Model-based fault detection in diesel engines air-path

Riccardo Ceccarelli

UNIVERSITÉ DE GRENOBLE

THÈSE

Pour obtenir le grade de

DOCTEUR DE L'UNIVERSITÉ DE GRENOBLE

Spécialité : **Automatique Productique**

Arrêté ministériel : 7 août 2006

Présentée par

Riccardo CECCARELLI

Thèse dirigée par **Carlos CANUDAS DE WIT** et
codirigée par **Philippe MOULIN**

préparée au sein du **Laboratoire de Grenoble, GIPSA-LAB**
dans **l'École Doctorale EEATS**

Diagnostic à base de modèle de la boucle d'air des moteurs Diesel

Thèse soutenue publiquement le **21 Septembre 2012**
devant le jury composé de :

M. Olivier SENAME
Professeur INP Grenoble, Président
M. Mohammed M'SAAD
Professeur ENSI Caen, Rapporteur
M. Luigi GLIELMO
Professeur Universita' del Sannio, Rapporteur
M. Pietro DOLCINI
Docteur Ingénieur, Renault, Membre
M. Philippe MOULIN
Docteur Ingénieur IFP Energies Nouvelles, Membre
C. CANUDAS DE WIT
Directeur de Recherche au CNRS, Membre

UNIVERSITÉ DE GRENOBLE

PhD THESIS

To obtain the degree of

DOCTEUR DE L'UNIVERSITÉ DE GRENOBLE

Speciality : **Automatic Control and Industrial Production**

Arrêté ministériel : 7 août 2006

Presented by

Riccardo CECCARELLI

Thesis surpervisor : **Carlos CANUDAS DE WIT**
Co-supervisor : **Philippe MOULIN**

Developed at **Laboratoire de Grenoble, GIPSA-LAB**
in **l'École Doctorale EEATS**

Model-based fault detection in Diesel engines air-path

Defended in public the **21 Septembre 2012**
In front of the board made by :

M. Olivier SENAME
Professor INP Grenoble, Président
M. Mohammed M'SAAD
Professor ENSI Caen, Rapporteur
M. Luigi GLIELMO
Professor Universita' del Sannio, Rapporteur
M. Pietro DOLCINI
DoctorIngénieur, Renault, Membre
M. Philippe MOULIN
Doctor Ingénieur IFP Energies Nouvelles, Membre
C. CANUDAS DE WIT
Directeur de Recherche au CNRS, Membre

Riccardo CECCARELLI

Gipsa-lab Grenoble Images Parole Signal Automatique, Unité Mathématiques et Systèmes, GIPSA-LAB, 961 rue de la Houille Blanche, BP 46, F - 38402, GRENOBLE Cedex, France

IFPEN, 1&4 av. du Bois Préu, 92852 Rueil-Malmaison, France.

E-mail: r.ceccarelli AT gmail.com

Key words. - Internal combustion engine, Faults Detection, Dynamic Threshold Generation, Air-path, OBD

Mots clés. - Moteur Combustion interne, Diagnostic, Generation Dynamique de Seuil, Boucle d'Air, OBD

September 19, 2012

Nihil est tam arduum quod ingegno vincas

Seneca

Remerciements:

To write acknowledgements is always difficult as there is the fear of not being good enough to convey the sense of gratitude or to forget someone.
I would like to thank Professor Carlos Canudas de Witt and Doctor Philippe Moulin who gave me the chance to work on this thesis. With them I considerably learned both on the scientific and professional sides. A special thank you goes to Gilles Corde, Head of the Department of Automatique, Traitement du signal et Informatique temps réel at the IFP Energies Nouvelle where I worked for three years.
Thanks goes to Professor Luigi Glielmo and Professor Mohammed M'Saad for being part of the Jury in the role of reviewers. Equally, thank you to Professor Olivier Sename and Doctor Pietro Dolcini for being President and Examiner.
I would like to mention the people of the Department for the nice time spent together in and out of the office.
Thomas Leroy, Mathieu Hillion, Emmanuel Enguyen e Thomas Coppin, thank you for sharing with me unforgettable time.
My thanks also to the the Italians at the IFP: Antonio Sciarretta, Angela Di Lella, Tiziana Armaroli, Marta Gasparrini, Clelia Tomasi, Gianluca Zito e Lorenzo Serrao.
Finally thanks to my family and Haruna.

Model-based Fault Detection in Diesel Engines Air-Path

Misura ció che è misurabile, e rendi misurabile ciò che non lo è.

Galileo Galilei

Abstract

The study of model-based fault detection for mass production Diesel engines is the aim of this thesis. The necessity of continuous vehicles health monitoring is now enforced by the Euro VI pollutant legislation, which will probably be tightened in its future revisions. In this context developing a robust strategy that could be easily calibrated and work with different systems (due to production variability) would be a tremendous advantage for car manufacturers. The study developed here tries to answer to those necessities by proposing a generic methodology based on local adaptive observers for scalar nonlinear state-affine systems. The fault detection, isolation and estimation problems are thus solved in a compact way. Moreover, the uncertainties due to measurement or model biases and time drifts lead to the necessity of improving the detection methodology by the use of robust thresholds that could avoid undesired false alarms. In this thesis a variable threshold is proposed based on the observability condition and the sensitivity analysis of the parameter impacted by the fault with respect to input or model uncertainties. This approach allows, among other things, to be used as an analysis tool for the individuation of the system operating points for which the diagnosis is more reliable and more robust to inputs uncertainties. The discussed approach has been successfully implemented and experimentally tested on a real Diesel engine for the intake leak detection and for the turbine efficiency loss drift detection in a co-simulation environment showing its advantages in term of detection reliability, calibration effort and engines diagnosis operating condition analysis.

Resume

Cette thèse a pour but l'étude de la détection basée sur modèle de défauts pour les moteurs Diesel produits en grande série. La nécessité d'une surveillance continue de l'état de santé des véhicules est maintenant renforcée par la législation Euro VI sur les émissions polluantes, qui sera probablement rendue encore plus contraignante dans ses prochaines révisions. Dans ce contexte, le développement de stratégies robustes, faciles à calibrer et valides pour des systèmes dispersés (car produits en grande série) procurerait un avantage considérable aux constructeurs automobile. L'étude développée ici tente de répondre à ces besoins en proposant une méthodologie générique. On utilise des observateurs adaptatifs locaux pour des systèmes scalaires non linéaires et affines par rapport à l'état, pour résoudre les problèmes de la détection de défauts, de son isolation et de son estimation d'une façon compacte. De plus, les incertitudes liées aux biais de mesure et de modèle et aux dérives temporelles nécessitent d'améliorer les méthodes de détection par l'utilisation de seuils robustes pour éviter les fausses détections. Dans cette thèse, on propose un seuil variable basé sur la condition d'observabilité du paramètre impacté par le défaut et sur une étude de sensibilité par rapport aux incertitudes sur les entrées ou sur le modèle. Cette méthode permet, entre autres, de fournir un outil d'analyse pour la sélection des conditions de fonctionnement du système pour lesquels le diagnostic est plus fiable et plus robuste par rapport aux incertitudes sur les entrées. L'approche présentée a été appliquée avec succès et validée de façon expérimentale sur un moteur Diesel pour le problème de détection de fuite dans le système d'admission d'air, puis dans un environnement de simulation pour le problème de détection de dérive d'efficacité turbine. On montre ainsi ses avantages en termes de fiabilité de détection, d'effort de calibration, et pour l'analyse des conditions de fonctionnement moteur adaptées au diagnostic.

Contents

Préface

La législation Européenne qui réglemente les normes d'émissions polluantes et incite à l'amélioration des performance des moteurs à combustion interne force les constructeurs automobile à la recherche continue de solutions techniques dans les domaines des lois de commandes et du diagnostic.

La Communauté Européenne, à partir de 1993 avec l'introduction de la réglementation *EURO I*, a commencé à définir les limites acceptées pour les émissions à l'échappement pour les nouveaux véhicules vendus dans les états membres de l' Europe. La réglementation standardise par ses directives les limites pour chaque catégorie de véhicule et type de technologie de combustion : allumage commandé (essence) ou par compression (Diesel).

Dans le cas des moteurs Diesel les produits de combustion qui sont réglementés sont les oxydes d'azote (NO_x), les monoxydes de carbone (CO), les particules fines (PM) et les hydrocarbures non brûlés (HC). Depuis *EURO I* la législation a continué à évoluer, devenant de plus en plus contraignante à la faveur d'une politique qui tient compte du respect de l'environnement comme illustré dans la Figure 1. Dans le détail, l'histogramme montre comment, de manière continue, les particules fines et les oxydes d'azote ont été progressivement limités. A chaque étape de la législation correspond l'introduction de solutions techniques innovantes et tout particulièrement une évolution des lois de commande qui doivent contrôler l'interaction de systèmes de plus en plus complexes : circuit(s) de recirculation des gaz brûlés (EGR), groupe turbocompresseur, système d'injection (groupée ou séquentielle), common rail et filtre à particules (DPF) pour mentionner les plus communs.

A partir de l'introduction de *EURO III*, le législateur a introduit des limites qui

doivent être respectées dans la durée, de fait cette date marque le début de l'introduction des systèmes de diagnostic embarqué (OBD). La dernière directive pour la régulation des gaz d'échappement est *EURO VI* [40] qui impose une réduction sensible des polluants et, pour la première fois, impose un système de diagnostique embarqué pour surveiller le moteur et une réduction drastique des seuils de détection des pannes. Cette tendance, dans l'esprit de moteurs de plus en plus respectueux de l'environnement, sera confirmée dans le futur (*EURO VII* et suivants).

L'obligation de surveiller de manière continue le véhicule pendant toute sa durée vie afin de respecter les contraintes sur les émissions polluantes, ammène les constructeurs automobiles à développer des stratégies de diagnostic qui puissent vérifier l'état de santé du moteur. L'objectif premier est donc d'éviter le mauvais fonctionnement du système surveillé et donc la conformité à la réglementation. L'aspect majeur de cette nouvelle réglementation, *EURO VI*, est la nécessité d'avoir des systèmes de diagnostic qui puissent être fiables dans toutes les zones de fonctionnement du moteur: ils doivent être validés au long du cycle de conduite Europeen - NEDC - qui est représentatif des conditions de fonctionnement du moteur pendant une conduite urbaine (ECE) et extra-urbaine (EUDC).

Le problème à traiter consiste donc dans le developpement d'une stratégie de détection des pannes qui puisse etre fiable dans des zones de fonctionnement où le systeme est tres peu excité (ECE cycle) et, très important, il doit fonctionner pour des systèmes tres différents entre eux. Cette dernière spécification est principalement dûe à la grande dispersion de production des moteurs et des leurs composants (capteurs et actionneurs). Si cette dispersion n'est pas prise en compte en phase de développement des stratégies, elle peut causer des fausses detections et avoir un impact économique qui n'est pas négligeable pour les constructeurs (réparations de composant en bon état, garages, insatisfaction des clients...). Afin de réduire les fausses alarmes liées aux dispersions de production, les constructeurs doivent habituellement faire face à de couteuses (temps et ressources) procédures de calibrations de leurs seuils de détection; ce qui peut, éventuellement, conduire à des retard de mise sur le marché.

Dans ce contexte, IFP Energies Nouvelles en collaboration avec le GIPSA Lab[1], dans

[1]Grenoble Images Parole Signal Automatique - INP Grenoble

le cadre de cette thèse, a évalué et étudié des approches de diagnostic basées sur des modèles physiques, c'est à dire "model-based fault detection". Spécifiquement, l'étude a porté sur l'évaluation des advantages et des limites de l'utilisation des observateurs dynamiques pour la détection et reconstruction des pannes dans les moteurs Diesel en visant la réduction, lorsque c'est possible, de l'effort de calibration des stratégies par rapport aux problèmes de dispersion de production déjà présenté.

Dans cette thèse, on prouve que, pour une classe spécifique de pannes, il est toujours possible d'utiliser des observateurs dynamiques locaux qui permettent l'estimation directe de la panne si les mesures utilisées par les stratégies sont pas affectées par d'autres erreurs, l'estimé est utilisé comme terme résiduel. De plus, grâce à une approche basée sur modèle, il a été possible de proposer une méthodologie pour le développement d'un seuil variable qui est basé sur l'analyse de sensibilité de la panne estimée en tenant compte des incertitudes des mesures dûes aux dispersions de production.

Le document est organisé comme suit: une introduction générale au problème de la détection de pannes est l'object du Chapitre 1, en particulier sont présentées les differentes metodologies de diagnostic, les approches spécifiquement utilisées dans le cas des moteurs Diesel et l'approche proposée. Le Chapitre 2 est entièrement dédié à l'introduction des sous-systèmes constituant la *boucle d'air* d'un moteur Diesel. Les systèmes sont présentés d'un point de vue fonctionnel et pour chacun des hypothèses de travail sont proposées et un modèle pour le diagnostic est présenté. L'objectif de ce chapitre n'est pas de fournir une description exhaustive de la *boucle d'air* mais de donner une caractérisation la plus complète possible des composants principaux qui seront utilisés dans la suite de ce travail. Dans le Chapitre 3, la première des deux applications étudiées est présentée: la détection d'une fuite dans le collecteur d'admission. Ce problème nous a permis d'étudier et développer deux observateurs non linéaires pour l'estimation du diamètre de la fuite, obtenus selon la théorie de Lyapounov (une comparaison qualitative est l'objet de l'Annexe B). Dans le même chapitre, deux typologies de pannes sur les capteurs ont été définies et utilisées par la suite dans l'analyse de sensibilité du paramètre estimé par l'observateur, c'est à dire le diamètre de la fuite, par rapport au cas où l'observateur utilise des mesures affectées par les erreurs. Cette approche nous a permis de développer un seuil variable qui adapte

son niveau en fonction de la sensibilité de l'estimé et, plus important, en fonction de la condition d'observabilité permettant ainsi de réduire la confiance de la panne estimée dans les zones pour lesquelles les algorithmes sont numériquement mal conditionnés. La stratégie proposée est donc testée expérimentalement sur le banc moteur (Annexe A) et les résultats sont présentés et commentés.

Une fois que la nouvelle approche a été définie, elle est validée sur une autre partie de la *boucle d'air* dans le Chapitre 4 : le système du turbocompresseur. L'intérêt ici est d'être capable d'estimer une perte d'efficacité de la turbine. Le chapitre veut montrer comment la stratégie proposée peut être facilement appliquée sur d'autres parties du système avec un effort de calibration limité. De plus, par le biais de l'analyse de sensibilité, il a été possible de comprendre les facteurs qui ont en impact majeur dans l'erreur d'estimation et (Annexe C) il permet aussi de déterminer les points de fonctionnement du moteur où la stratégie de diagnostic est la plus fiable et moins sensible aux erreurs de mesure.

Le Chaptire 5 est dedié aux conclusions et perspectives de ce travail.

Preface

Environment pollution legislation and internal combustion engine performances impose to car manufacturers a continuous research of technical solutions both in monitoring and controlling.
The European Community, starting in 1993 with *EURO I*, started to define the acceptable limits for exhaust emissions of new vehicles sold in EU member states. The emission standards regulated by the European Union directives impose specific limits for different vehicle categories and combustion technologies: spark or compression ignition.

In the case of Diesel engines the exhaust emissions subject to the regulation are the nitrogen oxides (NO_x), carbon monoxide (CO), particulate matter (PM) and non combusted hydrocarbons (HC). Since *EURO 1* the legislation evolved with new challenging and more environmentally friendly constraints as shown in Figure 1. This figure shows how fast and progressive was the intent to reduce the pollutant matters from the exhaust gases. For each step in the regulation an equivalent technological progress has been done and particular attention has been paid to engine control strategy which had to deal with more and more complex systems: exhaust gas recirculation circuit(s), turbocharger stage(s), fuel multi-injections system, common rails, Diesel Oxidation Catalyst (DOC) and Diesel particulate filter (DPF) to mention the most common.

Since *EURO III*, the legislator has introduced specific limits for aged vehicles, which leads to the development of on-board diagnosis (OBD) systems. The last European directive for exhaust gases regulation is *EURO VI* [40] which imposes a sensible reduction in the pollutant and, for the first time, a specific demand in fault detection of the engine

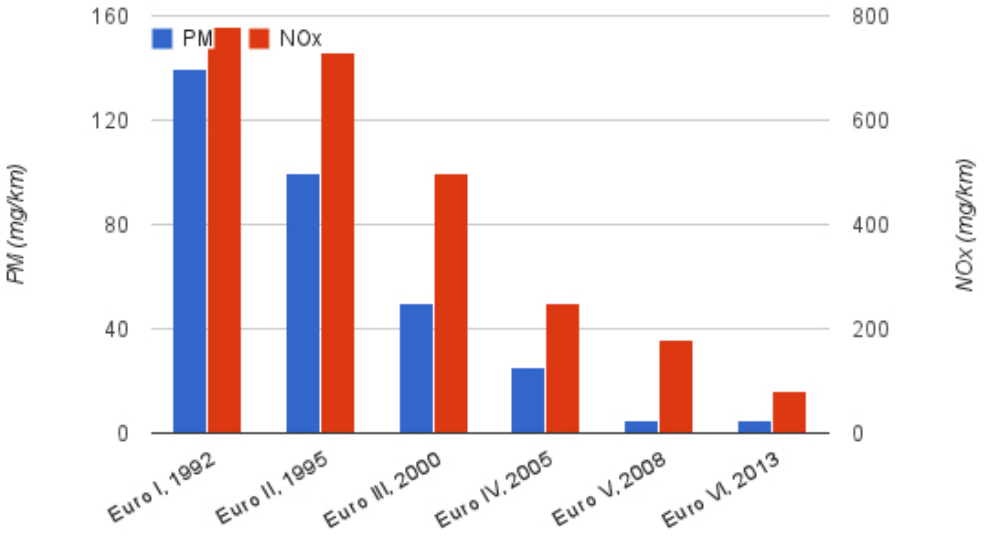

Figure 1: Nitrogen oxides and particulate matter emission standards for Diesel cars

as a system all along its life and a drastic reduction of the OBD threshold. This trend will probably be confirmed in the future (*EURO VII* and beyond).
This requirement of a continuous monitoring all along the vehicle life imposes to the car manufacturer to develop specific fault detection strategies in order to be able to health monitor the engine. The goal is to avoid a malfunctioning of the system and the non compliancy of the emission. The key part introduced in this last regulation is that the monitor system should work continuously in all possible engine operating conditions and in particular should be tested on the new European driving cycle - NEDC - which represents both urban and extra-urban driving conditions.

The problem to face consists in the design of fault detection strategies that should work in very poolyr excited conditions (ECE cycle) and, more important, should work for very different systems. In fact, the high production variability of the engines and of their components (sensors and actuators) can lead to very different systems to monitor. This variability could induce to false fault detection and could have, therefore, an

important economical impact for car manufacturers (garage services, fault free components replacement, customers unsatisfaction, ...).
In order to reduce false alarms with respect to production variability, car manufacturers face very exhaustive threshold calibration processes. This is something that could lead to very long lead time with catastrophic consequences.

In this context, the IFP Energies Nouvelles in collaboration with the GIPSA Lab[2] wanted to evaluate and study possible solutions with a model-based approach which is the goal of this thesis.
In particular, their interest was to study and evaluate what would be the advantages and limits of using dynamical observers applied to the fault detection of Diesel engines and reduce the calibration effort due to the above explained production variabilities.

In this thesis, it is shown that, for a certain class of faults, it is possible to use successfully local dynamical observers which give direct benefits in the estimation of the fault magnitude when the sensor measurement are faults free, otherwise use the estimation as the residual term [3]. Moreover, thanks to the model based approach, it has been possible to propose a methodology for threshold design which is based on the sensitivity analysis of the estimated parameter with respect to the measurement uncertainties.

The document is organised as follow: a fault detection overview is provided in Chapter 1, in particular the different diagnostic methodologies will be presented , a background of the Diesel engines fault detection and a description of the proposed approach.
The Diesel engine's *air-path* is presented in Chapter 2. The different constitutive components are presented and a brief description of their role at system view is reported, particular attention in this chapter is given to the modelling of each part. The aim is not to present the whole *air-path* but to provide a complete characterisation of the most

[2]Grenoble Images Parole Signal Automatique - INP Grenoble
[3]The *residual* is the name of the signal associated with a fault monitored in a diagnostic strategy

important components that have been analysed and studied in this work.
In Chapter 3, the first of the two studied faults is presented: the intake manifold leak detection. This problem allows to develop two different nonlinear adaptive observers based on the Lyapounov theory for the leak diameter estimation (their qualitative comparison is the subject of Appendix B). In the same chapter, the modelling of two classes of sensor faults as been defined and then used for the sensitivity analysis of the estimate with respect to measurement faults used in the observer. This analysis allows to design the proposed variable threshold which shows to adapt its level not only on the sensitivity based on the measurement uncertainties but, more important, to the parameter observability condition allowing to not consider the estimation where the observer estimation risk is poor. The proposed strategy is then experimentally tested on the engine test bed (A) and results are reported and commented.
Once the strategy was defined, in Chapter 4, it has been tested on a different part of the system: the turbocharger. The interest here was to detect turbine efficiency loss.
The work presented in this chapter shows how the proposed methodology can be applied to different systems with limited effort. The sensitivity analysis allows to isolate the major source of error in the turbine efficiency estimation and the same analysis (see Appendix C) revealed to be a powerful tool to understand the engine operating points in which the fault detection strategy is more reliable and less sensitive to measurement errors.
General conclusions and perspectives are reported in Chapter 5.

Chapter 1

Introduction to Diesel Engines Fault Detection Problems

In the field of automotive engines, environmentally based legislative regulation as the European On-Board Diagnostics (EOBD) specifies strong requirements on the diagnosis system performance. Fault detection is a complex task to be achieved, by definition a fault is an event that modifies the operation of the process in such a way that its performance is degraded and/or its mission cannot be achieved. In Diesel engines *events* could be of different types, i.e., actuators and sensors failure or modification of the system structure (leaks). The aim of this chapter is to introduce the fault detection problem with respect to the Diesel engine.

1.1 Fault detection: an overview

Diesel engines can be seen, as shown in Figure 1.1, as a system where faults can happen on different parts: actuators, process and sensors. The main aim of a fault detection scheme is to detect the presence of these faults. Moreover, once the fault is detected, the next step is to localise: *isolated*.

In order to detect and isolate the system anomalies it is necessary to generate signals, *residual*, which are sensible to a set of possible faults. By definition a residuals is a signal which is equal to zero when no fault acts on the system and different from zero

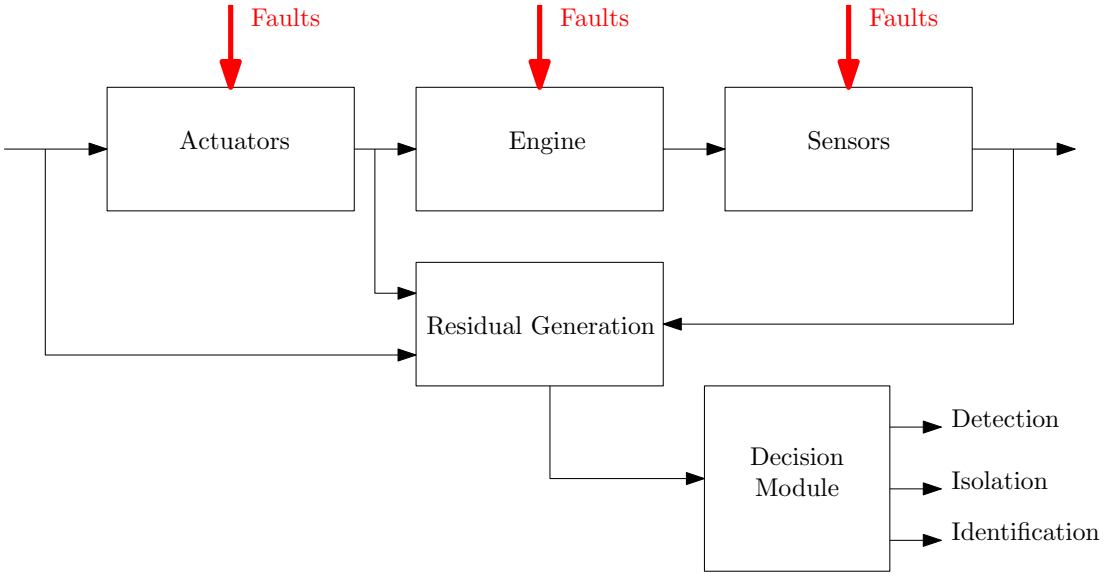

Figure 1.1: General scheme: faults act on different parts of the system

otherwise.

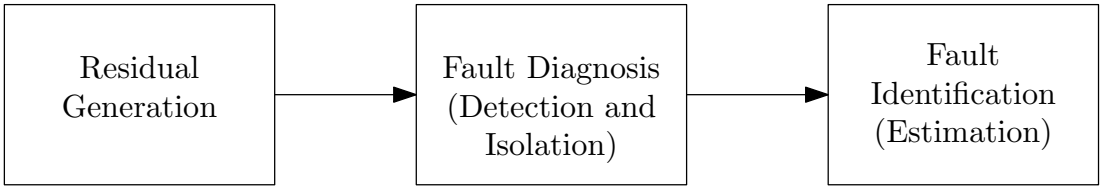

Figure 1.2: Fault Detection, Isolation and Identification scheme.

In a more general way, the Fault Detection and Isolation (FDI) problem can be decoupled in two main steps:

- generation of residual signals;
- analysis of the residuals.

The residuals analysis implies the detection, the isolation and the identification of the fault (Figure 1.2). In general, referring to FDI problem, the detection is the only mandatory part whereas isolation and identification (the estimation of the amplitude of the fault) have a lower priority even if their effect is really useful. In particular,

identification can be necessary in fault-tolerant control where the control algorithms could be designed with respect to the detected fault.

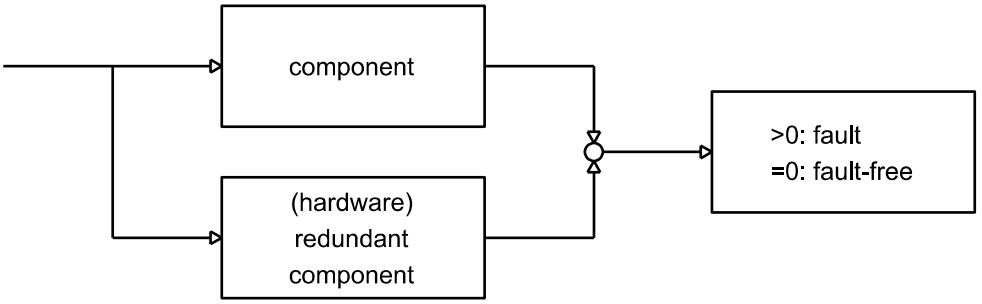

Figure 1.3: Hardware redundancy fault detection scheme

The residual generation can be done in very different ways, in [19] a good introduction to the FDI problem for engineering application is presented. In term of approaches used in engines faults detection [32] here is an overview of the most common approches:

- **Hardware redundancy** - the reconstruction of the process component is made by using an identical (redundant) hardware component (see Fig 1.3). The fault is detected if there is a deviation of one of the two (or more) components. The main advantage is the reliability of the method and the isolation problem is resolved automatically thanks to the nature of the strategy. The principal drawback and also the main reason why the methodology is not welcomed by vehicles manufactures is the cost: redundant components can increase the final cost of the car to not marketable prices;

- **Knowledge Based** - prior knowledge of physical process is used to ascertain when a fault condition has occurred. This approach is probably the most common in real applications however it is not used alone but in support of other strategies. As a matter of fact, the previous knowledge based on physical behavior and direct experience is the most useful piece of information that can be used to interpret the reliability of the strategy and for calibrating the algorithms used. Fuzzy logic approaches, that use knowledge based information rules, can be classified in this family; a good example of this methodology application in engines fault detection

can be found in [12] and in Figure 1.4 an example of rules extracted from the cited work is reported.

Table 3 Rule base

Number	Engine power	Fuel consumption	Engine temperature	CO emission	HC emission	CO_2 emission	O_2 emission	Excess air ratio	State of internal combustion engine
1	Normal	Normal	Normal	Normal	Normal	Normal	Normal	Normal	No fault
2	Normal	Low	Normal	Low	Low	Low	High	High	Lean mixture
3	Low	Very low	Very high	Very low	Very high	Very low	Very High	Very high	Very lean mixture
4	High	High	Normal	High	High	Low	Low	Low	Rich mixture
5	Low	Very high	Normal	Very high	Very high	Very low	Very low	Very low	Very rich mixture
6	Normal	Normal	Normal	High	Normal	Low	High	Normal	Faulty atomisation
7	Very low	Normal	Normal	Normal	Very high	Low	High	Normal	Faulty ignition
8	Low	Normal	Normal	High	Very high	Low	Low	Low	Low compression
9	Low	Normal	High	Normal	Normal	Normal	Normal	Normal	Excessive friction
10	Very low	Normal	Very high	Normal	Very low	Normal	Low	Normal	Overheating
11	Normal	High	Normal	Normal	Normal	Normal	Normal	Normal	Fuel system leakage

Figure 1.4: Rule base table used in Celik and Bayir work on fuzzy logic applied in fault detection of internal combustion engines (extract from JAUTO366 © IMechE 2007)

- **Signal Based** - the signal is analyzed or filtered to yield further information regarding the faults detection. The assumption here is that there are signals that carry useful informations about possible faults and, through a good signal processing (both in time and/or in frequency), it is possible to extract them. In fault detection jargon the signal processing phase (trend analysis, limit values check, mean, variance...) generates the so called *symptoms*, signals that should be then treated in a second analysis stage, *the symptom analysis*, for the final association with the fault (see Fig. 1.6). The approach could be really useful if

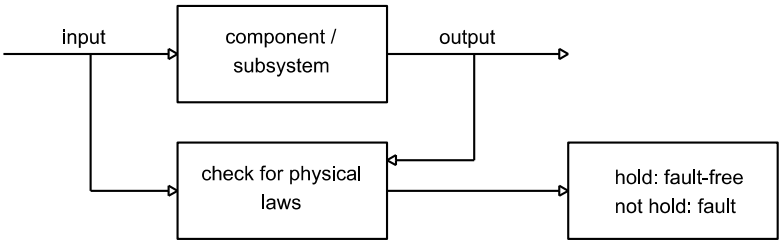

Figure 1.5: Plausability check scheme

reliable measurements are available and if the faulty behavior has a clear signature. In this category falls the *Plausibility test*, sketched in Figure 1.5 which, in its

simplest form, checks that the sensor signals are within the expected physical plausible ranges.

- **Data Based** - a neural network can be used to train a "black box" process model, without having a detailed understanding of the physical processes involved. The model is then compared to the actual physical process to determine an out of tolerance condition. The main advantage of this approach is that no physical knowledge of the process is required but the network generalization relies on the data quality and diversity (the model is ideally trained in all possible operating conditions). Among the advantages that make neural networks appealing is the elaboration speed and the limited memory footprint on the microcontrollers. The main drawback of this approach is that the network has to be trained every time the process change on a data base that is not always available or could be provided in a short elapse of time.

- **Model Based** - deviation between a theoretical model and the physical process are used to determine fault conditions. In its simplest form, the software model acts as a simulated redundant component, in this case we speak about *software redundancy concept* or *analytical redundancy*. The advantage of the approach is the easy and cheaper implementation, moreover it is suitable when the measurement under analysis is not directly measurable but can reconstructed. The main drawback is that no technical process can be modelled exactly as parameter differences and unknown disturbances will affect the residual terms. In addiction, the isolation and estimation of the faults require a second stage analysis: this can be classified as a problem of filtering/extracting useful information from the residual signals.

All these strategies have pro and cons, but, with the increasing complexity of Diesel engines more and more efforts are devoted to model based techniques. The reason, as already mentioned, lays in the possibility, given by the model, to reconstruct internal quantities which are not directly measurable and useful for FDI tasks.

All model-based techniques can be summarized in three main classes [32] as following:

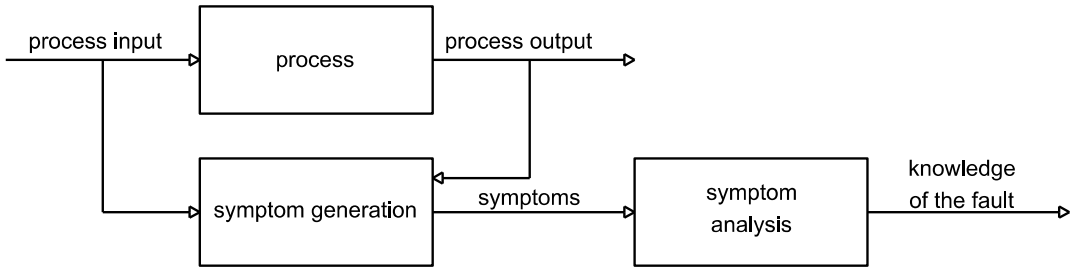

Figure 1.6: Signal processing fault detection scheme

- **Observation and State Estimation** - measured or calculated variables are limit checked to ensure they are within tolerance;
- **Parity Equation** - using a model of the process, the outputs of the model are compared directly to the outputs from the physical process (residuals). When the residuals exceed a pre-determined threshold value, an alarm condition is generated;
- **Parameter Estimation** - parameters are calculated from the physical process and are compared against parameter values calculated from process models or against known good reference values.

A detailed approach to model-based FDI, especially for linear system, can be found in [19]. Chen's work [14] provides a very exhaustive survey on framework for robust fault detection approaches.
A survey of the existing model based techniques in FDI in the subject of [26] and [25]; for those interested automotive, [32] gives an overview to the current trends in engines diagnosis.

1.2 Observer based FDI

In the previous section are provided different types of approaches to FDI. The first step in FDI is the residual signals generation and one of the possible ways to generate residuals is by the means of observers. With reference to the figure 1.7 observers are

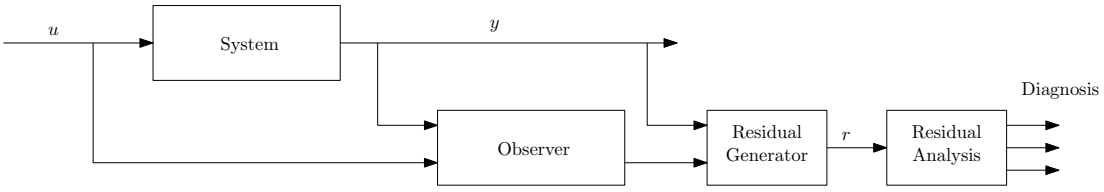

Figure 1.7: Observer based residual generation scheme

used to reconstruct some variables of the system in order to be compared then with the available measurements. By this comparison residual signals are generated. The most evident term that can be used as residual is the output errors of the observer but also other signals combination are possible.

1.2.1 Linear system

The observer approach for FDI in linear system has a wide background, since 1980 the use of closed loop observers for residual generation has been studied.
The good knowledge of linear system and control theory allow researchers to manage such a kind of systems with respect to fault detection.
The main aim in observers design for residual generation is to decouple the estimation from the observer's inputs and, eventually, increase the robustness of the estimation with respect to model uncertainty. These characteristics, in linear system, have a very well developed mathematical tools which allows to analyze the system properties and then design, if it is possible, specific observers in a systematic way.
Moreover, the possibility to design output observers decoupled from some of their inputs can help during the isolation process. As an example, under some strict conditions, a class of observers called *unknown input observer* (UIO), can be employed to generate residual signals which are not sensitive to specific inputs. This property simplifies, once a fault is present, the isolation task: as each observer of the bank is insensitive to a specific input (actuator or sensor), when the fault occurs on an input, only a subset of the residuals will react to its presence and so, by inference, it is possible to go back to which part of the system is affected by the fault. Other observer design approaches, using structural property of the system, are well documented in [16]. A description of

some of these methodology can be found in [14], [41] and [26].
In the linear domain, one of the most used observer is the Kalman filter due to its optimality in the estimation when measurement and process noise are present. This is particularly true when the fault detection and isolation strategy is designed for detecting sensor and actuator failures [30].
For multiple faults detection [1] presents an analytic redundancy approach based on reduced observer.

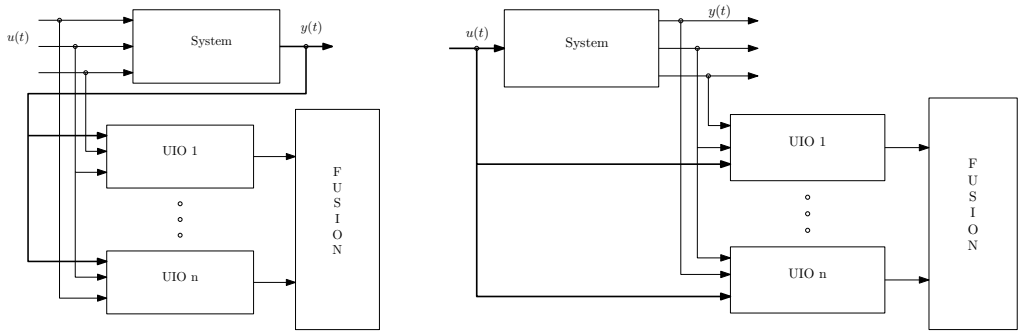

(a) Inputs - actuators (b) Outputs - sensors

Figure 1.8: Bank of observers (UIO) excited by all inputs 1.8(a) and all outputs 1.8(b)

In Figure 1.8 are shown the two described strategies for actuators and sensors fault detection in a linear system case by the use of a bank of unknown input observer.

1.2.2 Nonlinear system

Nonlinearities are present in almost every system and their knowledge, combined with the ability of taking them into account in the modelling process, can improve the quality and fidelity of the model itself. However, in a model-based diagnosis framework, those nonlinearities can increase the complexity of the strategy design.
The reason and the main difference from the linear case, has to be found in the absence of a systematic framework for treating nonlinear systems; each nonlinearity have to be studied and tried to be classified in a more generic family of known mathematical problems [6], more specifically for the FDI problem, Garcia and Frank, presented a survey in [3].

The most common way to manage nonlinear systems is to linearise them around some equilibrium point [14] and use the previously exposed linear techniques for residuals generation and isolation problem.
Another possible approach is the use of the nonlinear sliding mode observers [18] and [45] which are applied to the estimation of unknown inputs and faults in a class of nonlinear systems in [43].
Another example of nonlinear observer application is the tire/road contact friction estimation proposed in [8].
The engine and its air-path belong to this class of problems and a specific solution has been studied.

1.3 Engine fault detection

The Fault Detection and Isolation strategies for automotive engines have been more and more in car manufacturers research and The research on FDI strategies for automotive engines have been driven mainly by legislation, with the introduction of OBD (On Board Diagnosis) regulation and has been possible with the progress in technology, i.e., with the development of increasingly powerful microprocessors.
First works on automotive FDI was mainly oriented to spark-ignition engines, whereas Diesel engines are nowadays considered with increasing interest for research and development of FDI strategies.

1.3.1 State of art

Modern on-board diagnosis systems are based on the analysis of some measured signals, which are compared to pre-defined thresholds.
Model-based fault detection approach, based on parity equations and threshold checking, is very common in nowadays strategies applied to car engines. The key idea of this methodology is the use of a model of the system to generate *virtual measurements* which are compared to available sensors signals.

A very complete FDI scheme for a Diesel engine with turbo charger, using parity equation approach, is provided in [27] and [42] where physical equations and neural networks are used to model different parts of the system.
A similar approach in fault detection and isolation was developed by Mitsubishi Motors Corporation by state comparison with model behavior where are discussed the advantages of a model-based approach to cope with the OBD-II requirements.

An observer based approach to FDI problem for SI engine with exhaust gas recirculation is proposed in [31] and [29]. The fault diagnosis, i.e., detection and isolation, is performed by generating residuals based on multiple nonlinear sliding-mode observers. Once unmeasured engine's variables are estimated, residuals are generated as a difference of measures and model-based estimation made by these observer's reconstructed signals.

Further relevant contributions are those proposed by Nyberg in [38], [37] and [39], where a diagnosis method is presented based on a structure of hypothesis. The method consists in the detection of faults in the air mass sensor, throttle angle sensor, manifold pressure boost and the presence of leakages in the air system, i.e., intake manifold and before the throttle for SI engines. The key idea in Nyberg's works is to define *behavioral models* for each functioning conditions of the system, i.e., defined a nominal behaviour model (fault free) and other different models, each one expressing a particular faulty operating condition (behaviors), it is possible to determine which behavior best match the measurements through a structured hypothesis test. This result leads to the fault detection and isolation.

Another type of approach in fault detection, by using identification algorithms, is proposed in [33] for the exhaust gas recirculation system (EGR) . A real-time (recursive-least-squares method) parameters identification is used to diagnose different types of faults: low flow or high flow faults. The authors proposed to identify parameters of the EGR model in nominal behavior and then, by an on-line estimation, looked if there was a drift of such variables which corresponded to the presence of some faults.

As explained, the problem of fault detection relies on the continuous check of the residual signal against the threshold. The choice of the threshold value is always a compromise between the ability to quickly detect a fault and the necessity to avoid false alarm due to measurements or model error. In [34], Montes and Pisu, design a fault detection strategy to detect throttle and intake manifold pressure sensor faults for internal combustion engines in idle speed. The interesting aspect here is the approach they adopted for the threshold design: a variable threshold that is driven by the torque estimation through a first order polynomial. The result is a stairs threshold signal. Finally, a complete summary of the current strategies in automotive fault detection and the future trends are detailed in [32].

1.3.2 Proposed approach

The state of art proposed in the previous section shows that the model-based methodology for engine diagnosis is a promising way to approach the problem. The aim of this thesis is to evaluate, with respect to the air-path system of a Diesel engine, the use of a model-based closed-loop observer for FDI problems. In particular, the proposed approach should work with commonly available sensors and be robust to process and measure uncertainties due to production variability. This last problem is common in vehicles production and implies long calibration process.

In section 1.1 the problem of the diagnosis has been broken up in three sequential

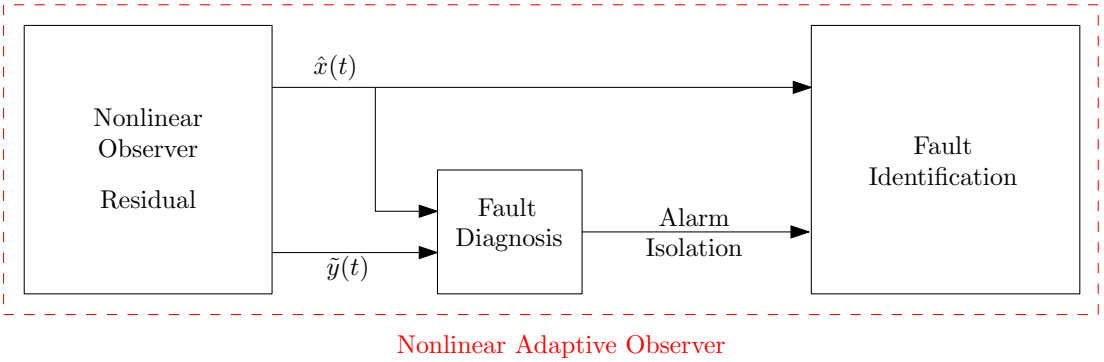

Figure 1.9: Adaptive Observers motivation for FDI on Diesel engine. Observer estimate state $\hat{x}(t)$ and the observer's output error $\tilde{y}(t)$.

steps: residuals generation, analysis and identification. The proposed strategy is to use a particular class of observers, i.e., adaptive nonlinear observers, locally implemented which have the property of simultaneously estimate state and parameters in order to merge, if possible, the FDI diagnosis in one step.

The use of this class of observers can be found in [17] for the estimation of the friction coefficient for an automotive clutch engagement or in [23] where it is proposed a model augmentation for bias compensation in a truck engine application.

The reason of this choice is motivated by the fact that, if the fault amplitude is linked to a parameter, the residual signal would be the parameter itself, i.e., equal to zero when there is no fault and different from zero otherwise. This last choice dictates the signal to be monitored. Moreover, the estimated parameter amplitude is the magnitude of the fault, i.e., the identification problem.
In figure 1.9 is shown how a nonlinear adaptive observer comprises the detection, isolation and identification phases.

For the detection phase, the sensors production variability combined with the engines construction uncertainty leads to the necessity of a robust threshold that can efficiently help to trig faults and avoid false alarms. As the fault's estimation (parameter) relies on the model equation accuracy, it is possible to estimate and bound the estimation error and use it for a robust threshold design strategy.
The proposed methodology for threshold design relies on the sensitivity analysis of the parameter estimation. Through this approach, combined with the observability condition of the estimation algorithm, it is possible to design a variable threshold that is driven completely by the available measurement and the maximum measurement uncertainties. Moreover, the sensitivity analysis, provides a useful tool to analyze the system and determine the operating points in which the fault detection strategy is more reliable.

This approach has been experimentally tested with success in a initial case study: the intake manifold leakage detection. The leakage had to be detected and the hole's

diameter had to be estimated.

In order to validate the strategy, the approach had been tested on another critical part of the Diesel engine air-path: the turbocharger. In this case, the aim of the fault detection was to determine the turbine efficiency loss.

Chapter 2

Models for Diesel Engines

In this chapter an introduction to the engine air-path is presented. The aim is to introduce the model used to simulate its behavior and to highlight some issues that will arise in the fault detection strategy. Particular attention will be paid to the model simplifications made to adapt it to the FDI problem, taking into account the available sensors present on mass production engines.
Each section will be devoted to a different part of the air-path of the engine used in this work:

- Cylinder filling
- Manifolds dynamics
- Valves model
- EGR cicuit model
- Turbocharger.

These models will provide some insight in the system operation and will be used later in the fault detection strategy. This chapter deals with the nominal system. The hypotheses and models of faults will be introduced in the next chapters.

2.1 Diesel Engines Air-Path: An overview

The purpose of the air-path is to convoy and control the gases used during the normal Diesel engine operative condition. In figure 2.1 a schematic of a Diesel engine is

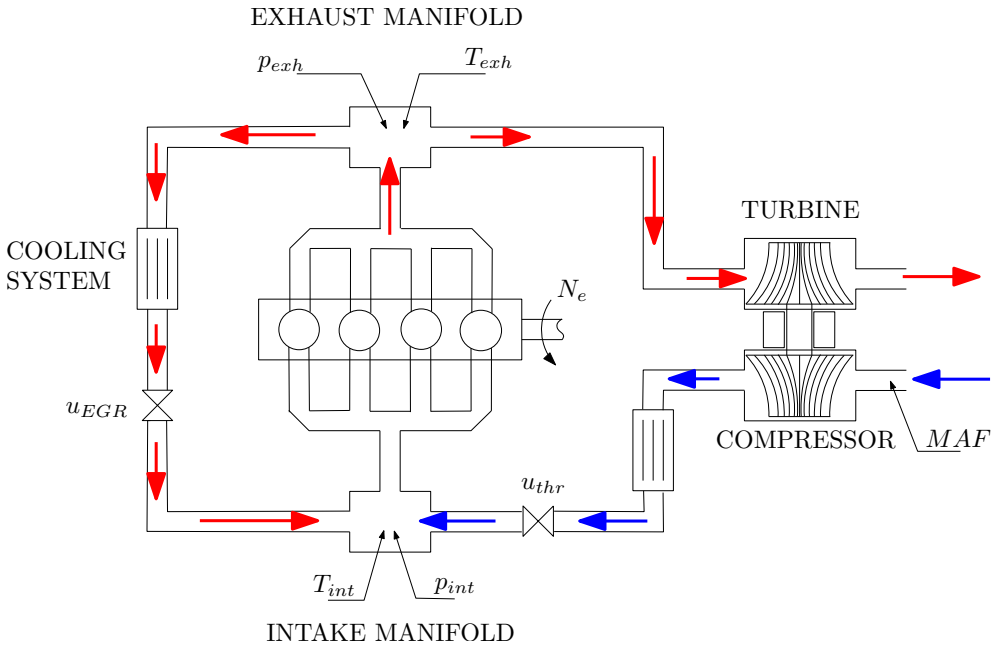

Figure 2.1: Diesel engine scheme: An overview.

presented. The aim of this scheme is to give a general and complete behavioural view of the gases flow and introduce the different subsystems below detailed.

The engine combustion chamber is filled, in normal condition, by fresh air (blue path): the air is compressed first and then, after a cooling system, is collected in the intake manifold where is aspired in the engine by the depression caused by the piston movements. This first part of the air-path is generally referred to as *intake system*.

After the combustion is completed, hot gases are used to drag the turbine which drive the compressor, presented before, and continue to the after-traitement system (not shown in the figure) to reduce pollutant emission. This part is generally referred as *exhaust system*.

There is a third part that has been introduced in the air-path a decade ago, i.e., *the exhaust gas recirculation system*: EGR circuit. The aim of this third circuit is to allow gases produced by combustion to be mixed with the intake air. The interest of such

approach is strictly related to a better control of the combustion and so of the pollutant emissions. A detailed analysis of the impact of the uses of the burned gases recirculation can be found in [13],[2].

2.2 Engine

The system considered in this work is a Diesel engine with variable geometry turbocharger and high pressure exhaust gas recirculation circuit.
As explained before the aim here is to present the model used for simulation and make some remark usefull later in the fault detection part. Hence, for air-path fault detection, the engine is seen as a source for gases energy (kinetical and thermal).

Engine Mass Flows

The engine can be approximated as a volumetric pump [20] and the flow aspirated in the cylinders can be modeled as proportional to the engine's speed as follow

$$\dot{m}_{asp} = \eta_v(p_{int}, N_e)\frac{p_{int}}{T_{int}R}V_{cyl}\frac{N_e}{2 \times 60} \tag{2.1}$$

where T_{int} and p_{int} are, respectively, the intake temperature (in Kelvin) and pressure (in Pascal), N_e is the engine's speed (in rpm), R is the universal specific constant for gases and V_{cyl} stands for the displaced volume, i.e., the combustion chamber's volume when the piston is at the bottom dead center (BDC) minus the volume of the cylinder when the piston is at the top dead center (TDC). The engine model as a volumetric pump, due to different causes (internal gases recirculation, cross-coupling between cylinders...), has to be corrected by a term that represents the capacity of the engine, in that particular operating condition, to fulfill the cylinder displaced volume: the volumetric efficiency η_v which is generally obtained experimentally (Fig. 2.2). In the following, for notation simplicity the aspired mass flow (2.1) can appear as

$$\dot{m}_{asp} = \eta_v(p_{int}, N_e) \cdot p_{int} \cdot \beta_{int}(T_{int}, N_e) \tag{2.2}$$

where

$$\beta_{int}(T_{int}, N_e) = \frac{1}{T_{int}R}V_{cyl}\frac{N_e}{2 \times 60} \tag{2.3}$$

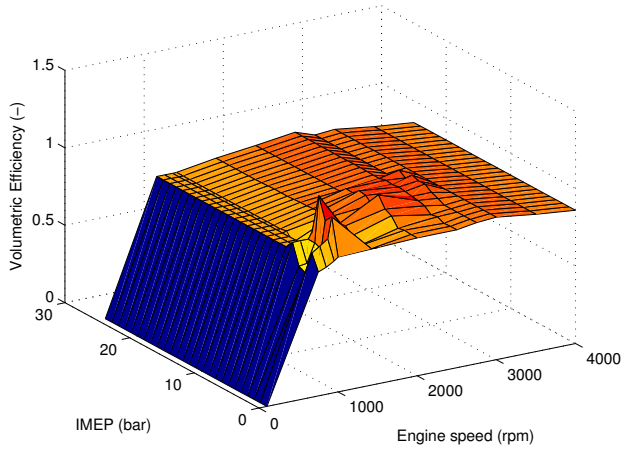

Figure 2.2: Diesel engines' experimental volumetric efficiency look-up table obtained for the European driving cycle NEDC.

Remark 2.1.

In figures 2.3(a) and 2.3(b) the engine volumetric efficiency map derivative with respect to the $IMEP$ (image of the engine produce torque) is shown. As figures shows, the η_v term does not change significantly with respect to the change of the produced torque, except for the the very low loads (the bottom left corner of Fig. 2.3(b)). In this operating zone, it is particularly difficult to exactly measure all the variables needed to describe η_v. Usually the map Fig. 2.2 is obtained as interpolation of some steady state engine working points. The same kind of remarks can be made for the sensitivity of the engine efficiency with respect to its speed. These consideration lead to some working hypothesis:

- *η_v is bounded and as well as its derivative;*
- *as its derivative is almost equal to zero, the engine volumetric efficiency can be considered constant for control purposes.*

2.3 The Intake Manifold

The intake manifold is a volume where different gases are mixed and aspirated (Fig. 2.4). As a thermodynamic system, the variables representative of the state of the system are the pressure p_{int} and the temperature T_{int}. Under the hypothesis that the

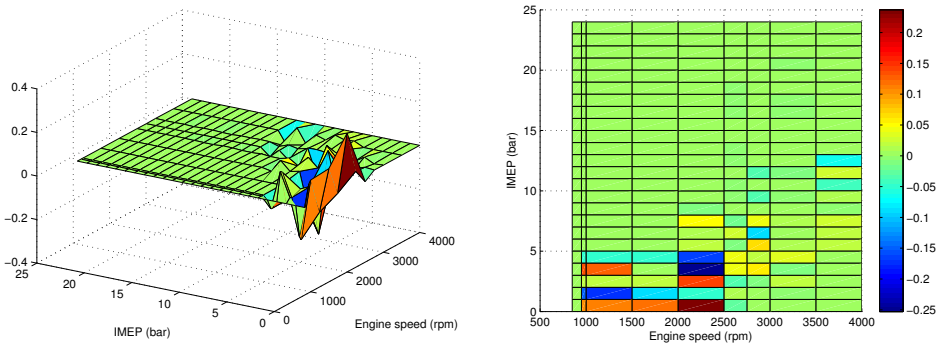

(a) 3D map

(b) Top view

Figure 2.3: Partial derivative of the efficiency map with respect to IMEP.

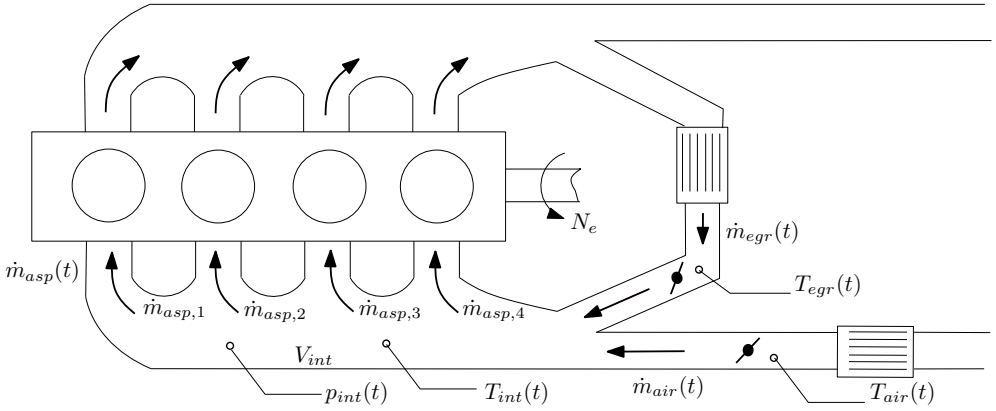

Figure 2.4: Intake manifold model details.

system is isolated, there are not heat exchange with the ambient, the system can be modeled as *adiabatic*.

2.3.1 Adiabatic Model

The adiabatic model [20] is particularly suited when the temperature variations are not negligible. The model is derived under the hypothesis that mass and energies balance stand, i.e,

$$\frac{d}{dt}m(t) = \dot{m}_{in}(t) - \dot{m}_{out}(t) \tag{2.4}$$

$$\frac{d}{dt}U(t) = \dot{H}_{in}(t) - \dot{H}_{out}(t) \tag{2.5}$$

where $m(t)$is the total gases mass inside the manifold, $\dot{m}_{in}$ and $\dot{m}_{out}$ are the mass flow rates coming in and out the manifold, $U(t)$ is the internal energy and $\dot{H}$ stands for entalpy flows. With reference to the figure 2.4,

$$\dot{m}_{in}(t) = \dot{m}_{air}(t) + \dot{m}_{egr}(t) \tag{2.6}$$

$$\dot{m}_{out}(t) = \dot{m}_{asp,1}(t) + \dot{m}_{asp,2}(t) + \dot{m}_{asp,3}(t) + \dot{m}_{asp,4}(t) \tag{2.7}$$

Assumption 2.1.

In the rest of this document, all the flows will be considered positive.

If it is assumed that the fluid can be modeled as perfect gases, no heat or mass transfer through the walls, and that no substantial changes in potential and energy in the flow occur, under the assumption 2.1, the adiabatic model of the intake manifold is:

$$\begin{cases} \dot{p}_{int}(t) = \gamma \dfrac{R}{V_{int}} \left(\dot{m}_{air}(t) T_{air}(t) + \dot{m}_{egr}(t) T_{egr}(t) - \dot{m}_{asp}(t) T_{int}(t)\right) \\ \dot{T}_{int}(t) = \dfrac{R T_{int}(t)}{p_{int}(t) V_{int}} \left(\dot{m}_{air}(t)(\gamma T_{air}(t) - T_{int}(t)) - \dot{m}_{asp}(t)(\gamma - 1) T_{int}(t) + \right. \\ \qquad \left. \dot{m}_{egr}(t)(\gamma T_{egr}(t) - T_{int}(t))\right) \end{cases} \tag{2.8}$$

where all variables are described in Table 2.1.

Although the system (2.8) is a complete model for the intake manifold gases dynamic, the adiabatic model is still too complex [21]. The reasons are different: first, the temperature dynamic is much slower than the pressure dynamic, second, the model need measurements that are not generally available in mass production cars, i.e., the EGR temperature and flow rate and finally, the temperature sensors normally used have high time constants ($3 - 6$ s).

These considerations lead to the choice of an isothermal model, which has been shown is a good representation of the manifold dynamics and it will be the object of the following section.

Name	Description	Units
R	gas constant	$[J/kgK]$
c_p	specific heat at constant pressure	$[J/kgK]$
c_v	specific heat at constant volume	$[J/kgK]$
γ	ration of specific heat	$[-]$
T_{egr}	upstream EGR valve temperature	$[K]$
T_{int}	intake manifold temperature	$[K]$
T_{air}	downstream cooled compressor temperature	$[K]$
V_{int}	intake manifold volume	$[m^3]$
$\dot{m}_{air}$	compressor flow	$[kg/s]$
$\dot{m}_{egr}$	egr flow	$[kg/s]$
$\dot{m}_{asp}$	engine aspired flow	$[kg/s]$

Table 2.1: Variables definition - Adiabatic model

2.3.2 Isothermal Model

The Diesel engine considered in this thesis is supposed to work with exhaust gas recirculation, this might generate very high intake temperature variation. This, as already discussed in section 2.3.1, suggests the use of an adiabatic model because of the small volume of the intake and so the short dwell time of the gases trapped in it (negligible heat exchanges with the manifold wall).

Due to long response time of temperature sensors, even under the hypothesis of having all the necessary measurements, the adiabatic model, even if it is more accurate in transient [15], can be generally replaced with a isothermal one in real applicative context. The isothermal model is obtained from (2.8) by neglecting the temperature dynamics

$$\begin{cases} \dot{p}_{int}(t) &= \gamma \dfrac{RT_{int}(t)}{V_{int}} \left(\dot{m}_{air}(t) + \dot{m}_{egr}(t) - \dot{m}_{asp}(t)\right) \\ \\ T_{int}(t) &= T_{int,m}(t) \end{cases} \tag{2.9}$$

where $T_{int,m}$ is the available measurement provided by the intake temperature sensor. Generally, for notation simplicity, a new variable is introduced

$$\alpha_{int}(t) = \frac{RT_{int}(t)}{V_{int}} \tag{2.10}$$

which, experimentally, is always strictly positive and bounded, i.e.,

$$0 < \alpha_{int}(t) \leq \alpha_{int,MAX} \tag{2.11}$$

as the intake temperature is always different from zero and bounded.

2.4 Flow through an orifice

The air-path is a mix of different controlled flows, it is not always possible to have a direct measurement of them, because of cost and technical issues. Bernoulli law provides, given pressure measurements, in the cases of incompressible fluids, a good estimation of the flow rate. In the case of compressible fluids, i.e. gases flowing in the air-path pipes, more complex relations have to be considered.

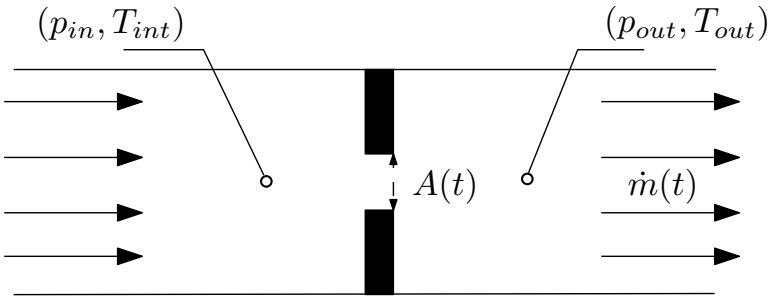

Figure 2.5: Flow through an orifice of variable section. Model scheme.

For engine control and diagnosis purposes, under some working hypothesis (see e.g. [20, 22]), a common way to model a flow through a variable restriction is

$$\dot{m}(t) = c_d A(t) \frac{p_{in}(t)}{\sqrt{RT_{in}(t)}} \sigma\left(\frac{p_{out}(t)}{p_{in}(t)}\right) \tag{2.12}$$

where

$$\sigma\left(\frac{p_{out}}{p_{in}}\right) = \begin{cases} \frac{1}{\sqrt{2}} & \text{if} \quad \frac{1}{2}p_{in} > p_{out} \\ \sqrt{2\frac{p_{out}}{p_{in}}\left(1 - \frac{p_{out}}{p_{in}}\right)} & \text{if} \quad \frac{1}{2}p_{in} \leq p_{out} \end{cases} \tag{2.13}$$

and the subscripts "in" and "out" stand for upstream and downstream values across a possibly variable-area section $A(t)$ (see Fig. 2.5 for more details on the variables).

The $\sigma(t)$ function (2.13) is a piecewise continuous and derivable function as depicted

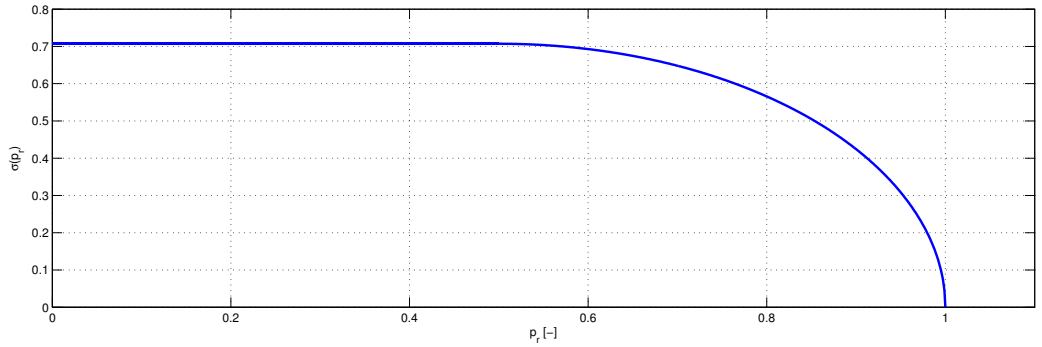

Figure 2.6: $\sigma(p_r)$ function's shape.

in figure 2.6. It is defined for $p_{out}/p_{in} \leq 1$, otherwise the equation (2.12) must be considered with a minus and considering the input and output pressures with respect to the sense of the flow.Physically a $p_{out}/p_{in} > 1$ means that the flow has changed its direction: back-flowing.

A last remark on the $\sigma(p_r)$ function is its stiffness for values of the pressure ratio grater of 0.9, this means that very small errors in pressure ratio lead to big variation of the estimated mass flow through the variable restriction. This last consideration is very important for understanding the limit of validation of the model. The c_d term stands for the *discharge coefficient* that is experimentally determined and allows to include the neglected losses due to the hypothesis done in the model, i.e., pressure drop across the section.

2.5 Exhaust Gas Recirculation circuit: EGR

The exhaust gas recirculation circuit has become, in Europe, a fundamental part of the design of modern Diesel engine. Its introduction in the car market as engines constitutive part coincide with the start of the EURO 3 regulation in order to match the imposed emission limitations.

The EGR strategy allows to reduce the oxygen concentration and so to slow down the combustion. Moreover, the inert exhaust gas displaces the amount of combustible matter in the cylinder which means the heat of combustion is less. Hence the formation

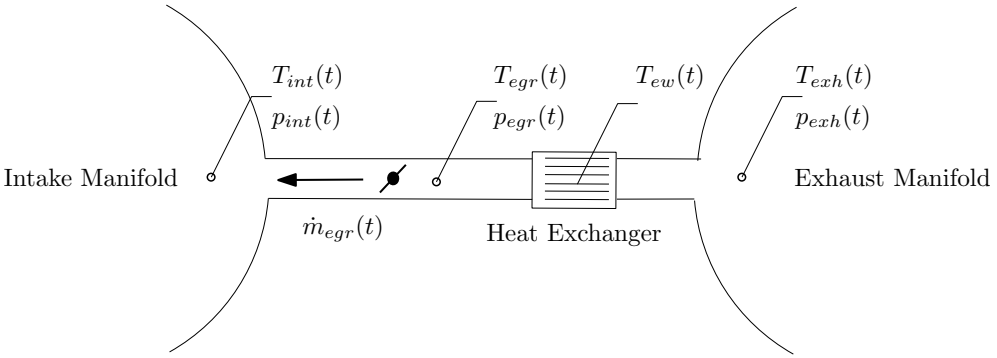

Figure 2.7: Exhaust gas recirculation circuit: a schematic view.

of NO_x is strictly related with the oxygen concentration and combustion temperature, the EGR strategy allows to reduce the NO_x emissions.

In order to increase the recirculated gas density and to decrease their temperature, the exhaust flow is generally cooled with a heat exchanger. The amount of recirculated burned gases is controlled by a valve.

A detailed scheme of the EGR circuit is depicted in figure 2.7 : exhaust gas discharged by the engine in the exhaust manifold (right), are cooled in the heat exchanger and the quantity of gas introduced in the intake manifold (left) are controlled by a specific valve.

The main effect of the heat exchanger is to cool the exhaust gas and, consequently,to a pressure drop. The pressure and temperature downstream of the exchanger are referred as p_{egr} and T_{egr}. In the contest of this thesis, the exchanger, is cooled by the engine water T_{ew}.

The model of the cooling system is therefore

$$\begin{cases} T_{egr} &= \eta_{egr\_HE}(t)T_{ew}(t) + \left(1 - \eta_{egr\_HE}(t)\right) T_{exh}(t) \\ \\ \eta_{egr\_HE} &= a_{egr\_HE}\dot{m}_{egr}(t) + b_{egr\_HE} \end{cases} \tag{2.14}$$

where the downstream temperature of the heat exchanger T_{egr} is a convex combination of the upstream gas temperature T_{exh} and the water temperature T_{ew} weighted by an experimental coefficient $\eta_{egr\_HE}(t)$, i.e. the heat exchanger conversion efficiency (experimentally obtained and provided by the manufacturer).

It is possible to express the efficiency as a linear function of EGR flow $\dot{m}_{egr}$, where a_{egr_HE} and b_{egr_HE} are two constants obtained from an optimization of the raw data. The point here is that the two equations are implicitly coupled and the EGR pressure and temperature sensors are not available in cars for two main reasons: the sensors are exposed to soots present in the exhaust gas, this make the measurements unreliable and on the other hand, the cost.

Another important point is the estimation of the EGR flow. The lack of a specific sensor, for the same reasons exposed above, obliges to estimate the EGR flow by a dedicated dynamical observer [13] based on the intake pressure measurement.

For diagnosis purposes, it will be detailed in the next chapter (i.e. the intake manifold leakage detection), the observer based approach for the estimation of the EGR flow is not suitable anymore with respect to the detection strategy used. The reason is that, in case of leakage on the intake manifold, the EGR mass flow observer will be not able to distinguish the fault from a decreasing amount of the EGR flow rate. Hence, the EGR gas stream is estimated by the equation (2.12). This way of modeling neglects the EGR heat exchanger and the EGR pipe length; these strong simplifications lead to a less accurate estimation of the EGR flow. In order estimate, under these hypothesis, the recirculated flow, an experimentally based discharge coefficient c_d has to be recalculated. Finally, the EGR flow model equation is

$$\dot{m}(t) = c_d(t)A(t)\frac{p_{exh}(t)}{\sqrt{RT_{int}}(t)}\sigma\left(\frac{p_{int}(t)}{p_{exh}(t)}\right) \tag{2.15}$$

where, due to the available sensors, the upstream temperature T_{egr} is replaced by the intake temperature T_{int}. In figure 2.8 is shown the comparison between the two considered temperatures when a low loads trajectory is simulated on a reference nonlinear model of the engine runs under AMEsim - Simulink co-simulation environment.

By this comparaison it is possible to see that the error between T_{egr} and T_{int}, when the EGR rate is close the 50 %, is less than 20° in the worst cases.

Remark 2.2.

As briefly described at the beginning of this paragraph, the EGR is probably one of the best strategy to control the NO_x production. The introduction of this circuit however can limit the operating zone of the compressor. In particular, the use of the EGR can push

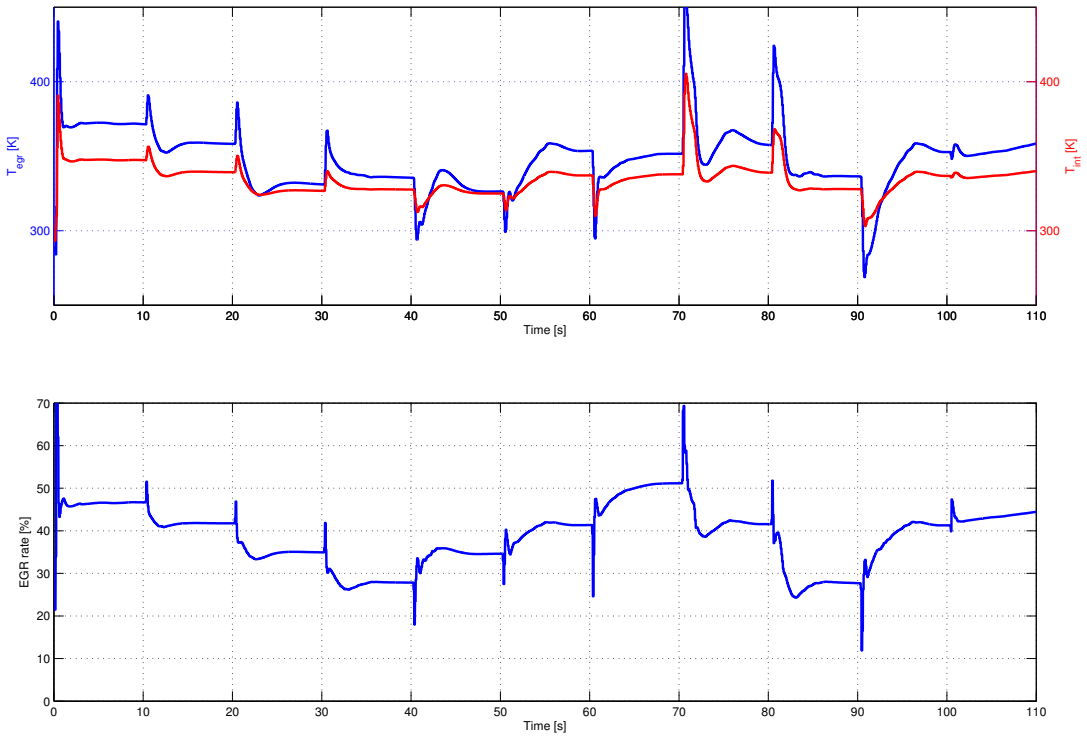

Figure 2.8: (top) T_{egr} versus T_{int} and (bottom) the EGR rate, along a load trajectory. The trajectory considered is made of *IMEP* steps keep for 10 seconds each. The particular sequence used in simulation is $IMEP = [4\ 5\ 6\ 7\ 6\ 5\ 2\ 5\ 7\ 5\ 4]\ bar$.

the compressor to its the surge line. Moreover, collecting part of exhaust gas directly in the exhaust manifold subtract energy to the turbine.
To cope with these issues, another EGR circuit is considered: the low pressure EGR. The long route EGR picks-up the exhaust gas downstream the turbine and injects it upstream the compressor.

2.6 Turbocharger

The turbocharger has become a fundamental part in nowadays engine. The main role of the turbocharger is to increase the air density in order to allow the engine to trap, for the same cylinders volume, more air hence more power. The advantage of

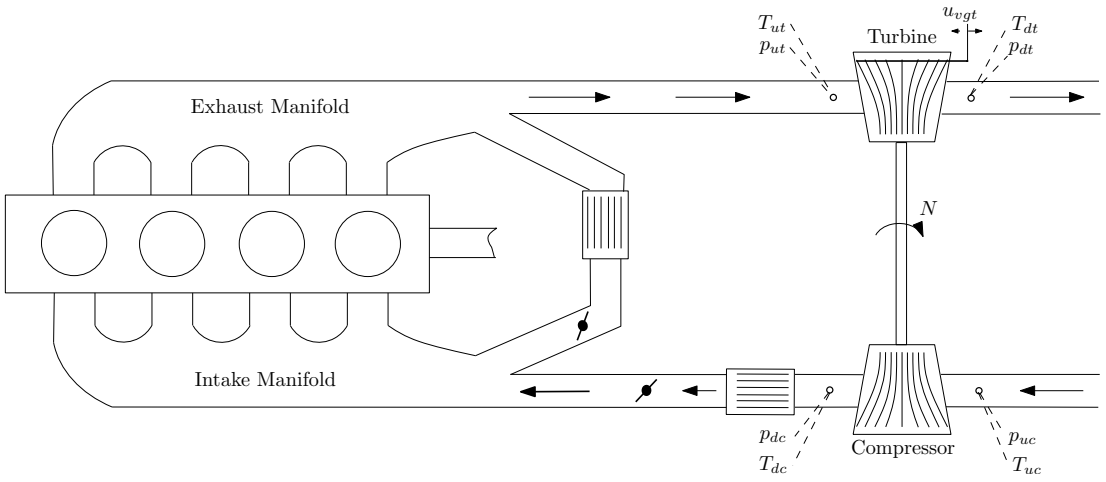

Figure 2.9: General scheme of Diesel engine with the turbocharger system detailed.

using a turbocharger, in Diesel engines, is the possibility to increase its power density. The turbochargers technological development led today to three main typologies: free-floating, with waste-gate and variable geometry turbochargers [22].
In this work a variable geometry turbine (VGT) is considered. The particularity of such type of turbine is to have the possibility to control the input section of the turbine as function of the exhaust gas mass flow rate and pressure.
The model presented in the next section is suited for control purposes, an exhaustive physical modeling description can be found in [22], [35] and [44].

The turbocharger dynamic is its rotational speed N which is derived from the power balance of the turbocharger shaft.

$$P_t - P_c = JN\frac{dN}{dt} \tag{2.16}$$

where J is the moment of inertia of the turbocharger, P_t is the power developed by the turbine and P_c the power to drive the compressor. The turbine and the compressor powers can be expressed as

$$P_t = W_t c_p \eta_t T_{ut}\left[1 - \left(\frac{1}{\Pi_t}\right)^{\frac{\gamma-1}{\gamma}}\right] \tag{2.17}$$

$$P_c = W_c c_p \frac{1}{\eta_c} T_{uc}\left[\Pi_c^{\frac{\gamma-1}{\gamma}} - 1\right] \tag{2.18}$$

where the η_t and η_c are the turbine and compressor efficiency terms used to correct the isentropic powers into the real ones. Π_t and Π_c are respectively the pressure ratio across the turbine and the compressor. c_p is the specific heat at constant pressure and γ is the ratio of specific heats. In order to simplify the reading of this section, due to the large amount of variables needed for the model, a summary of all them is presented in Table 2.2. The compressor efficiency η_c is given by a static map (Fig. 2.10(a)) which depends

Name	Unit	Definition
N	[rad/s]	Turbocharger shaft speed
p_{ut}	[Pa]	Turbine upstream pressure
p_{dt}	[Pa]	Turbine downstream pressure
p_{uc}	[Pa]	Comppressor upstream pressure
p_{dc}	[Pa]	Compressor downstream pressure
p_{ref}	[Pa]	Const. reference pressure
T_{ut}	[K]	Turbine upstream temperature
T_{dt}	[K]	Turbine downstream temperature
T_{uc}	[K]	Compressor upstream temperature
T_{dc}	[K]	Compressor downstream temperature
T_{ref}	[K]	Const. reference temperature
Π_t	[-]	p_{ut}/p_{dt} Turbine pressure ratio
Π_c	[-]	p_{dc}/p_{uc} Comp. pressure ratio
W_t	[Kg/s]	Turbine flow rate
W_c	[Kg/s]	Compressor flow rate
W_f	[Kg/s]	Injected fuel flow rate
η_c	[-]	Compressor efficiency
η_t	[-]	Turbine efficiency
u_{VGT}	[%]	VGT opening control
T_{amb}	[K]	Const. atmospheric temperature
p_{amb}	[Pa]	Const. atmospheric pressure

Table 2.2: Nomenclature for Turbocharger Model

on the corrected compressor speed $N_{c,corr}$ and on the corrected mass flow $W_{c,corr}$

$$\eta_c = \phi_{\eta_c}(W_{c,corr}, N_{c,corr}) \tag{2.19}$$

where

$$N_{c,corr} = N\frac{\sqrt{T_{ref}}}{\sqrt{T_{uc}}} \qquad W_{c,corr} = W_c\frac{p_{ref}}{\sqrt{T_{ref}}}\frac{\sqrt{T_{uc}}}{p_{uc}} \tag{2.20}$$

In the same way, the variable geometry turbine efficiency η_t is given by another static

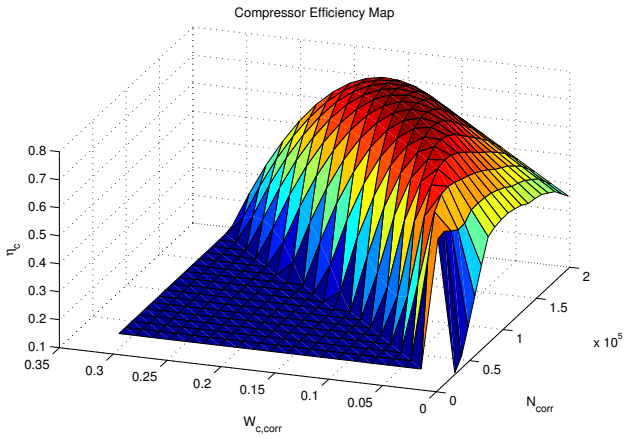

(a) Compressor efficiency map

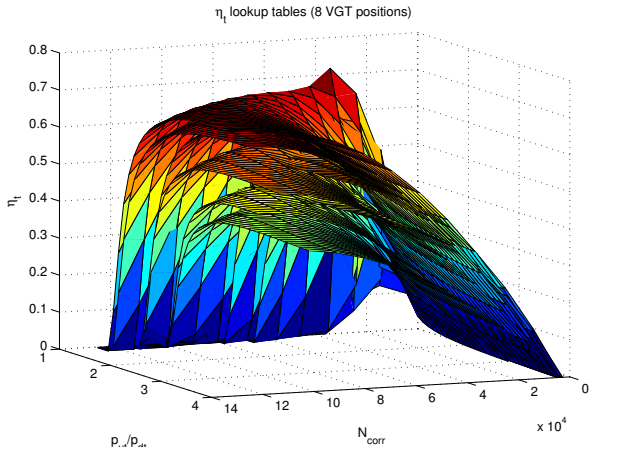

(b) Turbine efficiency map

Figure 2.10: Efficiency maps for a turbocharger with a variable geometry turbine - 8 different VGT's position

map (Fig. 2.10(b)) which is function of the VGT position.

$$\eta_t = \phi_{\eta_t}\left(W_{t,corr}, N_{t,corr}, u_{VGT}\right) \tag{2.21}$$

where $N_{t,corr} = N\frac{\sqrt{T_{ref}}}{\sqrt{T_{ut}}}$ and $W_{t,corr} = W_t\frac{p_{ref}}{\sqrt{T_{ref}}}\frac{\sqrt{T_{ut}}}{p_{ut}}$. For completeness, two more maps are generally provided with the turbocharger, i.e. ϕ_{Π_c} and $\phi_{W_{t,corr}}$ which are the compressor pressure ratio Π_c and the corrected turbine flow rate $W_{t,corr}$

$$\Pi_c = \phi_{\Pi_c}\left(W_{c,corr}, N_{c,corr}\right) \tag{2.22}$$

$$W_{t,corr} = \phi_{W_{t,corr}}\left(\Pi_t, N_{t,corr}, u_{VGT}\right) \tag{2.23}$$

Remark 2.3.

All the turbocharger look-up tables are obtained in steady state condition and provided by the manufacturer and are generally very accurate in the zone for which the turbocharger is designed to operates (i.e. high engine loads).

Chapter 3

Fault-Detection for Intake Leakage

3.1 Introduction

The purpose of this chapter is to introduce a first type of fault in the air-path: a leakage in the intake manifold. The interest in this type of fault is that, even if it is extremely rare the formation of a hole on the manifold surface, it could happen that the materials fatigue and vibration may lead to pipes disconnection. Hence, the leak detection becomes a critical task to be achieved, especially when an intensive use of burned gas is made by means of the EGR circuit, in order to prevent direct pollutant emissions in the ambient. Moreover, the incapacity of detecting a leak in the intake receiver can lead to a wrong estimation of the gas flow through the after-treatment system. The direct consequence, in a Diesel engine, is a inadequate control strategy of the Diesel Oxidation Converter (DOC), with a result, in the worst scenario, of over-heating of the DOC itself and the consequent failure.

The chapter is organized as follow: a model for the leakage is introduced and the model for diagnosis is presented. An adaptive observer for the estimation of the leak diameter is presented and compared with two observers estimation. Once a residual is generated different type of detection threshold are evaluated. In particular a dynamical generated threshold is proposed.

3.2 Model for diagnosis

The intake manifold can be described by an isothermal receiver in which the pressure is the state variable (Section 2.3). This approach is supported by the fact that both the temperature and the pressure are measured and available.
Starting from the equation (2.9), it is possible to include the leakage as a fourth flow term in the mass balance on the right hand side of the dynamic. The model for the intake manifold pressure becomes

$$\begin{cases} \dot{p}_{int}(t) &= \gamma \dfrac{RT_{int}(t)}{V_{int}} \left(\dot{m}_{air}(t) + \dot{m}_{egr}(t) - \dot{m}_{asp}(t) - \dot{m}_{leak}(t) \right) \\ \\ T_{int}(t) &= T_{int,m}(t) \end{cases} \tag{3.1}$$

where the leakage can be modeled as flow through a restriction expressed in equations (2.12) and (2.13). In particular, for a given hole section A_{leak}, the leakage can be explicitly expressed as

$$\dot{m}_{leak}(t) = A_{leak} \frac{p_{int}(t)}{\sqrt{RT_{int}(t)}} \sigma \left(\frac{p_{amb}(t)}{p_{int}(t)} \right) \tag{3.2}$$

The proposed strategy, as explained in the introduction, is to directly estimate the hole diameter by means of a dynamical observer. Hence, the diameter must appear explicitly in the equation (3.2). For doing that the term referring to the opening section of the leak A_{leak} is rewritten as

$$A_{leak} = \theta \cdot A_{leak,max} \tag{3.3}$$

where θ is related to the diameter by

$$\theta = \frac{D_{leak}^2 \pi}{4 A_{leak,max}}$$

and $A_{leak,max}$ is a constant and correspond to the maximum opening surface of the leak, i.e., the entire surface of the manifold. In other words, in the worst case scenario, the manifold will be completely disconnected from the pipes. This type of choice is arbitrary, any other maximum value can be selected. The θ term is a parameter that can be any value from zero to the unit, corresponding to the two extreme cases: there is not any leak or the leak surface on the manifold is equal to the considered $A_{leak,max}$.

State-space model for leakage diagnosis

The aim of a state-space modeling is to put in evidence the structure of the system with respect to the state variable chosen. Starting from equation (3.1) is possible to express the model as follows

$$\begin{cases} \dot{x}(t) &= -a(x(t),z(t))x(t) - \psi(x(t),z(t))\theta(t) + \phi(x(t),z(t)) \\ y(t) &= x(t) \end{cases} \tag{3.4}$$

where the state $x(t) = p_{int}$ is scalar, $z \in \mathbb{R}^8$ is a vector containing the available measured variables (see TABLE 3.1 for details) and y stands for the measured output. Finally, θ is the parameter to be estimated that is, as explained before, the percentage of the maximal leak section (3.6) such that $\dot{m}_{Leak}(t) = \theta \cdot \psi(x(t), z(t))$. In the following $y(t)$ and $x(t)$ will be used without distinction. Moreover the following functions have been introduced

$$a(x(t),z(t)) = \alpha_{int}(z_2(t))\beta_{int}(z_2(t),z_7(t))\eta_v(x(t),z_7(t)) \tag{3.5}$$

$$\psi(x(t),z(t)) = \alpha_{int}(z_2(t))A_{leak,max}\frac{x(t)}{\sqrt{Rz_2(t)}}\sigma\left(\frac{z_8(t)}{x(t)}\right) \tag{3.6}$$

$$\phi(x(t),z(t)) = \alpha_{int}(z_2(t))(z_1(t) + \dot{m}_{egr}(z_2(t),z_3(t),z_5(t))) \tag{3.7}$$

where $\psi(x(t), z(t))$ is the gas mass flow rate through the hole when $A_{leak} = A_{leak,max}$,

Variable name	Meas. name	Description	Units
z_1	D_{air}	Mass air flow	[kg/s]
z_2	T_{int}	Intake temperature	[K]
z_3	p_{exh}	Exhaust pressure	[Pa]
z_4	T_{exh}	Exhaust temperature	[K]
z_5	u_{egr}	EGR valve position	[%]
z_6	u_{thr}	Throttle valve position	[%]
z_7	N_e	Engine speed	[rad/s]
z_8	p_{amb}	Ambient pressure	[Pa]

Table 3.1: Available measurements

$a(x(t), z(t))x(t)$ is the flow $\dot{m}_{asp}(t)$ aspirated by the engine and $\phi(x(t), z(t))$ stands to

sum of air and the EGR flow incoming in the intake manifold. For more details on the other variables, refer to Chapter 2 for a complete description of the models and hypothesis adopted.
As the intake pressure is measured, it is possible to inject $y(t)$ directly inside the equations (3.5),(3.6) and (3.7) in order to obtain three completely known functions of the available measurements.

The reference model for intake leak detection becomes

$$\begin{cases} \dot{x}(t) &= -a(t)x(t) - \psi(t)\theta(t) + \phi(t) \\ \dot{\theta}(t) &= 0 \\ y(t) &= x(t) \end{cases} \tag{3.8}$$

where a, ψ and ϕ, for notation simplicity, have been written as function of the time implying that they are completely known functions. Note that the original system model (3.1) has been extended with the additional equation $\dot{\theta} = 0$, which implicitly assumes that this parameter is constant or it varies very slowly in the time. This hypothesis is reasonable because it is possible to suppose that the leak formation is a step-like function of the time.
Moreover it is interesting to point out that, by means of the proposed hypothesis, the system (3.8) is a linear time-varying system with respect to the new state $[x(t)\ \theta(t)]$.

In the following of this chapter different types of adaptive observers will be used to estimate the leak diameter and used as residual term for the detection and identification of the fault.

Remark 3.1.

It is important to note that $\psi(\frac{p_{amb}}{p_{int}})$ is a positive differentiable bounded function (see section 2.4) and its derivative $\psi'(\cdot)$ is bounded too (provided $\frac{p_{out}}{p_{in}} \neq 1$). Same consideration can be done for the volumetric efficiency look-up table $\eta_v(p_{int}, N_e)$, which is a positive bounded function and its derivative $\eta_v'(\cdot)$ is bounded too (see section 2.2).

3.3 Observers

3.3.1 Adaptive - Lyapunov Based

The first adaptive observer is obtained by the analysis of a Lyapunov function in order to ensure the convergence of both the state and the parameter variable to the real values. Observers of this type have been widely used for different applications, some examples could be found in different fields of application [7, 8, 9, 17, 39], for more detail on the theory [4, 5, 28]. Consider the nonlinear adaptive observer:

$$\begin{cases} \dot{\hat{x}}(t) &= -a(t)\hat{x}(t) - \psi(t)\hat{\theta}(t) + \phi(t) + K_0(y(t) - \hat{x}(t)) \\ \dot{\hat{\theta}}(t) &= -\gamma\psi(t)(y(t) - \hat{x}(t)) \end{cases}$$

with positive constants γ and K_0. This observer, applied to the system under consideration, has the following properties:

i) The error signals $\tilde{x}$(t) and $\tilde{\theta}(t)$ are bounded

ii) $\lim_{t\to\infty} \tilde{x}(t) = 0$

iii) In addition, if $\lim_{t\to\infty} \psi(t) \neq 0$, then

$$\lim_{t\to\infty} \tilde{\theta}(t) = 0$$

The convergence rate of the state and parameter estimation can be tuned by the γ and K_0 gains.

Proof 3.1.

The first proposed observer is a Lyapunov-based designed. The proposed structure is:

$$\begin{cases} \dot{\hat{x}}(t) &= -a(t)\hat{x}(t) - \psi(t)\hat{\theta}(t) + \phi(t) + K_0(y(t) - \hat{x}(t)) \\ \dot{\hat{\theta}} &= \xi(t, \hat{x}(t)) \end{cases} \tag{3.9}$$

where $K_0 > 0$ is the gain influencing the pressure estimation convergence rate, and $\xi(t, \hat{x}(t))$ is the adaptation law to be designed. The error system equations in terms

of the error variables: $\tilde{x}(t) = x(t) - \hat{x}(t) = y(t) - \hat{x}(t)$ and $\tilde{\theta}(t) = \theta - \hat{\theta}(t)$ is:

$$\begin{aligned} \dot{\tilde{x}}(t) &= -a(t)\tilde{x}(t) - \psi(t)\tilde{\theta}(t) - K_0\tilde{x}(t) && (3.10) \\ \dot{\tilde{\theta}}(t) &= -\dot{\hat{\theta}}(t) = -\xi(t, \hat{x}(t)) && (3.11) \end{aligned}$$

Consider the following scalar Lyapunov function

$$V = V(\tilde{x}(t), \tilde{\theta}(t)) = \frac{1}{2}\tilde{x}^2(t) + \frac{1}{2\gamma}\tilde{\theta}^2(t)$$

Its time-derivative along the equation dynamics is given by

$$\dot{V} = -a(t)\tilde{x}^2(t) - K_0\tilde{x}^2(t) - \psi\tilde{\theta}(t)\tilde{x}(t) - \frac{1}{\gamma}\tilde{\theta}(t)\xi(t, \hat{x}(t))$$

If the adaptation law $\xi(t, \hat{x}(t))$ is designed to cancel the last two term in $\dot{V}$, i.e.,

$$\xi(t, \hat{x}(t)) = -\gamma\psi(t)\tilde{x}(t) = -\gamma\psi(t)(y(t) - \hat{x}(t)) \tag{3.12}$$

and moreover $a(t) > 0\ \forall t$ and a $K_0 > 0$ is choosen, then

$$\dot{V} = -(K_0 + a(t))\tilde{x}^2(t) \leq 0.$$

As, $V(\tilde{x}, \tilde{\theta})$ is a positive continuous function and $\dot{V} \leq 0$ then $V(\tilde{x}, \tilde{\theta})$ has a limit as $t \to \infty$. Moreover,

$$\begin{aligned} V(0) &\geq V(0) - V(\tilde{x}(t), \tilde{\theta}(t)) = -\textstyle\int_0^t \dot{V}(\tau)d\tau \\ &\geq (K_0)\textstyle\int_0^t \tilde{x}^2(\tau)d\tau \end{aligned} \tag{3.13}$$

where the last inequality holds because of (3.5) and (2.11),

$$0 \leq a(t) \leq a_M \tag{3.14}$$

and so $\tilde{x} \in L_2$. As $\tilde{x} \in L_\infty$ and $\tilde{\theta} \in L_\infty$ and for (3.10), (3.11) it is true that $\dot{\tilde{x}}(t) \in L_\infty$ and $\dot{\tilde{\theta}} \in L_\infty$.

By applying Barbalat's lemma [28] to $\tilde{x}$ it is possible to conclude that

$$\lim_{t\to\infty} \tilde{x}(t) = 0 \tag{3.15}$$

Thus, as $\dot{\tilde{x}}$ is uniformly continuous and bounded (cf. the remark 3.1) it is possible to apply again Barbalat's lemma showing that $\dot{\tilde{x}}(t) = 0$ as $t \to \infty$. From the error equation (3.10) the following limit holds

$$\lim_{t\to\infty} \psi(t)\tilde{\theta} = 0$$

Therefore, if

$$\lim_{t\to\infty} \psi(t) \neq 0 \tag{3.16}$$

also

$$\lim_{t\to\infty} \tilde{\theta}(t) = 0$$

It is important here to remark that the equilibrium point $[0, 0]^T$ is uniformly asymptotically stable: UAS [24].

However the dynamics are linear, applying the theorem 4.11 in [28], it is possible to conclude that $[\tilde{x}, \tilde{\theta}]^T$, if the observability condition (3.16) is fulfilled, are exponentially stable. In other words, $\exists(\tau_{int}, \lambda_{int}) \in (\mathbb{R}^+\backslash\{0\})^2$ s.t. $\forall t \in R^+$

$$|\tilde{x}(t)| \leq \tau_{int} e^{-\lambda_{int} t} \text{ and } |\tilde{\theta}(t)| \leq \tau_{int} e^{-\lambda_{int} t}$$

Remark 3.2.

Note that condition $\lim_{t\to\infty} \psi(t) \neq 0$ *is the observability condition, which is always fulfilled, unless the intake pressure approaches the ambient pressure. This situation may occur in two different ways:*

- *A large diameter hole appears in the receiver, leading to a decrease of the intake pressure until it reaches* p_{amb}.
- *For some engine operation points intake pressure is controlled to be close to* p_{amb}. *In this case observability condition for parameter* $\hat{\theta}$ *is weak.*

3.3.2 Modified Adaptive Observer

In the previous section an adaptive observer has been obtained from Lyapunov theory for the detection of a intake receiver hole. As mentioned previously, the condition under which the observer will converge is that the term $\psi(t)$ is different from zero, i.e., the leakage is observable.

This last remark suggests to use the observer only when the condition expressed in (3.16) is fulfilled. A possible way to integrate such behavior inside the observer is to integrate with respect to a new variable, function of the time: $\psi(t)$.

The proposed new observer has the following structure:

$$\begin{cases} \dfrac{d\hat{x}(t)}{dt} &= \phi(t) - a(t)\hat{x}(t) - \psi(t)\hat{\theta}_{leak}(t) + K_1\psi(t)\left(\tilde{x}(t) + \Sigma(t)\right) \\ \dfrac{d\hat{\theta(t)}}{dt} &= -K_\theta\alpha_{int}\psi(t)\left(\tilde{x}(t) + \Sigma(t)\right) \\ \dfrac{d\Sigma(t)}{dt} &= a(t)\tilde{x}(t) \end{cases} \tag{3.17}$$

and it can be shown that its convergence is uniformly asymptotically stable.

Remark 3.3.

In the rest of this document, in order to simplify the notation, the time dependency of the state $x(t)$, $\theta(t)$, $\Sigma(t)$ and the output variable $y(t)$ will be not written explicitly if not necessary for a better comprehension.

Proof 3.2.

The generic structure used for the observer is

$$\begin{cases} \dfrac{d\hat{x}}{dt} &= \phi(t) - a(t)\hat{x} - \psi(t)\hat{\theta}_{leak} + \beta(t) \\ \dfrac{d\hat{\theta}}{dt} &= \eta(t) \end{cases} \tag{3.18}$$

where $\beta(t)$ and $\eta(t)$ are two functions to be defined in order to insure the convergence of the observer. The error system is defined as follow

$$\begin{cases} \dfrac{d\tilde{x}}{dt} &= -a(t)\tilde{x} - \psi(t)\tilde{\theta}_{leak} - \beta(t) \\ \\ \dfrac{d\tilde{\theta}}{dt} &= -\eta(t) \end{cases} \tag{3.19}$$

where $\tilde{x}(t) = x(t) - \hat{x}(t)$ and $\tilde{\theta}(t) = \theta(t) - \hat{\theta}(t)$. As mentioned before, the aim of this new observer is to include the notion of the observability directly inside the integration time of the estimation, in order to satisfy such constraint a new variable is defined

$$s(t) = \int_0^t \psi(\tau)d\tau \tag{3.20}$$

where $\psi(t) > 0 \, \forall t \geq 0$, this condition is easily fulfilled in real Diesel engine operative points.

Remark 3.4.

Given two functions $x(t)$ and $s(t)$ such that

$$\frac{dx(t)}{dt} = f(x), \; s(t) = \int_0^t \psi(\tau)d\tau \tag{3.21}$$

it is possible to define

$$\hat{x}(s(t)) = x(t) \Leftrightarrow \hat{x}(s) = x(t(s)) \tag{3.22}$$

whose derivative is

$$\frac{d\hat{x}}{ds} = \frac{dx}{dt}\frac{dt}{ds} = \frac{f(x(t))}{\psi(t)} = \frac{f(\hat{x}(s))}{\psi(t(s))} \tag{3.23}$$

where we used

$$\frac{ds}{dt} = \psi(t) \tag{3.24}$$

.

Defining

$$\mu(t) = \tilde{x}(t) + \int_0^t a(\tau)\tilde{x}(\tau)d\tau \tag{3.25}$$

it is possible to write the system (3.19)

$$\begin{cases} \dfrac{d\mu(t)}{dt} &= -\psi(t)\tilde{\theta} - \beta(t) \\ \\ \dfrac{d\tilde{\theta}(t)}{dt} &= -\eta(t) \end{cases} \tag{3.26}$$

By using the equation (3.20) and by the Remark 3.4 is possible to rewrite the system (3.26) with respect the new variable $s(t)$

$$\begin{cases} \dfrac{d\mu(t(s))}{ds} &= \dfrac{1}{\psi(t)}\left(-\psi(t)\tilde{\theta} - \beta(t)\right) \\ \\ \dfrac{d\tilde{\theta}(t(s))}{ds} &= -\eta(t)\dfrac{1}{\psi(t)} \end{cases} \tag{3.27}$$

by defining $\beta(t) = \psi(t)\bar{\beta}(t)$ and $\eta(t) = \psi(t)\bar{\eta}(t)$, the system (3.26) can be written as function of $s(t)$ which is still a function of the time, as follow

$$\begin{cases} \dfrac{d\mu(t(s))}{ds} &= -\tilde{\theta} - \bar{\beta}(t) \\ \\ \dfrac{d\tilde{\theta}(t(s))}{ds} &= -\bar{\eta}(t) \end{cases} \tag{3.28}$$

To choose the $\bar{\eta}(t)$ and $\bar{\beta}(t)$ function, a Lyapunov-based design is applied (as already used in the Proof 3.1).

The candidate Lyapunov function is

$$V = V(\mu(t(s)), \tilde{\theta}(t(s)) = \frac{1}{2}\mu^2 + \frac{1}{2K_\theta}\tilde{\theta}^2 \tag{3.29}$$

where K_θ is a positive tuning constant to be defined. Evaluating the derivative of V along the system trajectory (3.28) leads to

$$\begin{aligned} \frac{dV}{ds} &= \mu\dot{\mu} + \frac{1}{K_\theta}\tilde{\theta}\dot{\tilde{\theta}} \\ &= \mu \cdot (-\tilde{\theta} - \bar{\beta}(t)) - \frac{1}{K_\theta}\tilde{\theta}\bar{\eta}(t) \\ &= -(\mu + \frac{1}{K_\theta}\bar{\eta}(t))\tilde{\theta} - \mu\bar{\beta}(t) \end{aligned} \tag{3.30}$$

in order to guarantee the semi-negativeness of the Lyapunov function,

$$\bar{\eta}(t) = -K_\theta \mu \tag{3.31}$$

$$\bar{\beta}(t) = K_1 \mu \tag{3.32}$$

where K_1 and K_θ are two positive tuning constants. By this choice, the equation (3.30) becomes

$$\begin{aligned} \frac{dV}{ds} &= -(\mu + \frac{1}{K_\theta}\bar{\eta}(t))\tilde{\theta} - \mu\bar{\beta}(t) \\ &= -K_1\mu^2 \leq 0 \end{aligned} \tag{3.33}$$

The (3.33) shows that $\dot{V}$ is semi-defined negative, it is only possible to conclude that $\mu \in L_2$. By the same analysis made in Proof 3.1 it is possible to show the convergence of $[\mu, \tilde{\theta}]^T \to 0$ as $t \to 0$. Hence the adaptive observer for the system (3.28) is

$$\begin{cases} \dfrac{d\mu(t(s))}{ds} = -\tilde{\theta}(t) - K_1\mu(t) \\ \\ \dfrac{d\tilde{\theta}(t(s))}{ds} = K_\theta\mu(t) \end{cases} \tag{3.34}$$

Starting from the left hand side of 3.34 by appling the derivation chain rule and using the equations 3.20 and 3.25

$$\begin{cases} \dfrac{d\mu(t(s))}{ds} = \dfrac{d\mu(t)}{dt}\cdot\dfrac{dt}{ds(t)} = \left(\dot{\tilde{x}}(t) + a(t)\tilde{x}(t)\right)\cdot\dfrac{1}{\psi(t)} \\ \\ \dfrac{d\tilde{\theta}(t(s))}{ds} = \dfrac{d\tilde{\theta}(t)}{ds(t)}\cdot\dfrac{dt}{ds(t)} = \dfrac{d\tilde{\theta}(t)}{dt}\cdot\dfrac{1}{\psi(t)} \end{cases} \tag{3.35}$$

combining the two previous equation systems and taking into the account that $\dot{\tilde{\theta}}(t) = -\hat{\theta}(t)$, it is possible to write the new system as follow

$$\begin{cases} \dfrac{d\tilde{x}(t)}{dt} = -a(t)\tilde{x} - \psi(t)\tilde{\theta} - \psi(t)K_1\left(\tilde{x} + \displaystyle\int_0^t a(\tau)\tilde{x}(\tau)d\tau\right) \\ \\ \dfrac{d\tilde{\theta}(t)}{dt} = K_\theta\psi(t)\left(\tilde{x} + \displaystyle\int_0^t a(\tau)\tilde{x}(\tau)d\tau\right) \end{cases} \tag{3.36}$$

By defining an additional state $\Sigma(t) = \int_0^t a(\tau)\tilde{x}(\tau)d\tau$ and by remember the state error definition $\tilde{x} = x - \hat{x}$ and $\tilde{\theta} = \theta - \hat{\theta}$ the observer (3.36) becomes (3.17).

3.3.3 Zhang Observer

In the very beginning of this work on the leakage detection, an observer developed by Zhang [46] was used as benchmark because of its exponential convergence. Even if the observer presented before (see section 3.3.1), due to the linearity, has the same convergence property it is interesting to show the different approach used by the author.

Zhang observer design

The general system class considered by Zhang [46] comprises state-affine nonlinear systems. In particular, given a system of the form

$$\begin{cases} \dot{x} &= -a(t)x + \psi(t)\theta + \phi(t) \\ \dot{\theta} &= 0 \\ y &= c(t)x \end{cases} \tag{3.37}$$

which are particularized here to scalar signals, it is possible to design an *exponentially convergent* adaptive observer to jointly estimate x and θ under the persistent excitation conditions given next.

Assumption 3.1.

Assume that the pair $(a(t), c(t))$ in system (3.37) is such that a bounded time-varying gain $K_Z(t)$ exists so that the system

$$\dot{\eta} = [a(t) - K_Z(t)c(t)]\eta \tag{3.38}$$

is globally exponentially stable.

Assumption 3.2.

Let $\Gamma(t)$ be a function generated by the ODE system

$$\dot{\Gamma} = [a(t) - K_Z(t)c(t)]\Gamma + \psi(t) \tag{3.39}$$

Assume the $\psi(t)$ is persistently exciting (PE) so that two positive constants δ, T exists such that $\forall t > 0$ the following inequality holds

$$\int_t^{t+T} |\Gamma(\tau)c(\tau)|d\tau \geq \delta I \tag{3.40}$$

Under these assumptions the following theorem is stated

Theorem 3.1.

[46] Let $\Lambda > 0$ be any positive gain. Under Assumption 3.1 and 3.2 and for constant θ, the ODE system

$$\begin{cases} \dot{\hat{x}} &= a(t)\hat{x} + \psi(t)\hat{\theta} + \phi(t) + [K(t) + \Lambda\Gamma^2 c(t)][y - c(t)\hat{x}] \\ \dot{\hat{\theta}} &= \Lambda\Gamma c(t)[y - c(t)\hat{x}] \\ \dot{\Gamma} &= [a(t) - K_Z(t)c(t)]\Gamma + \psi(t) \end{cases} \tag{3.41}$$

is a global exponential adaptive observer for system (3.37), i.e. for any initial conditions the observation errors $\hat{x}(t) - x(t)$ and $\hat{\theta}(t) - \theta$ tend to zero exponentially fast when $t \to \infty$

Application to the intake receiver

Zhang's observer seems to deal perfectly with the issue of the joint estimation of the intake pressure and the leak hole diameter. If the observer in equation (3.41) is specifically suited for the system (3.8)

$$\begin{cases} \dot{\hat{x}} &= -a(t)\hat{x} + \phi(t) - \psi(t)\hat{\theta} + (K_Z + \Lambda\Gamma^2)[y - \hat{x}] \\ \dot{\hat{\theta}} &= \Lambda\Gamma[y - \hat{x}] \\ \dot{\Gamma} &= -[a(t) + K_Z]\Gamma - \psi(t) \end{cases} \tag{3.42}$$

where Λ is a tuning gain. In the following assumptions (3.1) and (3.2) are correctly checked.

Assumption 3.1 is always verified: the volumetric efficiency is always a positive quantity and thus the aspiration process is inherently stable. Therefore, it suffices that

$K(t) > -a(t)\ \forall t$ to satisfy Assumption 3.1. For instance, a constant $K(t) = K_Z > 0$ can be found or, as proposed in [46] an optimal Kalman filter gain can be used as well.

Assumption 3.2, as already discussed (Remark 3.2), is on persistent excitation condition of leakage function $\psi(t)$ which depends on the valve pressure ratio across the valve. As $\psi(t)$ represents the maximal leakage flow for each operation condition, then $\psi(t)$ is equal to zero only if the intake pressure reaches the ambient pressure. In the next section it will be shown how the estimation of θ can be physically difficult or even impossible for some specific engine operative points, where intake pressure is close to ambient pressure. This is a generic condition for this physical system (observability condition), that is independent of the observer design.

As it has been detailed in the observer design of section 3.1, if the PE condition is not satisfied, $\tilde{\theta}$ can not be ensured to tend to zero, although the prediction error $\tilde{x}$ does.

3.3.4 Comparison

The three presented observers have different structures and their nonlinear nature do not allow an easy analytical comparison. Moreover due to the nature of the system under analysis, i.e. the intake manifold, and the magnitude of the signals used it is particularly not evident to emphasise the differences, if any, in simulation.
A first attempt to compare the Lyapounov observer with the one suggested by Zhang was the subject of [10] and a simulation of the parameter estimation is reported in figure 3.3. The results of this comparison was that any major difference between the two observers was visible also for the above explained reasons.
A more detailed qualitative analysis between the two proposed observers has been done and reported in Annex B.
The key difference is that the modified observer, due to its peculiar structure is faster than the Lypounov one and more robust to the system output disturbances (noise and spikes).

3.3.5 Observability condition

The model based approach to leak detection, as already argued in previous chapters, is a good strategy because it allows, by means of dynamical observers, to have a direct estimation of the fault based on the physics of the engine. As pointed out for all the observers presented, the *persistent excitation condition* must be fulfilled:

two positive constants δ, T exists such that $\forall t > 0$ the following inequality holds

$$\exists \delta,\ T \forall t > 0,\ \text{such that}\ \int_{t}^{t+T} |\psi(t)| d\tau \geq \delta \tag{3.43}$$

The above condition means that the observers will converge to the real leak diameter if the leakage has an impact on the intake manifold pressure dynamics. The reasons why the $\psi(t)$ term can go to zero can be different and were already discussed in the remark 3.2.

The study of this condition is important for the determination of the operating zone in which our fault detection and identification is reliable.

In the next of this section different load trajectories will be analyzed with respect to the condition (3.43). The function (3.6), $\psi(t)$, can go to zero only if $\sigma\left(p_{amb}/p_{int}\right)$ goes to zero as well, i.e. $p_r = 1$ (see figure 2.6). For this reason the study of the pressure ratio $p_r = p_{amb}/p_{int}$ is equivalent to the study of $\psi(t)$.

In figure 3.1 the evolution of p_r is shown during a load transient when there is not any leak on the intake receiver. It is interesting to notice that the pressure ratio, for some operating points, is close to one: this implies that $\psi(t) \approx 0$. These operative conditions imply that the observer might not converge to the real value. In particular, with reference to the figure 3.1 the leak pressure ratio p_r and so the $\psi(t)$ term is very close to the unit when the engine load is under the 6 *bar* of IMEP. The worst case is in the interval [60, 70] seconds, in which $p_r = 0.97$ (2 bar of IMEP).

Another important scenario to be analyzed is the urban driving cycle ECE (figure 3.2(b)), which is a part of a cycle used for emission certification of light duty vehicles in Europe. As depicted in figure 3.2(a) the $\psi(t)$ term is almost the time close to the unit, i.e. $p_r \geq 0.9$ and the period in which there are good condition for leak detection are during the acceleration, in particular during the period between 120 s and 140 s. The interest of checking the strategy on the urban driving cycle is that, for FDI task,

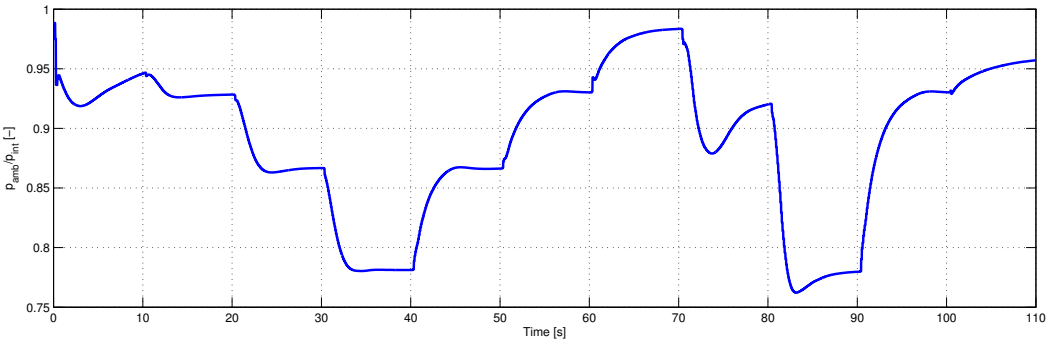

(a) p_{amb}/p_{int}

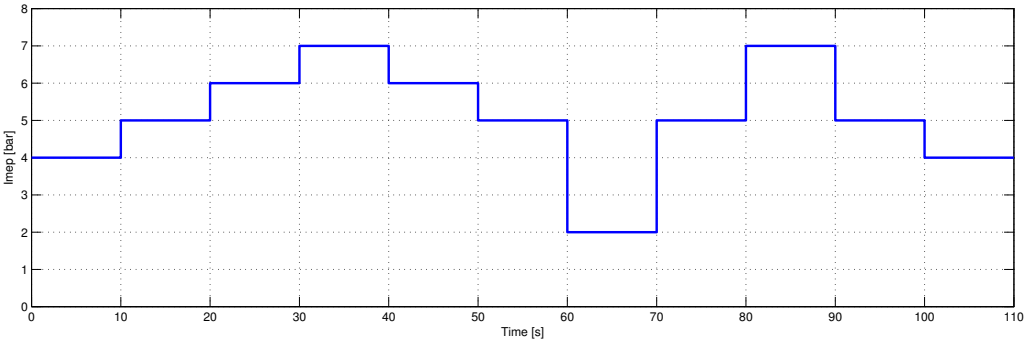

(b) IMEP trajectory

Figure 3.1: The observability condition measured (a) along a load trajectory (b) at 1500 rpm

represents a very difficult scenario, because there is not good observability condition and it is almost in presence of the gas recirculation. Moreover the European legislation certificates the FDI strategies on this cycle.
To conclude this section, it is important to note that the convergence speed of the observer is related on the observability condition, so for small value of the term $\phi(t)$, the time needed to the adaptive observer to settle can be long.

3.4 Threshold & Decision

Once the residual term is generated by the observers presented above, the next problem is how to determine when a fault occurs, in other words: *the problem of detection.*

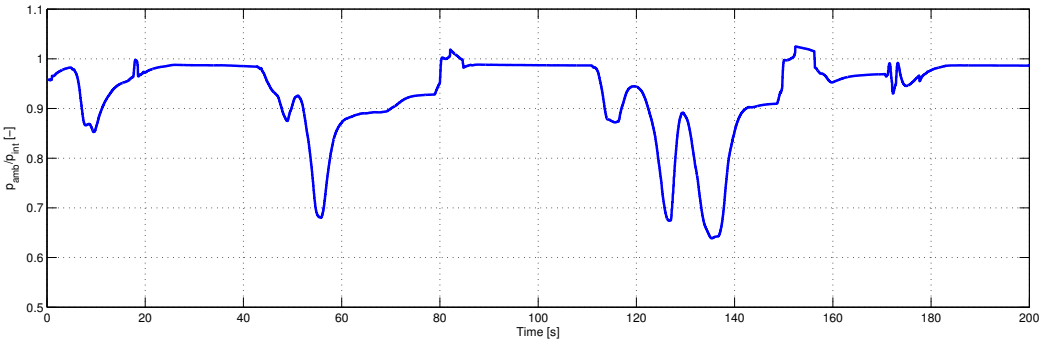

(a) p_{amb}/p_{int}

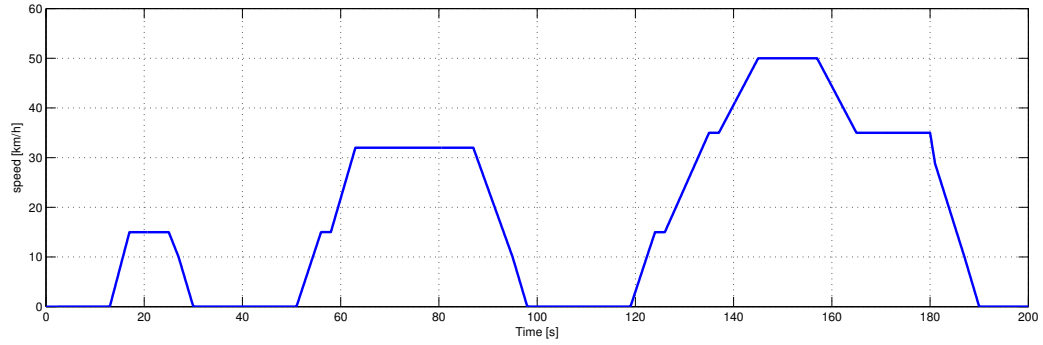

(b) ECE speed set-points

Figure 3.2: The observability condition measured along a urban driving cycle - ECE.

Different ways to design detection strategy can be found in literature ([16, 26, 34]) but these are all based on a threshold checking technique. The major issue is the design of threshold that avoids as much as possible false alarms and meanwhile allows the detection of small amplitude faults.

The aim of this section it to present a *dynamical model-based threshold* which allows to reduce the calibration time and, during the design phase, to better understand which are the critical sensors for the fault estimation accuracy.

3.4.1 Fixed Threshold

The first class of considered signal used for checking the presence of a fault are the so called “fixed thresholds". This class of thresholds are generally based on some heuristic

knowledge of the parameter or on large databases which provide a good estimation of the variance of the residual term.

The main drawback of this approach is that the obtained threshold is static for all the operative conditions and therefore can be conservative with respect to the sensitivity of the detection.

For the leak detection problem different tests, in simulation, have been made to deter-

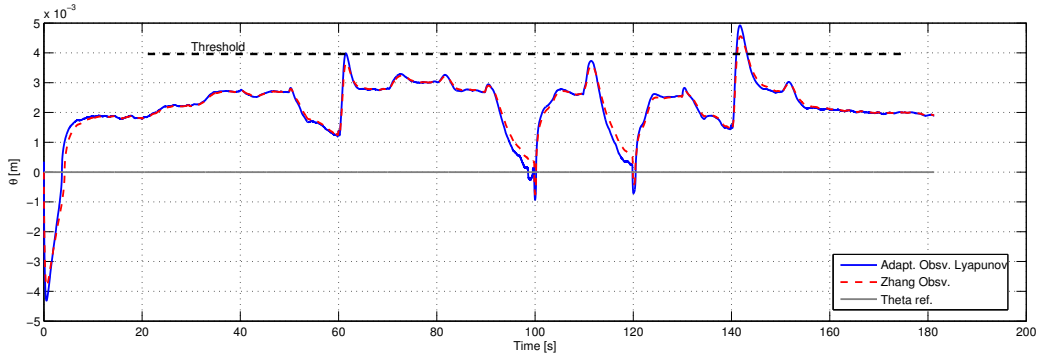

Figure 3.3: Fixed threshold determination. Lyapunov based and Zhang observer θ estimation during a simulation with a varying load.

mine the maximum variance of the residual θ estimated by the observer when no leak was present on the intake manifold. To give a more physical interpretation, the variance in the estimation can have different sources:

- model approximations: when the equations used in the observer are not always representative of the reality. For instance the EGR circuit is approximated with a simple flow through a valve (see section 2.4);
- observability condition, i.e., $\phi(t) \approx 0$ (see section 3.3.5) ;
- sensors biases and drifts: the sensors biased measurements are used to feed the observer yielding a biased estimation.

In figure 3.3 two different types of observers, the Lyapunov-based and Zhang's, have been used to estimate the hole diameter during a load trajectory in simulation to determine the variance of the estimated parameter. It appears that a possible choice of the fixed threshold is 4 mm, which means that leaks under this value cannot be detected.

3.4.2 Sensitivity-based Threshold

In this section, first it will be shown how the observability condition and possible errors can be taken into account during the design of the variable threshold then, an upper bound for two classes of modeling errors are provided: sensors measurement bias and the use of a faulty measure for estimate a mass flow by the equation (2.12).

3.4.3 Observer Sensitivity Analysis

Consider a general observer with the same structure as (3.9)

$$\begin{cases} \dot{\hat{x}} &= f(\hat{x}, z, y) + \psi(z, y)\hat{\theta} + \phi(z, y) + K_0\tilde{x} \\ \dot{\hat{\theta}} &= g(z, y)\tilde{x} \end{cases} \tag{3.44}$$

where, for analogy, $f(\hat{x}, z, y) = a(t)\hat{x}$ and $g(z, y) = -\gamma\psi(t)$.
As (3.8) is a stable system, the observer can be studied in stationary conditions. By this hypothesis (3.44) becomes

$$0 = f(\hat{x}, z, y) + \psi(z, y)\hat{\theta} + \phi(z, y) \tag{3.45}$$

where $\hat{\theta}$, in ideal case, is equal to

$$\hat{\theta} = -\frac{1}{\psi(z, y)}[f(\hat{x}, z, y) + \phi(z, y)] \tag{3.46}$$

As already discussed, the $\psi(z, y)$ term acts on convergence speed rate of the parameter. If $\psi(z, y) \neq 0$, it acts on final value of estimated parameter.

The result (3.46) is obtained if a perfect matching model of the system is used. In real case, equation (3.45) writes

$$\begin{aligned} 0 = \quad & f(\hat{x}, z^*, y^*) + \Delta f(\hat{x}, z^*, y^*) \\ & +\psi(z^*, y^*)\hat{\theta} + \phi(z^*, y^*) \\ & +\phi(z^* + \Delta z, y^*) \end{aligned} \tag{3.47}$$

where the symbol $*$ stands for the correct value of a measure or parameter and $\hat{\theta} = \theta^* + \Delta\theta$. The symbol Δ has to be considered as a small perturbation with respect to the correct function it refers to. In details the equation (3.47) shows different error types:

- $\Delta f(\hat{x}, z^*, y^*)$ stands for modeling error terms;

- $\phi(z^* + \Delta z, y^*)$ stands for terms correctly modeled but evaluated with a measure affected by errors;

- $\Delta\theta$ stands for the parameter estimation error;

The $\Delta\theta$ term represents the error made by the estimation, due to modeling and measurement errors. By (3.46) and neglecting the second order term, equation (3.47) becomes

$$\Delta\theta = -\frac{1}{\psi(z^*, y^*)}[\Delta f(\hat{x}, z^*, y^*) + \phi(z^* + \Delta z, y^*)] \tag{3.48}$$

which points out the effect of every error terms on the correct estimation of the hole's diameter. The idea, for the threshold design, is to find an upper bound to each error term of equation (3.48).

3.4.4 Error Models

With respect to the intake leakage detection problem, two different types of error are considered.

First error type

Consider $\xi \in \mathbb{R}$, the first class of considered errors is

$$\xi = \xi^* + \Delta\xi \tag{3.49}$$

An upper bound for $\Delta\xi$ is the object of the two following propositions.

Proposition 3.1.

Consider a scalar bounded variable $\epsilon(t)$ such that $|\epsilon(t)| \leq M_\epsilon$ with $M_\epsilon > 0$ then, if

$$\Delta\xi = \epsilon(t) \tag{3.50}$$

then

$$|\Delta\xi| \leq M_\epsilon \tag{3.51}$$

Proposition 3.2.

Consider a scalar bounded variable $\alpha(t)$ *such that* $|\frac{\alpha(t)}{1+\alpha(t)}| < M_\alpha$ *with* $M_\alpha > 0$. *If*

$$\Delta\xi = \alpha(t) \cdot \xi^* \tag{3.52}$$

then

$$|\Delta\xi| < M_\alpha|\xi| \tag{3.53}$$

Proof. From (3.49) and (3.52) holds

$$\xi^* = \frac{1}{1+\alpha}\xi \tag{3.54}$$

then, $\Delta\xi$ becames

$$\Delta\xi = \frac{\alpha}{1+\alpha}\xi \tag{3.55}$$

by moving to the absolute values and considering the assumption on α, it is possible to write

$$|\Delta\xi| < M_\alpha|\xi| \tag{3.56}$$

□

Second error type

Consider a scalar function $h : D \to \mathbb{R}$ and $\xi \in \mathbb{R}$ as defined in (3.49), the error considered here are of the type

$$h(\xi) = h(\xi^*) + \Delta h(\xi) \tag{3.57}$$

where a function is evaluated by using a biased variable of the type expressed in (3.50). The aim of the following proposition is to find an upper bound to $|\Delta h(\xi)|$.

Proposition 3.3.

Consider a scalar function $h : D \to \mathbb{R}$ *satisfying*

$$\begin{aligned} h(\xi) &\geq 0 \\ h'(\xi) &> 0 \\ h''(\xi) &< 0 \end{aligned} \tag{3.58}$$

and $\xi = \xi^* + \epsilon(t)$ *with* $|\epsilon(t)| \leq M_\epsilon$*, then an upper bound for the estimation error is*

$$|\Delta h(\xi)| \leq |h'(\xi - M_\epsilon)| M_\epsilon \tag{3.59}$$

Proof. From (3.49), (3.58), the following inequality holds

$$\Delta h(\xi) \leq h'(\xi^*) \Delta\xi \tag{3.60}$$

by the means of the hyphotesis on $h'(\xi) > 0$, it is possible to write the previous inequality with modules as

$$|\Delta h(\xi)| \leq |h'(\xi^*)| M_\epsilon \tag{3.61}$$

This last inequality is always true if ξ^* is known in order to evaluate the function first derivative. The only available measure is $\xi = \xi^* + \epsilon(t)$, so an estimation of an upper bound of $h'(\xi^*)$ is provided.
It is true that $\forall \xi \in D$, $\xi - M_\epsilon \leq \xi^*$. As $|h'(\xi^*)|$ is a positive decreasing function, it follows

$$|h'(\xi - M_\epsilon)| \geq |h'(\xi^*)| \tag{3.62}$$

This lead to prove that

$$|\Delta h(\xi)| \leq |h'(\xi - M_\epsilon)| M_\epsilon \tag{3.63}$$

□

3.4.5 Variable Threshold Design

The variable threshold is designed in order to be an upper bound to the $|\Delta\theta|$ appearing in (3.48).

For the particular application, i.e., intake leakage detection, model errors have been related to the first type of error (3.50). For example, the $\Delta f(\hat{x}, z^*, y^*)$, which represents the engine aspirated gas, is modeled as a constant bounded error, i.e., $\Delta f(\hat{x}, z^*, y^*) = \epsilon_{asp}(t)$, where $||\Delta f(\hat{x}, z^*, y^*)||_\infty = M_{asp}$.
Terms like $\phi(z^* + \Delta z, y^*)$ can be modeled by (3.57). With respect to studied system, such kind of term models the error due to the evaluation of EGR flow using (2.12) when the variable z_3 (Table 3.1) is affected by a bounded additive error, ϵ_{exh}, of the type discussed in Proposition 3.1 .
For the air mass flow sensor (MAF) it was modeled as an error of the first type with a multiplicative bias, as explained in Proposition 3.2, where the positive constant M_{air} is chose as the max tolerance provided by the manufacturer .

In conclusion the proposed threshold is

$$\theta_{th} = \frac{1}{\psi(z^*, y^*)} \left(M_{asp}|\dot{m}_{asp}| + M_{air}|z_1| + \left| \frac{\partial}{\partial z_3} \dot{m}_{egr}(z_3 - M_{exh}) \right| M_{exh} \right) \tag{3.64}$$

3.5 Experimental Results

The presented work for leak detection in the intake manifold has been tested in simulation and experimentally. The aim of this section is to show, with real data, the results obtained on a engine testbed available at the IFP (more details on the experimental setup can be found in the Appendix A).

Fixed threshold In order to confirm what obtained in simulations and theoretically in the previous sections of this chapter, the Figure 3.5 shows different leak diameter estimation, i.e. $\hat{\theta}(t)$, obtained from the Lyapunov design observer (in section 3.3.1) at different operating conditions: three different engine speeds and for each of them a load trajectory (Fig 3.4) has been imposed to the system.
These first results show that when any leak is present on the manifold surface the observer estimation varies in a range below of 4 mm, which was the variability already observed for choosing the fixed threshold. This variability is due two major causes: the presence of the exhaust gas recirculation, which is estimated and therefore introduces

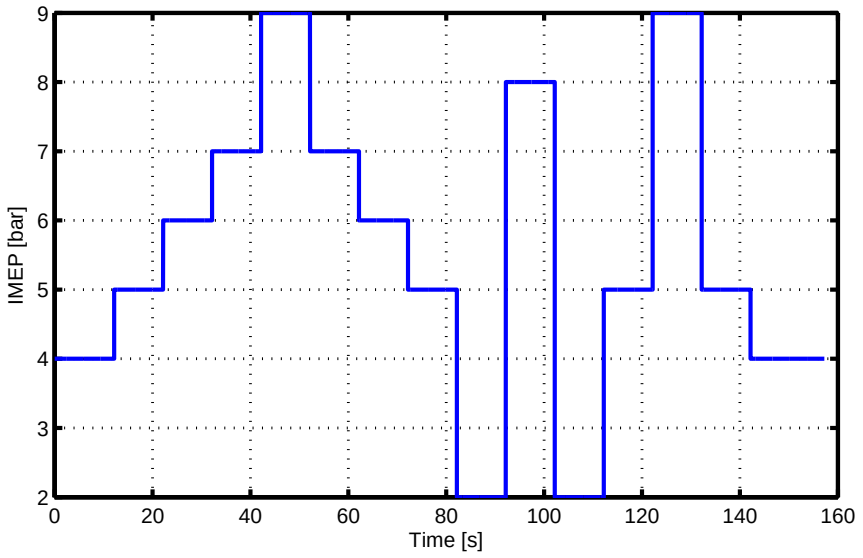

Figure 3.4: Imposed IMEP trajectory for experimental test

some errors due to the qualities of the calibrated model and the lack of the observability condition, i.e. $\psi(t) \approx 0$.

The Figures 3.5(a), 3.5(c) and 3.5(e) depict the leak diameter estimation at 1500 rpm, 2000 rpm and 2500 rpm respectively. It is important here to point out that, at these three different engine speeds, the pressure ratio across the intake manifold and the ambient air pressure is very different. This ratio is, as already argued before in the observability condition section, strictly related to the convergence speed and estimation quality of the observer. It is easy to see how for very low torque demand and low engine speed, corresponding here to a very bad condition (see Fig 3.5(b), the pressure ratio can reach the 0.96, in other word, in case of leakage the delta pressure between inside and outside the intake manifold would be really poor and so the leak estimation will be badly conditioned. Increasing the engine speed up to higher operating conditions has a benefit effect on the pressure ratio as shown in Figures 3.5(d) and 3.5(f). The effect is clearly visible in the corresponding estimation (Figures 3.5(c) and 3.5(e)) is closer to the real value, in that case zero. A last comment on Fig 3.5(e)) that shows negative values of theta. The shown data are raw on purpose for evaluating the observer performances and strategies, so in this particular case the negative values of the estimation are physically unfeasible, i.e. a negative diameter, the suggestion here is to reduce the

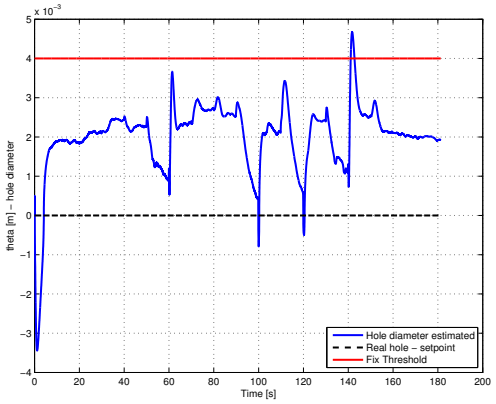

(a) Estimation without leak @1500 rpm

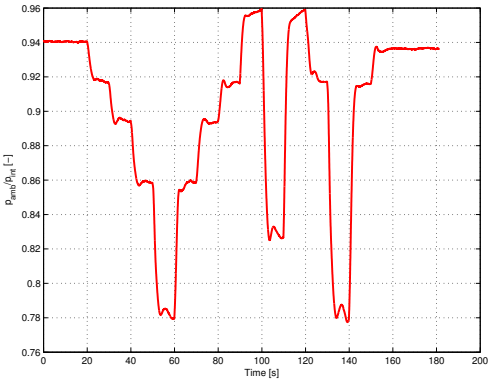

(b) Pressure Ratio across the manifold @1500 rpm

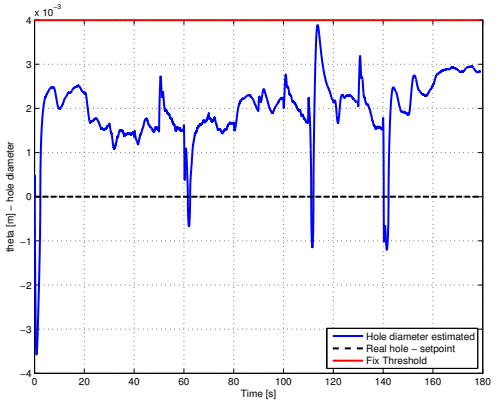

(c) Estimation without leak @2000 rpm

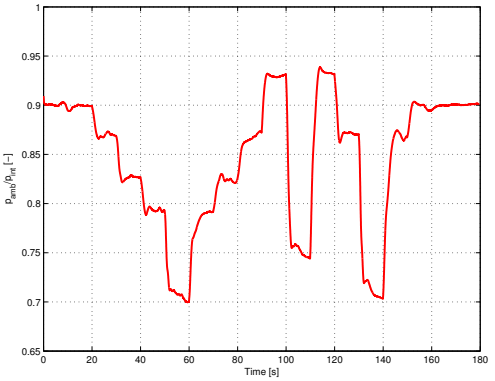

(d) Pressure Ratio across the manifold @2000 rpm

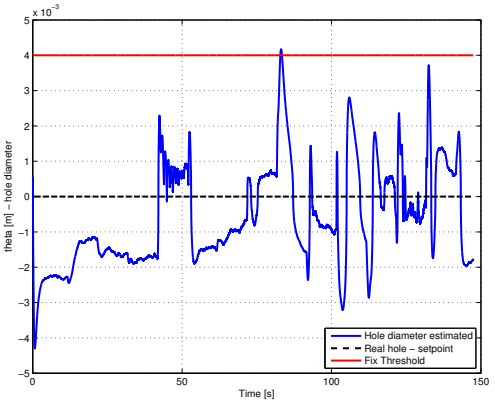

(e) Estimation without leak @2500 rpm

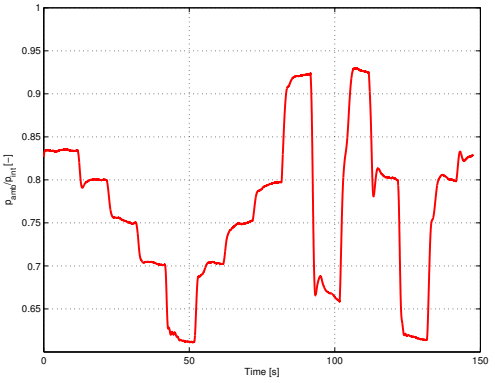

(f) Pressure Ratio across the manifold @2500 rpm

Figure 3.5: Experimental Results G9T NADI - Leak diameter estimation at different engine speeds along a torque trajectory

observer gains or applying a post filtering stage to the strategy in order to smooth the estimation against a lack of responsiveness of the fault detection.
Regarding the threshold choice, the experimental results show that 4 mm detection limit is a good choice but as explained before, the presence of a drift in the measurement or a bias in the sensors outcome must be take into the account. Moreover, setting a threshold to 4 mm eliminate the possibility *a priori* of detecting smaller leak hole that could, under specific working condition, be detected.

The second series of figures show the experimental results when a $5mm$ diameter leak is caused, by the mean of a valve, in the intake manifold. Figures 3.6(a), 3.6(c) and 3.6(e) show how the estimation is performed for different operating condition. As already spotted previously an increase in the engine speed leads to a better estimation precision of the EGR flow and a faster convergence of the estimation (see the pressure ratio on the right column - Fig 3.6(b), Fig 3.6(d) and Fig 3.6(f)): when the pressure ratio across the orifice is far from the unit the leak hole diameter estimation becomes more accurate.

Variable threshold In the previous paragraph, the observer performances for leak diameter estimation in the intake manifold have been shown with respect to a fixed threshold, which is a fast and accurate way if a good population of experimental data is available in order to set its level. The main drawback is that, if the detection algorithm should work in very different operating conditions, the threshold risks to be conservative (high value) in order to be robust to different sensors and measurements tolerance and models accuracy: this is almost required in order to reduce the number of possible false alarms.
In section 3.4.5, after modelling the possible error that could lead to an erroneous estimation, a variable threshold has been proposed and here applied in a real operating condition.
In the proposed sensitivity analysis, three different sources of error have been considered: possible additive biases in the exhaust pressure measurement, multiplicative biases in the mass air flow sensor that represent a good model of the sensor drift in time

and finally some multiplicative bias on the engine efficiency map due to experimental uncertainties.
In order to choose representative values for these error, the sensors datasheet 3σ production variabilities have been considered for each of the previously presented biases.
A summary of the used measurement and their maximum errors (3σ) is reported in Table 3.2.

Name	Max Δ	Unit
p_{int}	0	Pa
T_{int}	0	K
p_{exh}	$200e2$	Pa
MAF	5	%
η_v	5	%
p_{amb}	0	Pa

Table 3.2: Available measurements and maximum possible error considered (3σ)

All the further results are from test performed at 2000 rpm because it is a representative operating condition for an engine and allows to show significant results without doing a full campaign of tests and also because the effects of engine speeds on the estimation has been fully characterised in the previous paragraph.

The first set of results presented are about the leak estimation (Fig 3.7(a)) when a variable threshold is used considering a $M_{air} = 5\%$ and a $M_{asp} = 5\%$ and no EGR flow is allowed. The reason of this test is to validate the uncertainty of the engine efficiency map and to show how the variable threshold even in presence of these uncertainties is robust and avoids false detections (compared with the fixed threshold presented before, in that case a leak will be detected just for the mass air flow drift). Figure 3.7(b) reports the pressure ratio between the ambient air and the intake manifold to show how the concept of a diminishing observability is reflected in an increase of the threshold level: particular evident in the time intervals from 80 to 90 seconds and from 100 and 110 seconds. Once the validation and an eventual calibration of the threshold is done when no exhaust gas recirculation is present in the system, the EGR valve has been activated

in the engine combustion control supervisor. The fault detection results, in presence of EGR gases, are reported in Fig 3.8 when no hole is present - Fig 3.8(a) - and when a 5 mm diameter hole is produced on the intake manifold surface by the mean of a controlled valve - Fig 3.8(b) In both the tests the previous biases (M_{air} and M_{asp}) have not been removed.
What it is interesting to point out from those plots is:

- the threshold shape has changed between before and after the leak was generated. The fact that the threshold is more constant is due to the leak itself, in fact the presence of the leakage acts as a pressure regulator, i.e. a change in the torque demand (IMEP) correspond into a intake pressure change that will cause an increasing or decreasing leakage flow.

- as already presented, in very poor operating conditions, the threshold is over the estimation telling that in that intervals the estimation could be very slow to converge and badly conditioned and so it is better to not consider the estimation in those region.

To conclude a worst case scenario has been tested by adding a 200 mbar additive bias to the exhaust pressure measurement. The results are reported in Fig 3.9.

The proposed method relies on the sensitivity study of the estimation with respect to possible biases in the measurements. In order to bound the error, the threshold is designed with the maximum of each uncertainty which, if not completely known, can lead to a very conservative threshold. This means that the fault can be detected only for very high amplitudes. However, the use of the sensitivity allows to understand which is the impact of each sensor bias or drift and so use this analysis to choose the best sensor. In the next chapter the efficiency loss detection for a turbine is presented and a complete study of the sensitivity is shown. In particular it will be presented in details other possible use of this analysis to understand which are the best operating point to use the strategy in safest way.

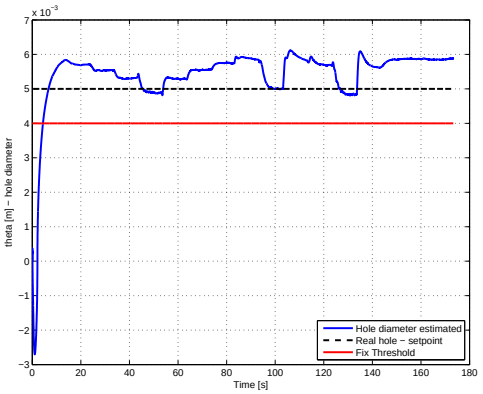

(a) 5mm Leak estimation @1500 rpm

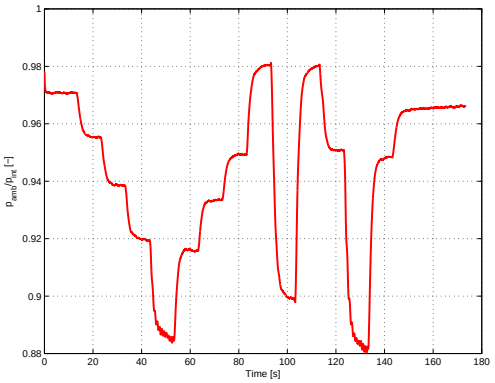

(b) Pressure Ratio across the hole @1500 rpm

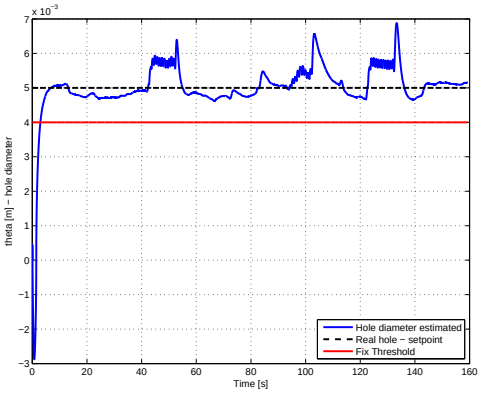

(c) 5mm Leak estimation @2000 rpm

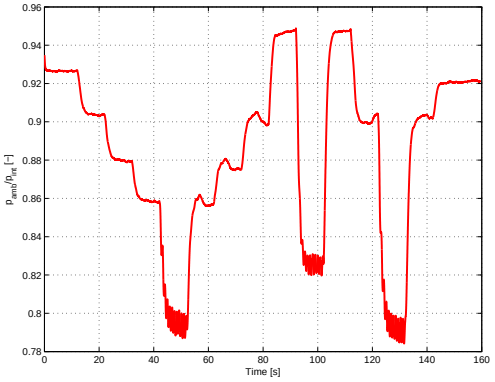

(d) Pressure Ratio across the hole @2000 rpm

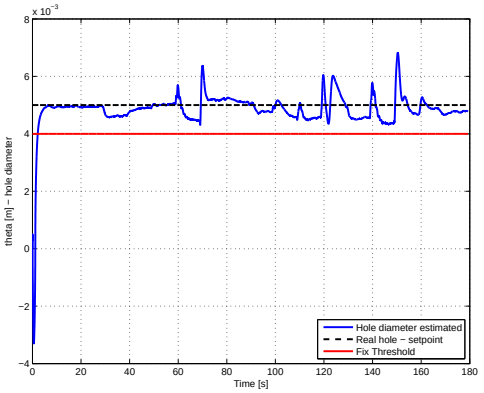

(e) 5mm Leak estimation @2500 rpm

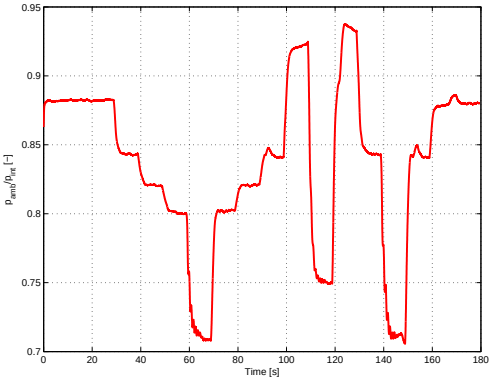

(f) Pressure Ratio across the hole @2500 rpm

Figure 3.6: Experimental Results G9T NADI - Leak diameter estimation when a 5mm diameter hole is present on the intake manifold at different engine speeds along a torque trajectory

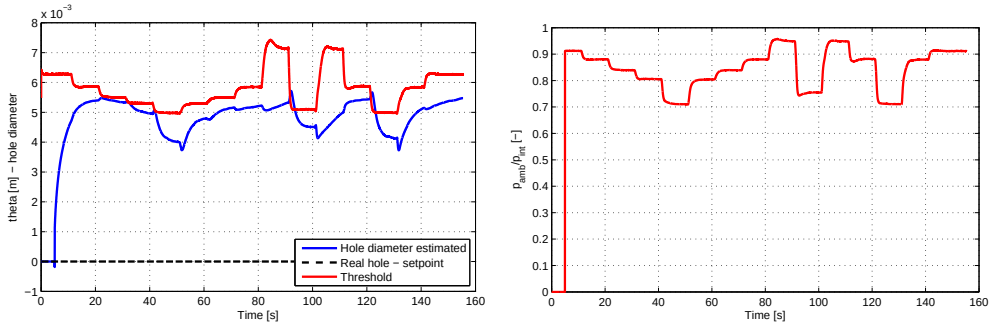

(a) Estimation without leak @2000 rpm (b) Pressure Ratio across the hole @2000 rpm

Figure 3.7: Experimental Results G9T NADI - No leakage, $M_{air} = 5\%$ multiplicative MAF error and no EGR flow along a load trajectory

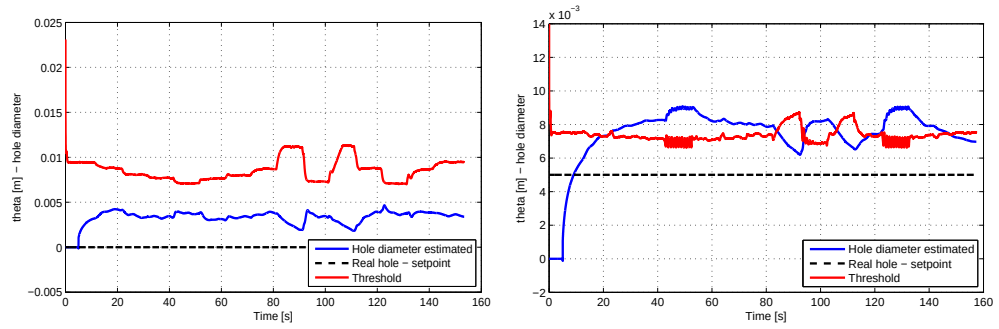

(a) Estimation without leak @2000 rpm (b) 5 mm Leak estimation @2000 rpm

Figure 3.8: Experimental Results G9T NADI - No leakage, $M_{air} = 5\%$ multiplicative MAF error and no EGR flow along a load trajectory @ 2000 rpm

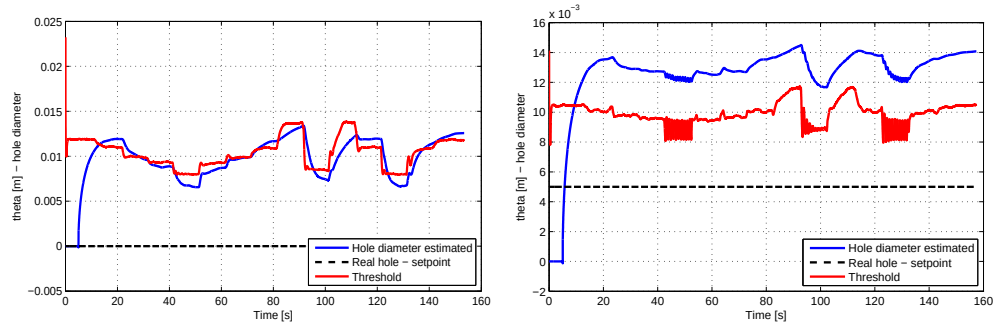

(a) Estimation without leak @2000 rpm (b) 5 mm Leak estimation @2000 rpm

Figure 3.9: Experimental Results G9T NADI - $M_{air} = 5\%$ multiplicative MAF error, $M_{asp} = 5\%$ multiplicative $\dot{m}_{asp}$ error and $M_{exh} = 200mbar$ additive p_{exh} error - EGR flow enabled along a load trajectory @ 2000 rpm

Chapter 4

Fault-Diagnostics for Turbine Efficiency Loss

The turbocharger is a key element in the air-path control of a Diesel engine, knowing its efficiency allow to design adaptive strategy to improve performances of the overall system. Due to its importance, the turbocharger has to be continuously monitored and any loss in its efficiency has to be detected.

This chapter introduces the working hypothesis and assumptions for deriving a simplified model suitable for real-time estimation. Therefore Lyapounov based adaptive observer, as the one proposed for leak's hole estimation in 3.3.1, is derived and the results of its application will be shown. The second part of this section is devoted to the design of a variable threshold based on the sensitivity study of the observer estimation.

4.1 Model for diagnosis

The turbocharger is a very complex system and an accurate model that take into account all the possible physical aspects is not suitable for online estimation algorithms such fault detection and estimation observers. Section 2.6 was devoted to introduce the role that the turbocharger plays in Diesel engine and deriving a model already suitable for control purposes. Even if the mathematical description obtained was strongly

simplified the model relies on different lookup tables and many measurements that, in almost cars, are not available.

Before describing the approach to the estimation and diagnosis of turbine efficiency, a further model simplification is needed. For such purpose some working hypothesis are here introduced:

- $T_{uc} \equiv T_{dt} \equiv T_{amb}$, where the atmospheric temperature is considered constant;
- $p_{uc} \equiv p_{dt} \equiv p_{amb}$, where the atmospheric pressure is considered constant;
- The turbocharger speed is not directly available as measurement, an estimation of it will be used. In [36] a simplified linear correlation is proposed for turbocharger speed estimation

$$N^2_{estim} = a\Pi_c + b \tag{4.1}$$

where a and b are two constants.

In a state space representation, by choosing the state $x = N^2$, from equations (2.16), (2.19), (2.21) the system can be rewritten as follow

$$\begin{cases} \dot{x}(t) &= \alpha_t(t)\phi_{W_t}(t)\phi_{\eta_t}(t) - \alpha_c(t)\frac{1}{\phi_{\eta_c}(t)} \\ y(t) &= x(t) \end{cases} \tag{4.2}$$

where the time variable t indicates that the functions are time-varying and depend on available measurements and $\phi_{W_t}(t)$ is a function of the same type of (2.23) without the correction term $\frac{p_{ref}}{\sqrt{T_{ref}}}\frac{\sqrt{T_{ut}}}{p_{ut}}$.
Moreover

$$\alpha_t(t) = \frac{2}{J}c_p T_{ut}\left[1 - \left(\frac{p_{dt}}{p_{ut}}\right)^{\frac{\gamma-1}{\gamma}}\right] \tag{4.3}$$

$$\alpha_c(t) = \frac{2}{J}W_c c_p T_{uc}\left[\left(\frac{p_{dc}}{p_{uc}}\right)^{\frac{\gamma-1}{\gamma}} - 1\right] \tag{4.4}$$

Remark 4.1.
For notation simplicity, the time variable will be no more used through the rest of this chapter.

4.2 Adaptive Observer

4.2.1 Lyapounov Based

In model-based fault detection, the use of observer is widely used. The reason of its success is that it allows to reconstruct signals not directly available from measurements or affected by errors . The interest of estimating the turbo efficiency is that, by comparison with the efficiency obtained by map (2.21), it is possible to get an error signal, i.e., *residual*, which allows to detect efficiency loss in the turbine.

Under the hypothesis that η_t is a slowly-varying parameter, i.e., $\dot{\eta}_t \approx 0$, the following observer is proposed

$$\begin{cases} \dot{\hat{x}} &= \alpha_t \phi_{W_t} \hat{\theta} - \alpha_c \dfrac{1}{\phi_{\eta_c}} + K(N^2_{estim} - \hat{x}) \\ \dot{\hat{\theta}} &= \dot{\hat{\eta}}_t \;=\; K_\theta \alpha_t \phi_{W_t} (N^2_{estim} - \hat{x}) \end{cases} \tag{4.5}$$

where K and K_θ are two tuning scalar constants: for the state observer convergence speed and the parameter adaptive law speed rate.

The correct estimation of η_t relies on the accuracy of the turbocharger speed N_{estim} provided by equation (4.1). In order to have a good estimation, after the calibration of the a and b terms, the Π_c values must be the most reliable. To guarantee the accuracy of Π_c the intake pressure sensor, p_{int}, must have a very high precision.

In Diesel engine the knowledge of the intake pressure is already a specification to be achieved and so the hypothesis to have a intake fault free pressure sensor is posed.

Moreover, the necessity of knowing the turbocharger speed is needed also for evaluating η_c and W_t in equations (2.19) and (2.23).

Besides the fault detection interest, the η_t continuous estimation may be useful in the turbocharger control strategy.

Proof 4.1.

The proof of the proposed observed relies on Lyapunov theory and conceptually will be the same type of the one used to prove the intake leak observer 3.9.

Defining the state error as $\tilde{x}(t) = x(t) - \hat{x}(t)$ and $\theta(t) = \theta - \hat{\theta}(t)$, where θ is the real turbine efficiency supposed here constant, i.e. $\dot{\theta} = 0$.

Under the above assumptions, the error system is

$$\begin{cases} \dot{\tilde{x}}(t) &= \alpha_t(t)\phi_{W_t}(t)\tilde{\theta}(t) - K(N_{est}^2 - \hat{x}(t)) \\ \dot{\tilde{\theta}}(t) &= \dot{\theta} - \dot{\hat{\theta}}(t) = -\dot{\hat{\theta}}(t) \end{cases} \tag{4.6}$$

Considering the following scalar Lyapounov function

$$V(\tilde{x}(t), \tilde{\theta}(t)) = \frac{1}{2}\tilde{x}^2(t) + \frac{1}{2}\tilde{\theta}^2(t) \tag{4.7}$$

and its time derivative along the equation dynamic is

$$\dot{V} = \tilde{x}\dot{\tilde{x}} + \frac{1}{K_\theta}\tilde{\theta}\dot{\tilde{\theta}} \tag{4.8}$$

expanding the previous equation by considering the error system dynamic 4.6

$$\dot{V} = -K(N_{est}^2 - \hat{x}(t))\tilde{x} + \alpha_t\phi_{W_t}\tilde{\theta}\tilde{x} - \frac{1}{K_\theta}\tilde{\theta}\dot{\hat{\theta}} \tag{4.9}$$

If the adaptation law is designed in order to cancel the last two term in $\dot{V}$, i.e.

$$\dot{\hat{\theta}} = K_\theta\alpha_t\phi_{W_t}\tilde{x} \tag{4.10}$$

and under the assumption that N_{est}^2 is considered as the best estimation of the turbo charger shaft speed and $K > 0$

$$\dot{V} = -K(N_{est}^2 - \hat{x}(t))\tilde{x} \leq 0 \tag{4.11}$$

the previous equation, under the assumption that intake pressure sensor p_{int} is fault free, which means that N_{est}^2 is an accurate estimate of the real turbo compressor shaft speed, can be rewritten in a standard Lyapounov form as follows

$$\dot{V} = -K\tilde{x}^2 \leq 0 \tag{4.12}$$

As $V(\tilde{x}, \tilde{\theta})$ is a positive continuous function and $\dot{V} \leq 0$ then $V(\tilde{x}, \tilde{\theta})$ has a limit as $t \to \infty$. Moreover,

$$\begin{aligned} V(0) &\geq V(0) - V(\tilde{x}(t), \tilde{\theta}(t)) = -\textstyle\int_0^t \dot{V}(\tau)d\tau \\ &\geq (K_0)\textstyle\int_0^t \tilde{x}^2(\tau)d\tau \end{aligned} \tag{4.13}$$

and so $\tilde{x} \in L_2$. As $\tilde{x} \in L_\infty$ and $\tilde{\theta} \in L_\infty$ and for (3.10), (3.11) it is true that $\dot{\tilde{x}}(t) \in L_\infty$ and $\dot{\tilde{\theta}} \in L_\infty$.

By applying Barbalat's lemma [28] to $\tilde{x}$ it is possible to conclude that

$$\lim_{t\to\infty} \tilde{x}(t) = 0 \tag{4.14}$$

Thus, as $\dot{\tilde{x}}$ is uniformly continuous and bounded ($\alpha_t(t)$, $\phi_{W_t}(t)$ and $\alpha_c(t)$ are positive differentiable bounded function and their derivate are bounded too) it is possible to apply again Barbalat's lemma showing that $\dot{\tilde{x}}(t) = 0$ as $t \to \infty$. From the error equation (4.6) the following limit holds

$$\lim_{t\to\infty} \alpha_t(t)\phi_{W_t}(t)\tilde{\theta}(t) = 0$$

Therefore, if

$$\lim_{t\to\infty} \alpha_t(t)\phi_{W_t}(t) \neq 0 \tag{4.15}$$

also

$$\lim_{t\to\infty} \tilde{\theta}(t) = 0$$

It is important here to remark that the equilibrium point $[0, 0]^T$ is uniformly asymptotically stable: UAS [24].

However the dynamics are linear, applying the theorem 4.11 in [28], it is possible to conclude that $[\tilde{x}, \tilde{\theta}]^T$, if the observability condition (4.15) is fulfilled, are exponentially stable. In other words, $\exists(\tau_{tc}, \lambda_{tc}) \in (\mathbb{R}^+\backslash\{0\})^2$ s.t. $\forall t \in R^+$

$$|\tilde{x}(t)| \leq \tau_{tc}e^{-\lambda_{tc}t} \text{ and } |\tilde{\theta}| \leq \tau_{tc}e^{-\lambda_{tc}t}$$

where the subscript "tc" stands for turbo compressor.

4.2.2 Observability condition

The condition under which the proposed observer is able to estimate its state is when the efficiency is observable, in other words when the condition expressed in equation 4.15 is fulfilled. Intuitively the turbine efficiency, when the turbo charger shaft speed is measured, can be determined when there is enough energy flowing through the turbine. It is possible to correlate the observability with the turbine power expressed as $\alpha_t(t)\phi_{W_t}(t)$.

How much this term is far from zero, greater will be the observability and so the ability to reconstruct the turbine efficiency.

As proposed in the section 3.3.5, it is here shown how the 'observability' vary along a standard ECE cycle. The top plot of the figure 4.1 shows the turbine power normalized

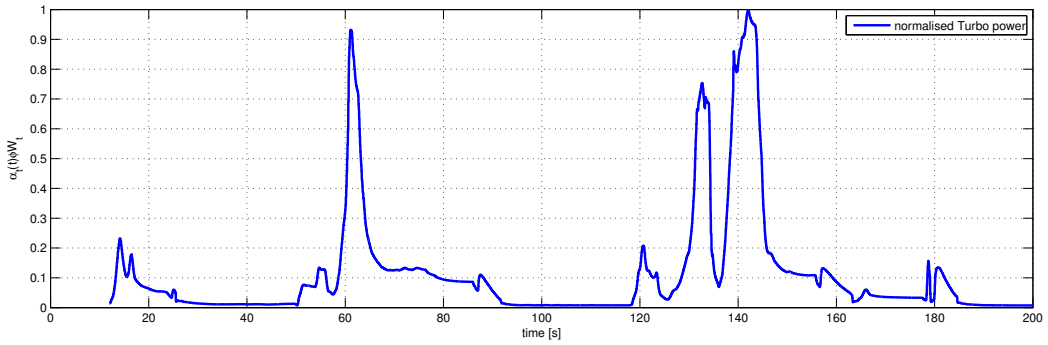

(a) $\alpha_t(t)\phi_{W_t}(t)$

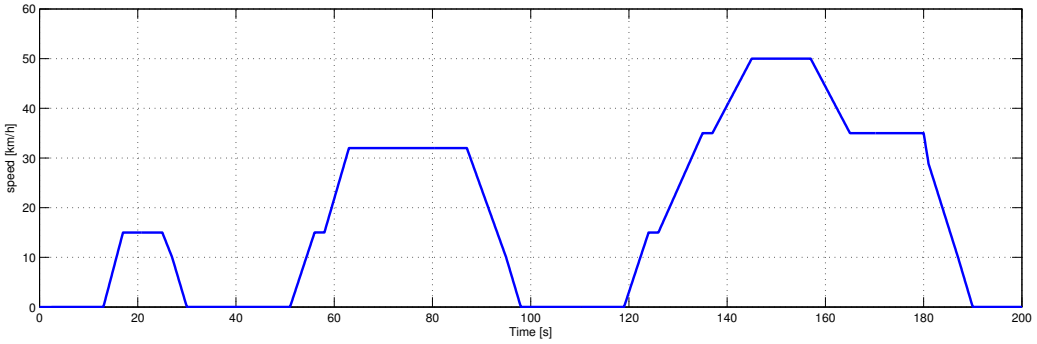

(b) ECE speed set-points

Figure 4.1: The observability condition measured along a urban driving cycle - ECE.

and it is possible to see that the term $\alpha_t(t)\phi_{W_t}(t)$ is high in relation to high speeds. Intuitively, that should not surprise, because high vehicle speeds correspond to high turbocharger power demand or equivalently to a high turbocharger shaft speed.

4.3 Threshold & Decision

4.3.1 Sensitivity analysis

In the previous section , the accuracy of the turbine's efficiency estimation has been discussed with respect to knowledge of the turbocharger shaft speed N. The estimation of η_t relies also on other available measurements. The object of this section is the observer sensitivity study in steady state condition in order to define what is the impact of the different sensors measurements biases in the estimation error. A similar approach have been used in [11].
In steady-state condition the parameter will converge to

$$\hat{\theta}_{ss} = \theta^* + \Delta\theta \tag{4.16}$$

where θ^* stands for the real value of the turbine efficiency, $\Delta\theta$ is the observer estimation error. The observer dynamic, after the transient, will be

$$0 = \alpha_t \phi_{W_t} \hat{\theta}_{ss} - \alpha_c \frac{1}{\phi_{\eta_c}} \tag{4.17}$$

and it is possible to explicit the $\hat{\theta}_{ss}$ as

$$\hat{\theta}_{ss} = \frac{\alpha_c}{\alpha_t \phi_{W_t} \phi_{\eta_c}} \tag{4.18}$$

In quasi-stationary condition the turbine flow $W_t = W_c + W_f$, where W_c is the compressor measured air flow (MAF sensor) and W_f is the fuel flow supposed known. In a Diesel Engine the injected fuel can be expressed as

$$W_f = W_c \cdot \frac{\Phi(t)}{14.7} \tag{4.19}$$

where $\Phi(t)$ is the measured equivalence ratio and considered a known function of the time. The double advantage in estimate the turbine flow through equation (4.19) is to avoid the use of the static map (2.23) and so the u_{VGT} control signal, which might not match with the real opening section of the variable geometry turbo (VGT), the second reason is that the equation (4.18) can be explicitly rewritten as

$$\hat{\theta}_{ss} = \frac{T_{amb} \cdot \left(\left(\frac{p_{int}}{p_{amb}} \right)^{\frac{\gamma-1}{\gamma}} - 1 \right)}{T_{exh} \cdot \alpha_f \cdot \left(1 - \left(\frac{p_{amb}}{p_{exh}} \right)^{\frac{\gamma-1}{\gamma}} \right) \cdot \phi_{\eta_c}(MAF_{corr}, N_{corr})} \tag{4.20}$$

where W_c term has been simplified from α_c and α_t function and $\alpha_f = 1 + \frac{\Phi(t)}{14.7}$. If, as already discussed previously, the intake manifold pressure sensor is supposed fault free and precise, in steady-state condition the turbine efficiency estimation is function of four terms which can be affected by biases: p_{exh}, T_{exh}, MAF and possible error in the η_c map.

A fifth signal error may be the equivalent ration term, Φ, but it is supposed here to be perfectly known and, anyhow, the impact on estimation error can be shown to be negligible.

The sensitivity of $\hat{\theta}_{ss}$ with respect to possible measurement bias, is studied by the explicit calculation of the first derivative of equation (4.20) with respect to the different four signals responsible of estimation error.

For notation simplicity, two substitution will be used through the rest of this section:

$$k_c = \frac{T_{amb}}{\alpha_f}\left(\left(\frac{p_{int}}{p_{amb}}\right)^{\frac{\gamma-1}{\gamma}} - 1\right) \tag{4.21}$$

$$\bar{\gamma} = \frac{\gamma - 1}{\gamma} \tag{4.22}$$

where K_c is a known function of time which depends only on fault free measurements and $\bar{\gamma}$ is a scalar constant.

Exhaust Manifold Temperature Sensor

The exhaust manifold temperature sensor is generally affected by an additive bias

$$T_{exh} = T^*_{exh} + \Delta T_{exh} \tag{4.23}$$

where ΔT_{exh} stands for bias and T^*_{exh} is the correct value of the temperature.

The sensitivity function of $\hat{\theta}_{ss}$ with respect to T_{exh} is

$$\frac{\partial \hat{\theta}_{ss}}{\partial T_{exh}} = -\frac{k_c}{T^2_{exh} \cdot \left(1 - \left(\frac{p_{amb}}{p_{exh}}\right)^{\bar{\gamma}}\right) \cdot \phi_{\eta_c}(MAF_{corr}, N_{corr})} \tag{4.24}$$

Exhaust Manifold Pressure Sensor

The exhaust manifold pressure sensor is affected by an additive bias

$$p_{exh} = p^*_{exh} + \Delta p_{exh} \tag{4.25}$$

where Δp_{exh} stands for bias and p^*_{exh} is the correct value of the pressure.
The sensitivity function of $\hat{\theta}_{ss}$ with respect to p_{exh} is

$$\frac{\partial \hat{\theta}_{ss}}{\partial p_{exh}} = -\frac{k_c \cdot \left(\left(\frac{p_{amb}}{p_{exh}} \right)^{\bar{\gamma}} \cdot \frac{\bar{\gamma}}{p_{exh}} \right)}{T_{exh} \cdot \left(1 - \left(\frac{p_{amb}}{p_{exh}} \right)^{\bar{\gamma}} \right)^2 \cdot \phi_{\eta_c}(MAF_{corr}, N_{corr})} \tag{4.26}$$

Compressor Efficiency Map

The compressor efficiency map provided by the manufacturer may have some uncertainties, in general this kind of error are modeled as proportional to signal bias

$$\eta_c = \eta^*_c + \Delta\eta_c \tag{4.27}$$

where η^*_c is the correct value of the compressor efficiency and $\Delta\eta_c = \delta_{\eta_c} \cdot \eta^*_c$ stands here for the proportional bias.
The sensitivity function of $\hat{\theta}_{ss}$ with respect to η_c (2.19) is

$$\frac{\partial \hat{\theta}_{ss}}{\partial \eta_c} = -\frac{k_c}{T_{exh} \cdot \left(1 - \left(\frac{p_{amb}}{p_{exh}} \right)^{\bar{\gamma}} \right) \cdot \phi^2_{\eta_c}(MAF_{corr}, N_{corr})} \tag{4.28}$$

where $\frac{d\eta_c}{d\phi_{\eta_c}} = 1$.

Compressor Flow Sensor

The mass air flow sensor (MAF) is one of the most important measurement for the control of a Diesel engine. It is, in general, a very accurate sensor but it may have some drift with the time. The bias is modeled

$$MAF = MAF^* + \Delta MAF \tag{4.29}$$

where MAF^* is the correct value of the compressor efficiency and $\Delta MAF = \delta_{MAF} \cdot MAF^*$ stands here for the proportional bias.
The sensitivity function of $\hat{\theta}_{ss}$ with respect to MAF is

$$\frac{\partial \hat{\theta}_{ss}}{\partial MAF} = -\frac{k_c \cdot \frac{\partial\ \phi_{\eta_c}}{\partial MAF}}{T_{exh} \cdot \left(1 - \left(\frac{p_{amb}}{p_{exh}} \right)^{\bar{\gamma}} \right) \cdot \phi^2_{\eta_c}(MAF_{corr}, N_{corr})} \tag{4.30}$$

where the $\frac{\partial \phi_{\eta_c}}{\partial MAF}$ term stands for the differention of the map (2.19) with respect to the MAF variable (Figure 2.10(b)).

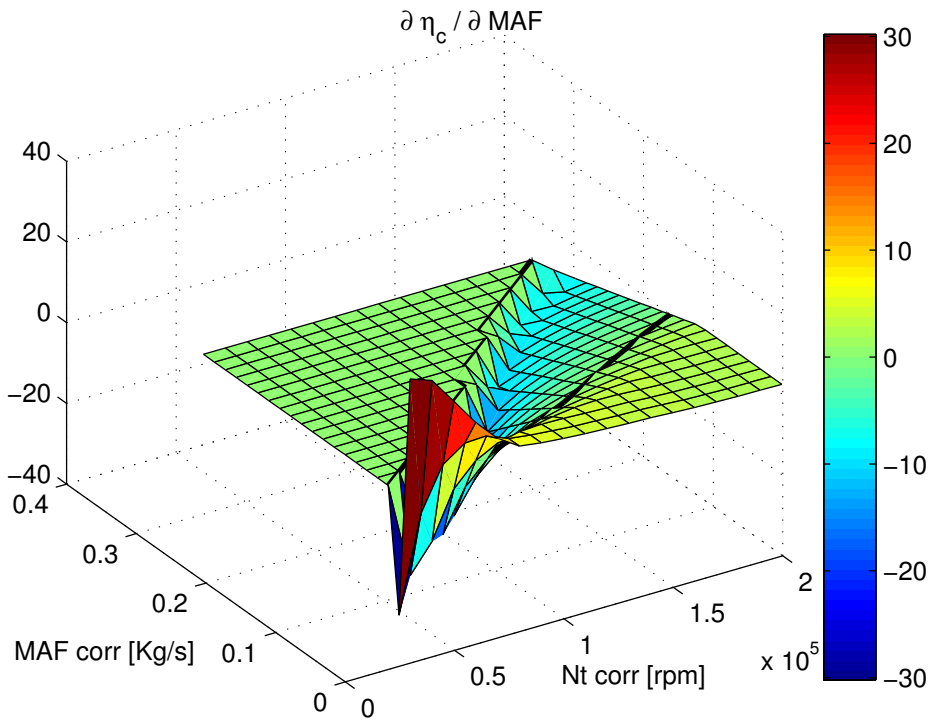

Figure 4.2: Derivative of compressor efficiency map with respect to MAF

Estimation Error Evaluation

In order to compare the sensitivity functions (4.24), (4.26), (4.28) and (4.30), an evaluation of the impact of each uncertainties on the turbine estimation error will be developed here.

By defining the estimation error as $\Delta\hat{\theta}_{ss} = \hat{\theta}_{ss} - \theta^*_{ss}$, a first order approximation of the error made by the observer because of the signal biases is

$$\Delta\hat{\theta}_{ss} = \frac{\partial\hat{\theta}_{ss}}{\partial\omega}\Delta\omega, \quad \text{with } \omega = \{p_{exh}, T_{exh}, MAF, \eta_c\} \tag{4.31}$$

Figure 4.3 shows the four sensitivity functions evaluation on different engine testbed steady-state experimental points at 2000 rpm, under the hypothesis that sensors error occurs once at time. The value of the bias are here reported:

- $\Delta p_{exh} = \pm 200$ mbar;
- $\Delta T_{exh} = \pm 20$ K;

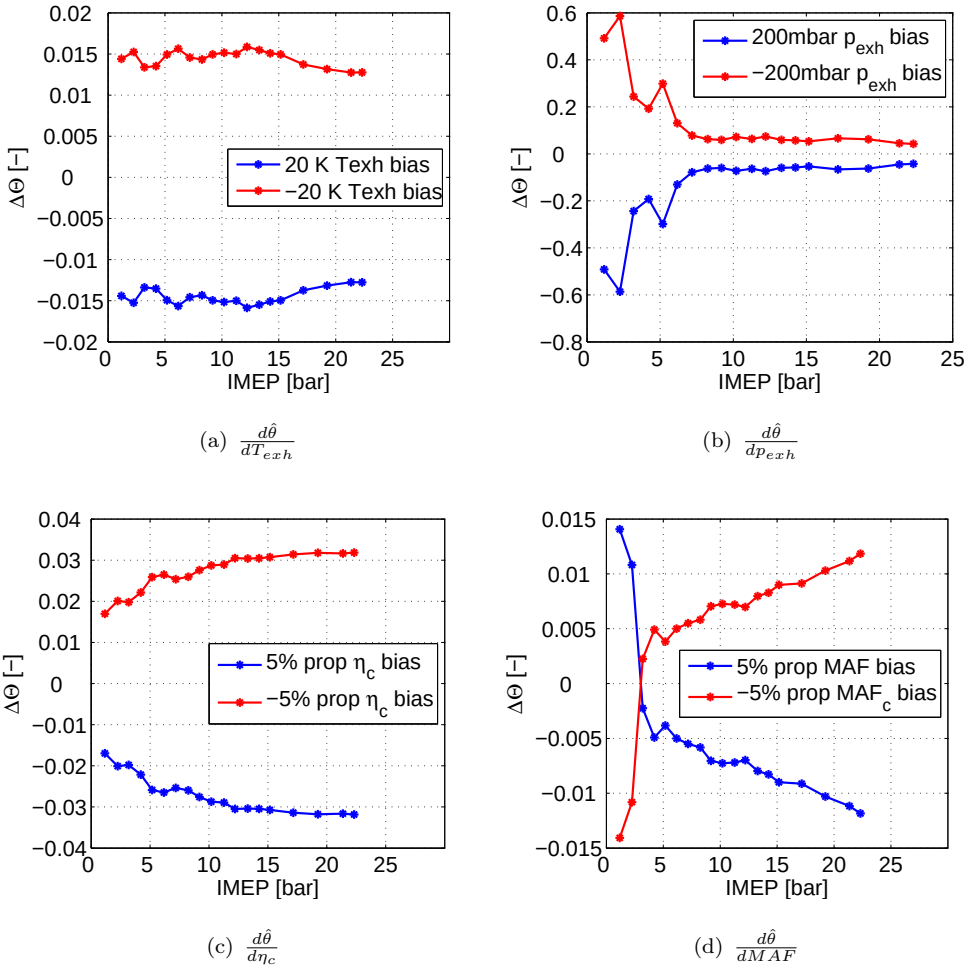

(a) $\frac{d\hat{\theta}}{dT_{exh}}$ (b) $\frac{d\hat{\theta}}{dp_{exh}}$

(c) $\frac{d\hat{\theta}}{d\eta_c}$ (d) $\frac{d\hat{\theta}}{dMAF}$

Figure 4.3: Sensitivity functions evaluated in different steady-state experimental points with measurements bias - 2000 rpm engin speed

- $\delta_{\eta_c} = \pm 5$ %;
- $\delta_{MAF} = \pm 5$ %;

Starting from the top-left figure and proceeding clockwise:

- ΔT_{exh}: the influence of turbine upstream temperature additive bias on $\Delta\hat{\theta}_{ss}$ is almost constant and less than 2%, (cfr. eq. 4.24);
- Δp_{exh}: exhaust manifold pressure bias is the most responsable component in estimation error. At low charge ($IMEP < 5$ bar) the error could be up to 60%

and even for higher IMEP it is not less than 5%, i.e., $5\% \leq \Delta\hat{\theta}_{ss} \leq 8\%$, (cfr. eq. 4.26);

- ΔMAF: as already argued before, if the MAF measurement is used both for the compressor flow and for the turbine flow, MAF bias acts only on the efficiency map of the compressor. The estimation error, for a 5% proportional to signal error on MAF measurement, is lower than 1.5%, (cfr. eq. 4.30);

- $\Delta\eta_c$: even error of 5% on the compressor efficiency map leads to estimation error lower than 3.5%, (cfr. eq. 4.28);

It is possible to understand the relevance of the exhaust manifold pressure sensor's accuracy and how it can impact the estimation error. Moreover, the sensitivity analysis gives a important information on how to choose the threshold as function of sensors biases and available measurements.

Residual Sensitivity

For the fault detection task, the purpose of the estimation, is to be able to generate an error signal, *residual*, which is different from zero only when there is an efficiency loss in the turbine. If the residual signal is defined as

$$r(t) = \hat{\theta}(t) - \phi_{\eta_t}(\Pi_t, N_{t,corr}, u_{VGT}) \tag{4.32}$$

where the ϕ_{η_t} now depends on Π_t and $N_{t,corr}$. In other words the turbine efficiency look up table depends on p_{exh} and T_{exh} measurements.

For sake of completeness, the ϕ_t term used in equation 4.32 is another possible way manufacturer provides turbine efficiency map and it will be used now for simplicity of analysis.

Residual is a confrontation between the estimation and a reference, but if the reference is itself affected by sensors error this can lead to false alarm. In the studied case only p_{exh} error as been considered in the analysis as a measurement that can impact

the reference by the means of Π_t. The exhaust temperature additional bias is not considered because of its small effect on the $N_{t,corr}$ due to the fact that appears under a square root, i.e. an additive error of even 50 Kelvin degrees will impact the correction term less of 0.002 .

In figure 4.4 the sensitivity of $\phi_{\eta_t}(\Pi_t, N_{corr}, u_{VGT})$ is evaluated with respect to p_{exh}

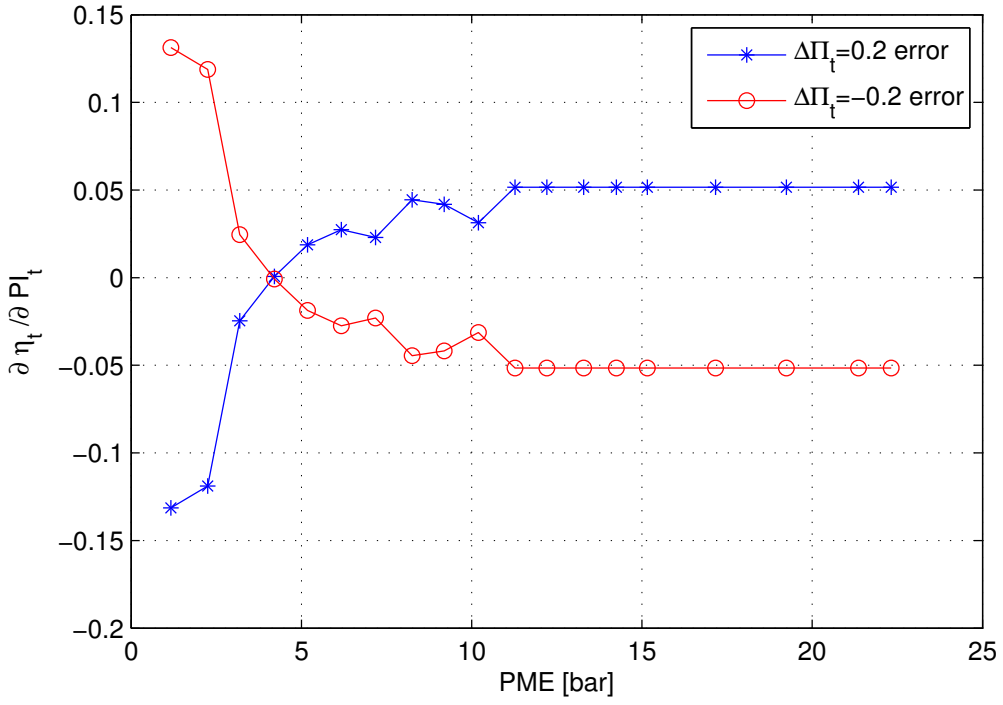

Figure 4.4: $\frac{\partial \phi_{\eta_t}(\Pi_t, N_{t,corr}, u_{VGT})}{\partial \Pi_t}$ evaluated in different steady-state experimental points with measurements bias, i.e., $\Delta\Pi_t = \pm 0.2$

when $\Delta p_{exh} = 200$ mbar in the same steady-state experimental points as previously. Two remarks come out form the observation of figure: for high IMEP the estimation error $\Delta\hat{\theta} < 6\%$ and the sensitivity function has opposite sign with respect to eq. (4.26) which means that in residual evaluation (eq. 4.32) the estimation error due to p_{exh} bias will be summed together.

4.3.2 Sensitivity-based Threshold

The ability and robustness to detect turbocharger loss of efficiency relies on the quality of the threshold adopted. As already explained for the leak detection the fixed threshold, if correctly choose, can be a fast and reliable approach if a good knowledge of the system under monitoring is available. This is quite common for the automotive industry, where huge historical database of system component behaviour and faults are available and allow to determine the best fixed threshold which allows to detect a fault and avoid false alarm as much as it can.
In this section it will be presented a possible way to choose the threshold using the sensitivity functions obtained previously in the following form

$$\begin{aligned} Th_r &= \frac{d\hat{\theta}_{ss}}{dT_{exh}}\Delta T_{exh} + \frac{d\hat{\theta}_{ss}}{dp_{exh}}\Delta p_{exh} + \\ &\quad \frac{d\hat{\theta}_{ss}}{d\eta_c}\Delta\eta_c + \frac{d\hat{\theta}_{ss}}{dMAF}\Delta MAF \end{aligned} \tag{4.33}$$

The threshold depends on the uncertainty of the sensors: the mass air flow, the exhaust pressure, the exhaust temperature and the possible error in the compressor efficiency map. If the maximum uncertainty for each of those sensors is known, i.e. the classic 3-sigma production variability, it is possible to evaluate, for a given operating condition of the engine, the impact of this uncertainty with respect to the accuracy of the estimation θ. In other words, the sensitivity function is used here as a measure of the error that the sensor biases can introduce in the estimation of the turbine efficiency.
A way to assess how the estimation error is distributed is to evaluate the threshold (4.33) for a given engine operating condition (here calculated along a power swing at 2000 rpm), where the $\delta\omega$ as defined in equation (4.31) is considered here only the maximum and minimum error for each sensor, i.e. as defined in section 4.3.1

As the number of possible sensor biases are four, it is possible to evaluate the proposed threshold for all fault possible combinations, i.e., sixteen combination if only maximum and minimum value are choosed.

The result is shown in figure 4.5, where it comes out that if the fault detection strategy is used when IMEP is greater than 6 bar, a fixed threshold can be choosen

Error code	T_{exh} err [K]	p_{exh} err [Pa]	MAF err [%]	η_c err [%]
1	-20	-200e2	-5	-5
2	-20	-200e2	-5	5
3	-20	-200e2	5	-5
4	-20	-200e2	5	5
5	-20	200e2	-5	-5
6	-20	200e2	-5	5
7	-20	200e2	5	-5
8	-20	200e2	5	5
9	20	-200e2	-5	-5
10	20	-200e2	-5	5
11	20	-200e2	5	-5
12	20	-200e2	5	5
13	20	200e2	-5	-5
14	20	200e2	-5	5
15	20	200e2	5	-5
16	20	200e2	5	5

Table 4.1: Error combination table sequence

equal to 0.15. The drawback of this strategy is that all the turbo efficiency loss lower than 0.15 will be not be detected.
By evaluating the equation (4.33) dynamically with the available measurements, a variable threshold is obtained which can be less conservative than the fixed one.

4.4 Simulations Results

Simulation for the proposed method was carried out using a co-simulation platform Matlab/Simulink© and AMEsim©. The AMEsim© model is used to simulate the engine behavior and it is calibrated on a 2.2L four cylinders Diesel engine available at IFP's test bed (A.2). The available sensors and their maximum bias considered in simulation are reported in Table 4.2. Moreover a maximum of 5%, proportional to

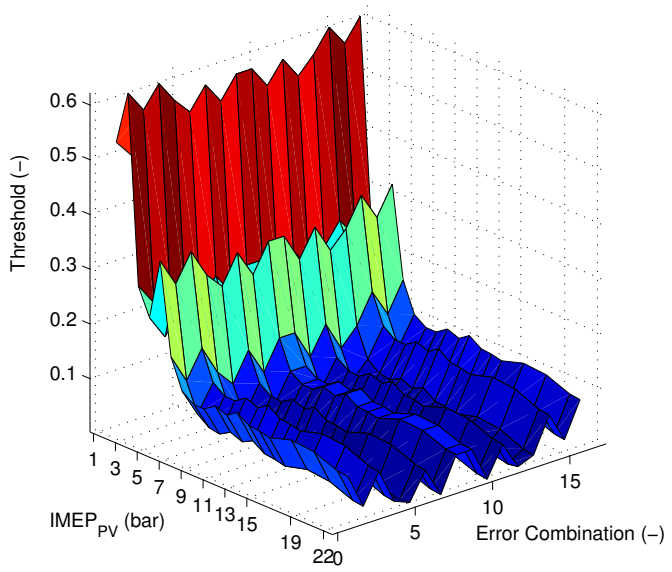

Figure 4.5: Threshold evaluation for all possible error combination (Table 4.1) in different engine experimental points

Name	Max Δ	Unit
T_{int}	0	K
p_{exh}	$\pm 200e2$	Pa
T_{exh}	± 20	K
u_{VGT}	0	%
MAF	± 5	%
Φ	0	-

Table 4.2: Available Measurements

value, uncertainty has been considered on the compressor efficiency map.
All simulations shown here are made at 2000 rpm constant engine speed and two torque trajectories have been used:

- LOW LOAD TRAJECTORY:

$$IMEP = [4\ 5\ 6\ 7\ 6\ 5\ 2\ 5\ 7\ 5\ 4]\ bar$$

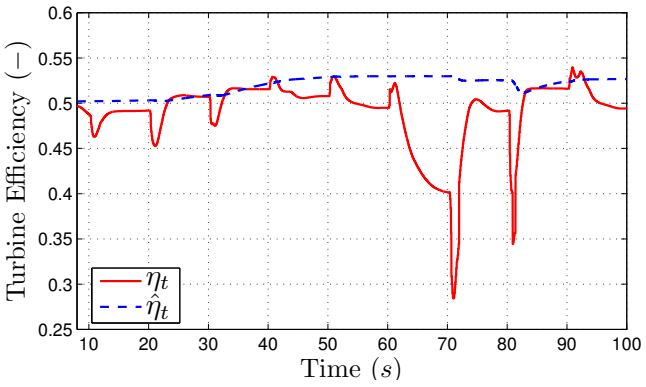

(a) Low Load - $\hat{\Theta}$

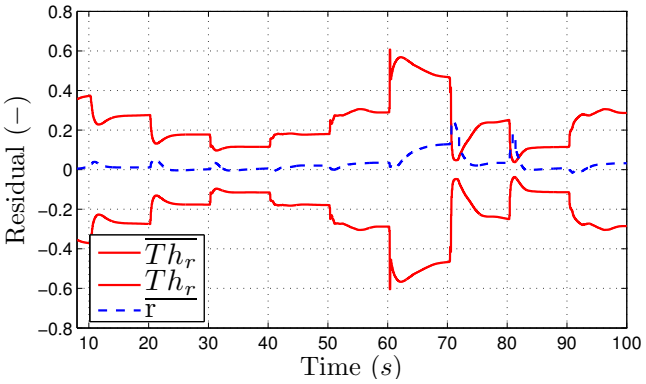

(b) Low Load - residual

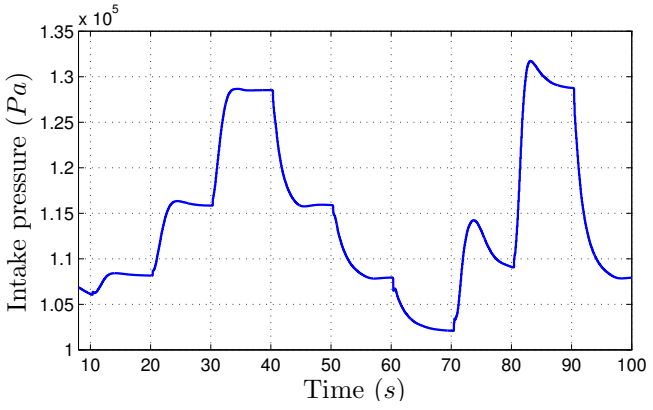

(c) Low Load - p_{int}

Figure 4.6: Adaptive observer turbo efficiency estimation - Engine speed 2000 rpm and Low Loads Trajectory - No sensors fault, $\Delta MAF = 3\%, \Delta\eta_c = 4\%,\ T_{exh} = -10K$

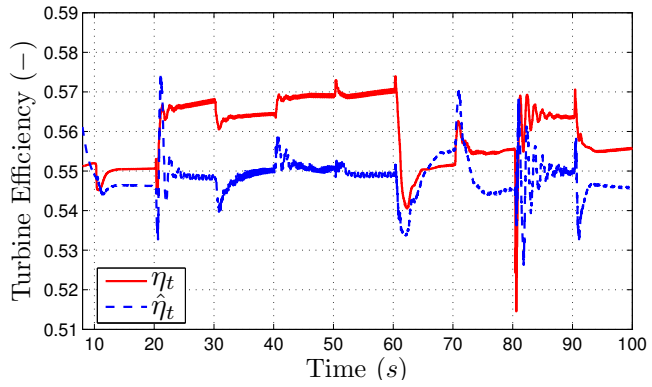

(a) High Load - $\hat{\Theta}$

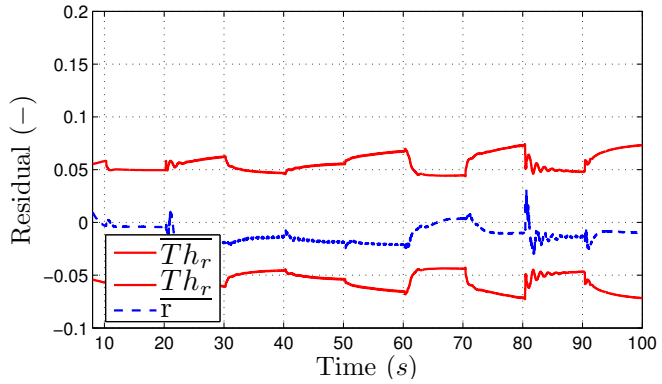

(b) High Load - residual

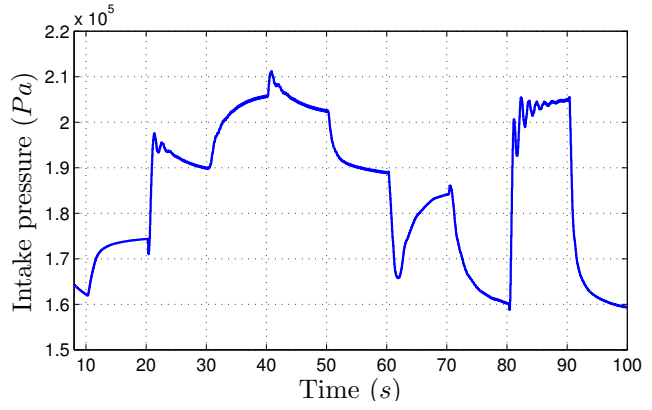

(c) High Load - p_{int}

Figure 4.7: Adaptive observer turbo efficiency estimation - Engine speed 2000 rpm and High Loads Trajectory - No sensors fault, $\Delta MAF = 3\%, \Delta\eta_c = 4\%,\ T_{exh} = -10K$

- HIGH LOAD TRAJECTORY:

$$IMEP = [10\ 11\ 13\ 15\ 14\ 13\ 12\ 10\ 15\ 10\ 13]\ bar$$

- Step Time: $T_{IMEP} = 10s$

the T_{IMEP} stands for the period in which the demanded torque is kept before changing to the next value of the trajectory.

The first set of figures (Fig. 4.7, 4.6) are about simulation at 2000 rpm where no loss in the turbine's efficiency is present. In Figures 4.6(a) and 4.7(a) the simulation results using the proposed adaptive observer (eq. 4.5) are shown: the dashed line is the estimated turbine efficiency $\hat{\theta}$ and, in solid line, is the turbine efficiency obtained by the static map (2.21).

The Figures 4.6(b) and 4.7(b) shown the residual (dashed), based on equation (4.32), with the proposed adaptive threshold evaluated on the maximum uncertainties defined before (Table 4.2).

Finally, figures 4.6(c) and 4.7(c) report the intake manifold pressure along the different trajectory. It is evident that the estimation of the turbine efficiency is more accurate for high IMEP which correspond to have high turbocharger speed. The accuracy of the estimation can be seen by the residual thresholds, for low loads (Fig. 4.6(b)) the thresholds absolute value is greater of 0.15 which is congruent with what obtained in Fig. 4.5. For high loads (Fig. 4.7(b)) the accuracy is greater, i.e., the thresholds absolute value is less than 0.075 along all the trajectory.

A last remark is about the threshold conservativeness. In intervals where the turbocharger speed is slow (ex. $60 \leq t \leq 70$ in Fig. 4.6(b)) the uncertainty on the estimation rise up and so the threshold avoid, if possible, false alarm.

Figure 4.8 shows different combination of functioning of the proposed method in low (left column) and high (right column) load trajectory. All the simulation are made with $\Delta MAF = 3\%, \Delta\eta_c = 4\%,\ T_{exh} = -10K$ and different exhaust manifold pressure bias Δp_{exh}. The reason of this choice is that, in the previous sensitivity analysis, the p_{exh} sensor appears to be the one which has the greater impact on the estimation error. To simulate the loss in the turbine efficiency a constant gain has been applied in the AMEsim© model turbine map.

In Figures 4.8(a) and 4.8(b) the residual results for a -10% of turbine efficiency loss is reported and it comes out that for low load trajectory it is impossible to detect the fault whereas, for high load, the detection can be done for all the analyzed points. If the threshold is generated for a p_{exh} maximum uncertainty of $200mbar$ and a same bias is applied on the p_{exh} measurement, the detection of loss in efficiency of the turbine is shown in figures 4.8(c),4.8(e), 4.8(d) and 4.8(f).
The proposed threshold is generated with the maximum uncertainties biases, which means that if the sensors has a bias lower with respect to this maximum, the threshold would be conservative. In order to reduce the conservativeness a dynamic Δp_{exh} is necessary or a more accurate sensor is suitable. For the specific problem a Δp_{exh} estimation is proposed by the means of the downstream EGR heat exchanger pressure p_{EGR}.

In order to complete the analysis, in Figure 4.9 and 4.10 the turbocharger fault detection algorithm has been applied along the first 200 seconds of the standard ECE cycle. Figure 4.9(a) shows the residual when a -10% turbine efficiency loss is simulated along the cycle: it is very hard to detect the fault due to the very high uncertainties in the estimation because of sensors bias and very low loads of this part of the cycle (Fig. 4.9(b)).
Figure 4.10(a) shows the residual when -10% of turbine efficiency loss is simulated along the standard EUDC cycle. The detection of the fault is possible in four intervals which correspond to high intake manifold pressure p_{int} (Fig. 4.10(b)). In particular, during the third and fourth acceleration phase (intervals between $[250s,\ 300s]$ and $[320s,\ 350s]$) the detection is clearly visible.
The detection in this intervals is due to the reduction of the threshold. This reduction corresponds to a good accuracy in estimation and so, by the observation of the threshold, it is possible to determine functioning zone for turbine efficiency loss detection.

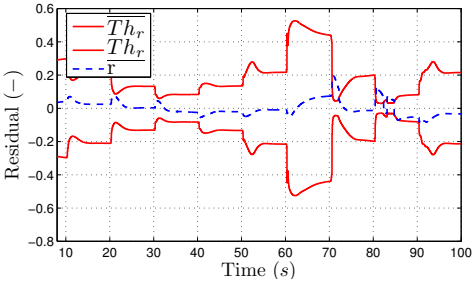

(a) Low Load, $\Delta\eta_t = -10\%$, $\Delta p_{exh} = 0mbar$

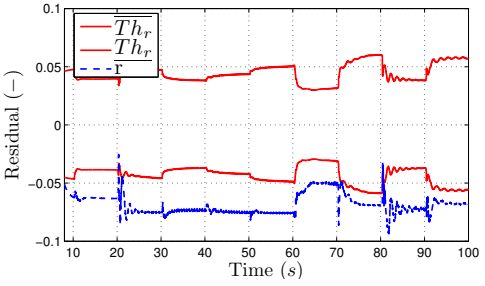

(b) High Load, $\Delta\eta_t = -10\%$, $\Delta p_{exh} = 0mbar$

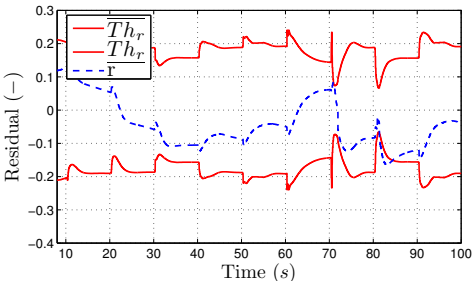

(c) Low Load, $\Delta\eta_t = 0$, $\Delta p_{exh} = 200mbar$

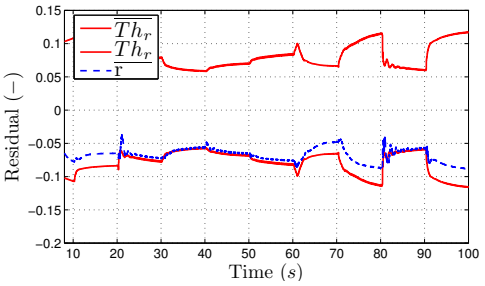

(d) High Load, $\Delta\eta_t = 0$, $\Delta p_{exh} = 200mbar$

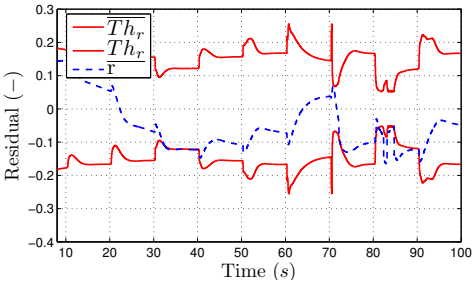

(e) Low Load, $\Delta\eta_t = -10\%$, $\Delta p_{exh} = 200mbar$

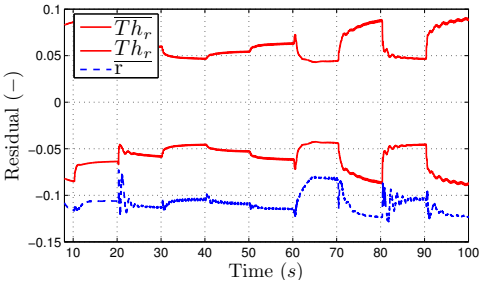

(f) High Load, $\Delta\eta_t = -10\%$, $\Delta p_{exh} = 200mbar$

Figure 4.8: Residual Analysis - Engine speed 2000 rpm - $\Delta MAF = 3\%, \Delta\eta_c = 4\%$, $T_{exh} = -10K$

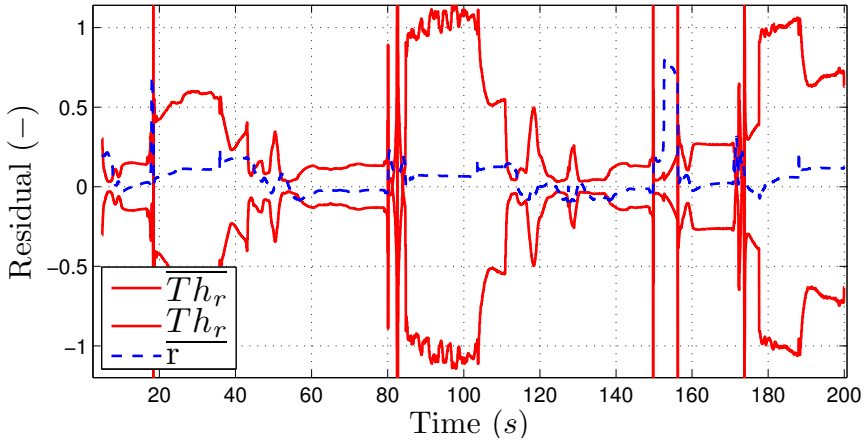

(a) ECE cycle Residual, $\Delta\eta_t = -10\%$, $\Delta p_{exh} = 0mbar$

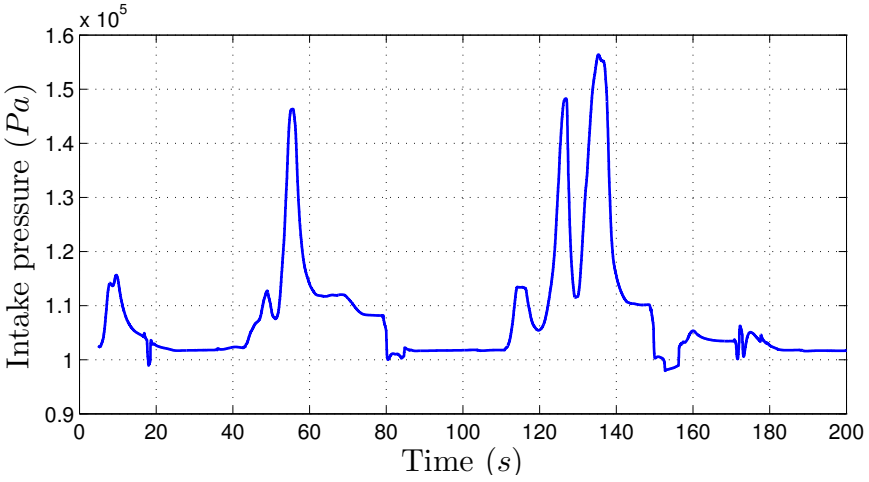

(b) p_{int} - ECE cycle, $\Delta\eta_t = -10\%$, $\Delta p_{exh} = 0mbar$

Figure 4.9: Residual Analysis - ECE cycle - $\Delta MAF = 3\%, \Delta\eta_c = 4\%,\ T_{exh} = -10K$

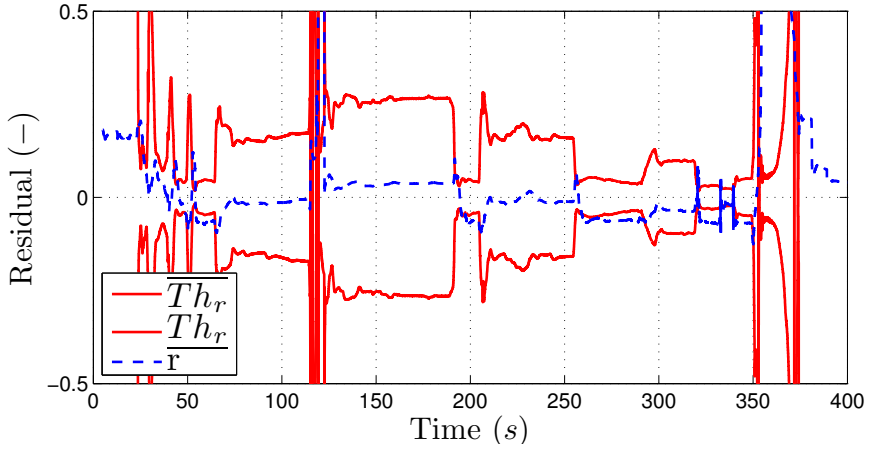

(a) Residual - EUDC cycle, $\Delta\eta_t = -10\%$, $\Delta p_{exh} = 0mbar$

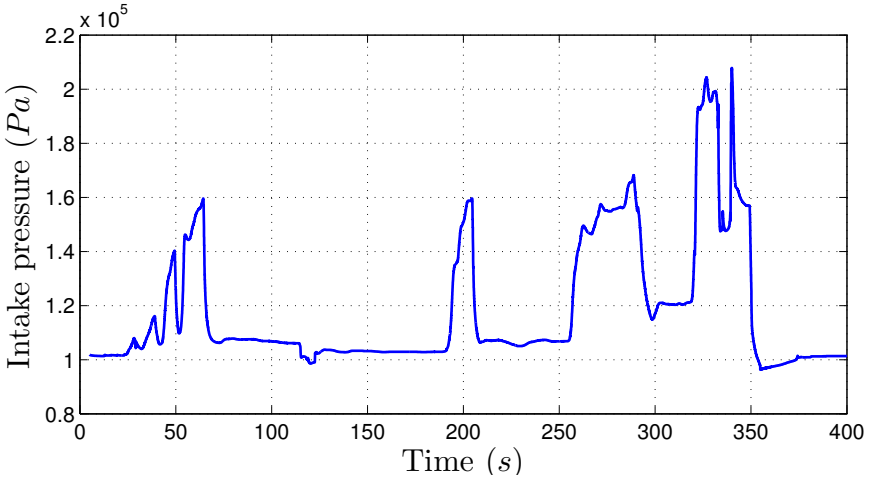

(b) p_{int} - EUDC cycle, $\Delta\eta_t = -10\%$, $\Delta p_{exh} = 0mbar$

Figure 4.10: Residual Analysis - EUDC cycle - $\Delta MAF = 3\%, \Delta\eta_c = 4\%,\ T_{exh} = -10K$

Chapter 5

Conclusions

English version

This thesis studies the fault detection for the air-path of a Diesel engine with a model based approach. The work has been conducted and tested around two major system failures:

- a leak in the intake manifold
- the turbine efficiency loss

whose detections are critical to the correct functioning of the engine and to respect the pollutant emissions law which enforce more and more the reliability of all the part of a vehicle all along its life (EURO-6).

In this work we deliberately choose to study the problem with a model-based approach taking into consideration some constraints:

- the strategy should work without adding more sensors than the ones already present in a mass produced vehicle;
- the strategy needs to be robust enough to work in several operating condition, i.e. along the European driving cycle;
- the strategy should not interfere with the existing control strategy.

The results of the work shows that, at least in the case study approached, the use of an adaptive observer is most suitable for fault detection strategy: it allows to detect, localise and, under sensors fault free, identify the amplitude of the fault. In a second phase of this work, the possible sensors uncertainties have been considered in the strategy and the necessity of a new threshold definition became necessary in order to avoid a conservative detection strategy based on a very high threshold level and reduce the calibration time.
The sensitivity analysis allowed to have, in a systematic way, how much each sensor measurement affects the estimation with respect to its uncertainty due to biases and drift. This analysis can be used in the fault detection design process, in particular when it is necessary to choose the sensors based on the accuracy (Appendix C).
Moreover, the use of the sensitivity function, coupled with additional conditions, such as the type of error model, provides a mean to design a variable threshold which adapts its amplitude to the observability condition.
The study of this last property, necessary for the estimation convergence, gives an important piece of information on the operating condition in which the estimation will converge fast to its value and with a better accuracy. This is particularly interesting as this is normally obtained by statistical method, e.g. Monte Carlo techniques, or by previous knowledge based on the experience.

In both treated faults, the analysis shows the success of the approach if a good estimation of the biases is known. Indeed, the proposed method provides an upper bound to all the uncertainties that each bias introduces in the observer estimation. In order to cope with this problem and allow to improve the capability to detect also small faults without loosing the robustness, it is necessary to recalibrate dynamically the threshold.

The intake manifold leak detection problem has shown that it is possible to detect hole as small as 2.5 mm in the best operating condition, even if the exhaust gas recirculation circuit is enabled. More generally, holes equal to or greater than 5 mm can be detected also when 5% multiplicative error is present in the mass air flow measurement and in the engine efficiency look-up table. In terms of detection operating regions, the

observability analysis combined with the model quality (in particular the EGR flow model) shows that the detection is reliable when the pressure ratio between the ambient pressure and the intake pressure is below 0.9 this result corresponds to an indicated mean effective pressure - IMEP - greater of 6 bar at 1500 rpm.

Regarding the turbine efficiency estimation and loss detection, once the model has been reduced to its simplest form, the proposed observer shows how good is the quality of the efficiency look-up table provided by the turbo compressor manufacturer in the nominal operative region (high turbocharger shaft speed) and in steady state condition. The advantage of having a dynamical estimation of the turbine efficiency is, if integrated into the control strategy, to have the possibility to improve the air-path control during the transient phases. The sensitivity analysis done in this case study was more complete and showed how to use it as a tool to calibrate a fixed threshold and more important to understand which sensor bias impacts more in the estimation error. The result was that the exhaust pressure sensor is the most responsible for the estimation accuracy and its uncertainty should be reduced to value smaller than the one considered (200mbar). As in the case of the leak detection, the observability combined with the sensitivity analysis suggests to trust the strategy in the high engine load points in order to be able to detect efficiency loss equal or greater than 10%.

All the presented results have been studied on a Diesel engine but the proposed approach is system independent. The model based technique main advantage is to reduce the calibration time if the engine is subject mechanical changes, which is particularly true in a design stage.

In conclusion, the presented work analyses the use of a model-based approach for the fault detection of the Diesel engine air-path showing that the strategy developed is successful if a good knowledge of sensor bias is available. Moreover, the advantage provided by the use of a dynamical observer is the possibility to use the observability and sensitivity analysis to evaluate operating conditions where to use the fault detection strategy. It has been shown that the proposed variable threshold provides only an upper

bound to the estimation error. This aspect leads, in some cases, to the impossibility of detecting faults before they reach very high level of magnitude. The strategy does not require, for the faults studied, any additional sensor unless strictly necessary and does not interfere with the used control strategy.

Perspectives

The continuous development of new technical solutions for better performing internal combustion engines leads to an increasing complexity of the system. Moreover, the next pollutant regulations will be more severe in system monitoring (EURO 6 and 7) and reliability over the time.

The increasing demand for specific fault detection strategy will be a challenge to be faced in the next years and a model based approach could be seen as one of the possible tool available to improve the FDI strategy.

In terms of future perspectives, the variable threshold conservativeness can be reduced by an online identification of the biases and drifts affecting the measurements. This can be done by numerical techniques like recursive least square algorithm if the persistent excitation condition is met (the system is sufficiently excited hence its measurements contain enough information on the biases that we want to estimate).
This implies that the FDI should be intrusive in the system: drive the control system in order to excite particular subsystems without breaking the global performances and respect the constraints.

Another important work is to develop the multi-faults detection. Even if the possibility that two failures appear at the same time is remote, the presence of different slow varying parameters in time is something that is more likely to happen. Being able to detect more faults at the same time will increase the robustness of the overall strategy.

In short terms, the application of this approach could be studied and implemented wherever possible to the post-treatment subsystem, in particular for Diesel engines, which is now a key part for the control and reduction of pollutant due to exhaust gases.

French version

Cette thèse a pour but l'étude et le développement de stratégies de diagnostic appliqué à la boucle d'air des moteurs Diesel. Le travail a été développé et testé pour deux pannes majeures qui peuvent apparaître dans un moteur thermique: - la présence d'une fuite dans le collecteur d'admission - la perte du rendement de la turbine, d'un groupe turbocompresseur Leur détection est critique pour le bon fonctionnement du moteur et donc pour le respect de la réglementation sur les émissions polluantes qui impose une surveillance continue, pendant tout la durée de vie du véhicule, de tous ses composants (EURO VI).

Dans le travail présenté on a choisi de traiter la problématique avec des méthodes basées sur les modèles c'est à dire model-based, en prenant comme hypothèses de travail les contraintes suivantes: - la stratégie doit fonctionner sans ajout de capteurs additionnels par rapport à ceux déjà disponibles dans la plupart des voitures commercialisées à ce jour; - la stratégie doit être suffisamment robuste pour être utilisée dans des zones de fonctionnement très différentes entre elles, c'est à dire durant un cycle de conduite Européen (ECE Cycle); - la méthodologie ne doit pas interférer avec la stratégie de contrôle du moteur;

Les résultats de cette thèse montrent que, au moins dans les deux problèmes traités, l'utilisation d'un observateur adaptatif est une solution viable pour la détection des pannes. Son utilisation permet de détecter la présences d'une panne, la localiser et, si les mesures utilisées par l'observateur sont précises, il a été montré qu'il était possible d'estimer l'amplitude de la panne. Dans une deuxième phase du travail, les incertitudes sur les mesures, donc les dispersions de production des capteurs ainsi que leurs défaillances éventuelles, ont été prises en considération dans la stratégie. Cela a permis de définir des seuils de détection variables, et ainsi d'éviter l'utilisation de seuils très conservatifs et pour réduire le temps de calibration de la stratégie.

L'analyse de sensibilité nous a permis, de manière systématique, d'estimer de quelle façon chaque incertitude de mesure (biais et dérive des capteurs) contribue à l'erreur d'estimation. Le résultat de cette analyse peut être utilisé en phase préliminaire quand il est nécessaire de définir les limites en termes de précision et de tolérance que chaque

capteur doit respecter pour obtenir une certaine précision et fiabilité dans l'estimation de la panne (Annexe C) De plus, l'utilisation de l'analyse de sensibilité avec des conditions additionnelles, comme la typologie de l'erreur de mesure, permet la conception d'un seuil de détection de la panne qui adapte son amplitude en fonction de l'observabilité de la panne sous surveillance. L'étude de cette dernière propriété, nécessaire pour garantir la convergence de l'observateur de l'estimation, peut être utilisée pour la détermination des zones de fonctionnement pour lesquelles l'estimation convergera plus rapidement et avec une meilleure précision: l'algorithme est fiable. Cet aspect est particulièrement intéressant d'un point de vue industriel, ces information étant habituellement obtenues avec des méthodes statistiques, par exemple méthode de Monte Carlo, ou avec l'analyse de grosses bases de données combinée à l'expertise industrielle dans le domaine.

Pour les problématiques examinées dans ce travail, l'utilisation de l'étude de la sensibilité pour la génération du seuil variable s'est révélée efficace si on dispose d'une bonne connaissance des incertitudes sur les mesures. En effet la méthodologie proposée fournit une limite supérieure pour toutes les incertitudes introduites sur l'estimation de l'observateur de chacune des erreurs de mesure. Afin de pouvoir résoudre ce problème et améliorer la capacité de détecter des pannes d'amplitudes mineures en gardant la robustesse de la méthodologie, il est nécessaire de recalibrer la seuil dynamiquement.

Le problème de la détection de fuite dans le collecteur d'admission abordé avec la méthode proposée a montré qu'il est possible de détecter des fuites, dues à des trous dans la surface du conduit, de 2.5 mm de diamètre si le moteur se trouve dans des zones de fonctionnement très favorables vis-à-vis du diagnostic, même en présence de recirculation de gaz brûlés (EGR). De façon plus générale, les résultats ont montré qu'il est toujours possible de détecter la présence de fuites de diamètre supérieur ou égal à 5 mm même si on se trouve en présence d'incertitude multiplicatives sur la cartographie de remplissage du moteur et sur la mesure fournie par le débitmètre de l'air provenant du compresseur. En termes de zones de fonctionnement, l'analyse de l'observabilité de la fuite combinée à celle de la fiabilité du modèle utilisé (en particulier la modélisation du débit des gaz d'échappement recirculés - EGR Flow) montre que la détection est précise et fiable quand le rapport des pressions entre l'intérieur et l'extérieur du collecteur est inférieur à 0.9, ce qui correspond à une pression indiquée moyenne (IMEP) supérieure

à 6 bar au régime moteur de 1500 rpm.

Pour le second problème, l'estimation du rendement de la turbine et la détection de sa perte, une fois que le modèle du turbocompresseur a été réduit à sa forme la plus simple, l'observateur peut être utilisé pour valider la cartographie fournie par le constructeur de la turbine sur les point stabilisés et normalement pour des zones de fonctionnement à très forte charge, c'est à dire grande vitesse de rotation. L'analyse de sensibilité pour ce problème a été très complète et montre son potentiel soit pour déterminer un seuil fixe, soit pour déterminer quel est le capteur et donc la mesure qui influence le plus l'erreur d'estimation. Le résultat est que le capteur de pression dans le collecteur d'échappement est le responsable principal de la précision de l'estimation et que l'incertitude maximale (3-sigma) considérée dans notre cas (200 mbar) doit être réduite pour que la méthodologie soit exploitable. Comme déjà démontré pour la détection des fuites, l'analyse de l'observabilité et l'étude de sensibilité suggèrent que la methodologie est particulièrement fiable sur les points de fonctionnement qui correspondent à une vitesse de rotation du turbocompresseur très élevée, c'est à dire à très forte charge. Sur ces points il est toujours possible de diagnostiquer des pertes de rendement supérieures ou égales à 10 de leur valeur nominale.

Les résultats de cette thèse ont été développés et présentés pour le diagnostic d'un moteur Diesel mais leur validité est absolument générale pour tout système qui ont les mêmes caractéristiques. L'étude a prouvé que l'un des avantages les plus importants dans l'utilisation d'une démarche basée sur un modèle est la réduction des temps de calibration. Cet avantage n'est pas négligeable surtout quand le moteur est sujet à des changements de partie mecanique, comme c'est le cas pendant la phase de son développement.

En conclusion, le travail présenté a montré les avantages d'une méthodologie de diagnostic basés sur l'utilisation de modèle physique appliqué à la boucle d'air d'un moteur thermique Diesel si on connait les incertitudes de mesure dûes aux dispersions de production des capteurs utilisés. De plus, un des avantages liés à l'emploi d'observateur dynamique réside dans la possibilité de déterminer les zones de fonctionnement où appliquer avec confiance la stratégie grâce à l'analyse de l'observabilité et la fonction de sensibilité. Pour ce qui concerne le seuil variable, il a été montré qu'il borne seulement

supérieurement l'incertitude de l'estimation. Cet aspect peut, dans certains cas, rendre impossible la détection de pannes avec des amplitudes faibles. Dans ce cas, une stratégie basée sur l'analyse statistique ou une analyse du résidu (dans le temps ou en fréquence) peut être plus efficace. On peut souligner que la stratégie proposée dans les cas étudiés ne demande aucun capteur additionnel et n'interfère pas avec la stratégie de contrôle déjà existante.

Perspectives

Le développement continu de solutions techniques pour améliorer les performance des moteurs à combustion interne entraine une complexification du système à contrôler et à surveiller. De plus, si les tendances sont confirmées, les prochaines réglementations sur la régulation des émissions polluantes (EURO VI et VII) seront de plus en plus sévères et nécessiteront une fiabilité dans le temps supérieure à la situation actuelle.

Selon ce scénario, la demande de stratégie de diagnostic, spécifique pour différentes parties du moteur, sera de plus en plus grande dans les années à venir et les methodologies basées sur modèles peuvent être vues comme un des instruments efficaces pour améliorer les stratégies de FDI.

Les perspectives futures de ces travaux concernent l'amélioration du seuil variable en le rendant moins conservatif par l'estimation en ligne des amplitudes des biais et des dérives qui affectent les mesures. L'identification peut être faite avec des méthodes numériques comme l'algorithme des moins carres récursifs si les conditions de persistance d'excitation sont garanties (le système doit être suffisamment excité par ses entrées et les mesures doivent contenir suffisamment d'information pour pouvoir reconstruire l'estimation considérée). Pour pouvoir aborder le problème de cette façon, la méthodologie de FDI doit devenir intrusive: le contrôle doit pouvoir exciter les sous systèmes d'intérêt en garantissant le respect des ses objectifs primaires: performance, consommation de carburant, agrément de conduite et respect des normes sur les émissions.

En termes d'évolution possible de la démarche, la capacité de pouvoir détecter plusieurs pannes en même temps reste très importante. Même si la probabilité que deux pannes puissent se manifester au même instant est très faible, la présence de dérives

lentes de certains paramètres dans le temps est réaliste et probable. Être capable de les détecter permettrait d'accroître la robustesse générale du diagnostic embarqué.

De façon plus en générale, la démarche proposée pourrait être étudiée et implémentée sur les systèmes de post traitement, en particulier pour les moteurs Diesel, qui sont maintenant une partie clé pour le contrôle et la réduction des émissions polluantes dans les gaz d'échappement.

Appendix A

Simulation and Experimental Facilities

In this report both simulative and experimental results have been presented. The aim of this section is to explain the software and mechanical setup used for developing and testing the proposed algorithms.

A key part in the analysis and development of new algorithms is the possibility to test them offline in operative conditions that are much closer to the real engine. This necessity is principally due to save occupancy time of the experimental facilities and so their operative costs.

A.1 Simulation Environment

All the algorithms have been tested in a co-simulation environment based on *Mathworks* Matlab and Simulink© softwares for the implementation of the engine controller and supervisor strategy and AMEsim © developed by *LMS Imagine* that has been used for the thermal and physical numerical simulation of the engine behaviour.
The IFP modelling team has developed a specific library, i.e. IFP-ENGINE, which contains the most important components that could be found in an engine and its

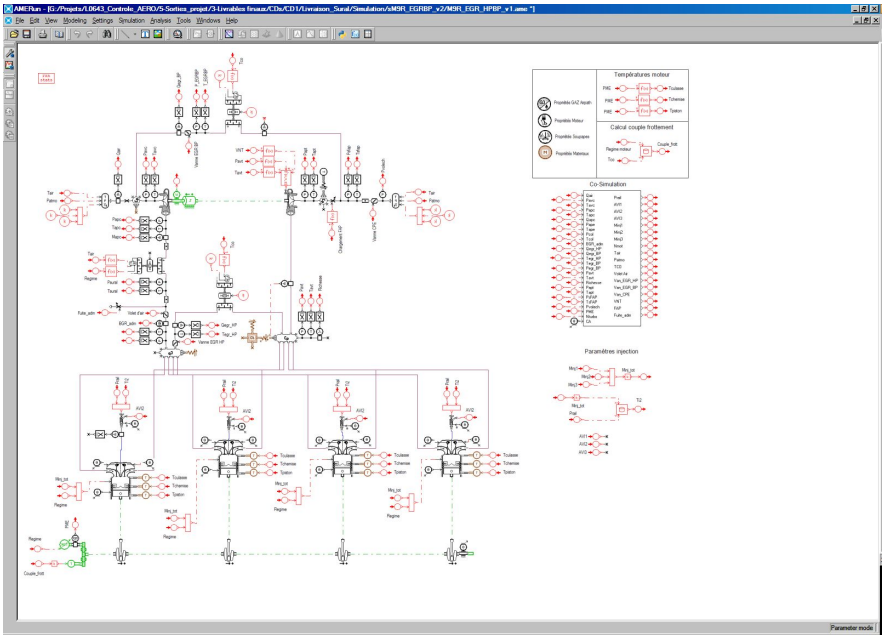

Figure A.1: Renault G9T Diesel engine - LMS AMEsim© model

subsystem. The library is created in to easily allow users to modify the mechanical configuration of the engine and calibrate each individual component regardless the mathematical and physical complexity underlying each element of the library. With respect to the fidelity of those models it should be noticed that they are intended for control co-simulation purposes, which means that they should catch the most important dynamic within a certain degree of precision. The reason of those limitation is principally due to the computation effort required to run the model with respect to the time required. In control development, as well for fault detection, there is a constant need to test the algorithm in many different engine operating points which can be really time consuming.

However, even if the AMEsim model is a simplified model, it is a complete description of the thermal and mechanical behaviour of the engine and all its components (turbocharger, valves, filters, heat exchangers...). Furthermore, in simulation, it is considered as a reference because it is the closest model to a real engine.
On Simulink's side, the used models are generally with lump parameters and they are a very good approximation of the system dynamic which leads to a natural discrepancy

between the two models; this aspect allows also to check also the robustness of the tested strategies with respect to model uncertainties.

In terms of data exchange between the two models, the co-simulation environment, by the mean of a C function embedded in Simulink, synchronises the signals and data exchanged. Generally the AMEsim model is designed to run with a good degree of precision by a fixed step solver and provides to Simulink all the measurements as if provided by the real sensors. It is in Simulink that is possible to arbitrary generate bias and drift in signals that the system controller and the FDI supervisor will then elaborate. In exchange the system controller will provide all the actuators set-points to drive the engine AMEsim model. This loop is performed every 0.1 ms.

A.2 Experimental Environment: the test bench

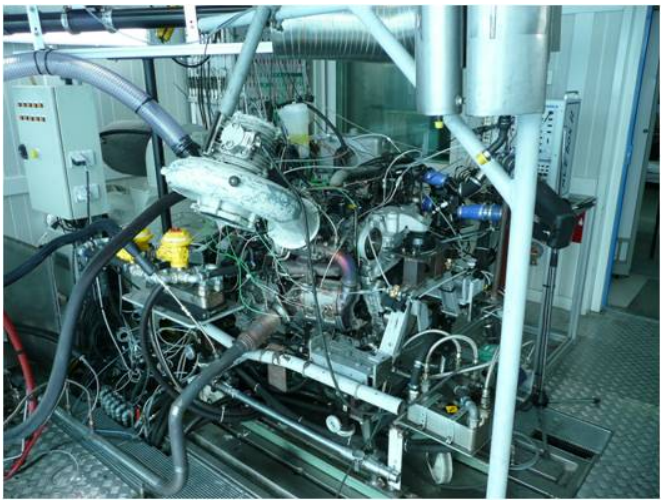

Figure A.2: IFP Test bench: Renault G9T Diesel engine (IFP courtesy)

The engine used as reference for this study is a Renault G9T 2.2 litres, 4 cylinders Diesel engine available at the IFP for research and development. The engine, when the work has been conducted, was already equipped with an exhaust gas recirculation circuit and a variable geometry turbocharger. Moreover an additional valve was installed to the intake manifold to simulate the leak.

The control strategy and so the fault detection strategy developed in Simulink is then built for a xTarget Pc which operates directly on a test bench computer and acts exactly in the same way as the co-simulation explained previously: it reads the sensors values, elaborate the best control action and sends the new desired set point to the actuators.

Appendix B

Adaptive Observers: a quantitative comparison

In Section 3.3 there were proposed two different observers for the intake manifold leak diameter estimation both derived from Lyapounov analysis.
The main difference between them is the change of coordinates which allow the modified observer (eq. 3.17) to evolute with respect to the observability condition: the better is the observability the faster will be the convergence of both the state and the parameter estimation.
In this chapter a quantitative analysis and comparison between the two proposed observer will be presented in term of performances and robustness.
In order to make the comparison, without any lack of information, more understandable in term of results a fake system will be used with exactly the same structure and nomenclature of the intake manifold model 3.4 but with different signal profiles. This case study will allow to have more control on the boundary conditions of the qualitative analysis.

B.1 The reference system

The system used as reference in this analysis is the following

$$\begin{cases} \dot{x}(t) &= -a(t)x(t) - \psi(t)\theta^* + \phi(t) \\ y(t) &= x(t) + \nu(t) \end{cases} \tag{B.1}$$

where $a(t)$, $\psi(t)$ and $\phi(t)$ are three completely known function of the time. In addition we added a noise ν to the output of the system which is considered not measurable and its wave form will specified later in this section.

In details the function $a(t)$ is always positive and in our study has been chosed to be:

$$a(t) = A * sin(t) + 2 * A \tag{B.2}$$

where A is a constant equal to 0.1.

The $\phi(t)$ term, which in the intake model was the sum of the EGR flow plus the air

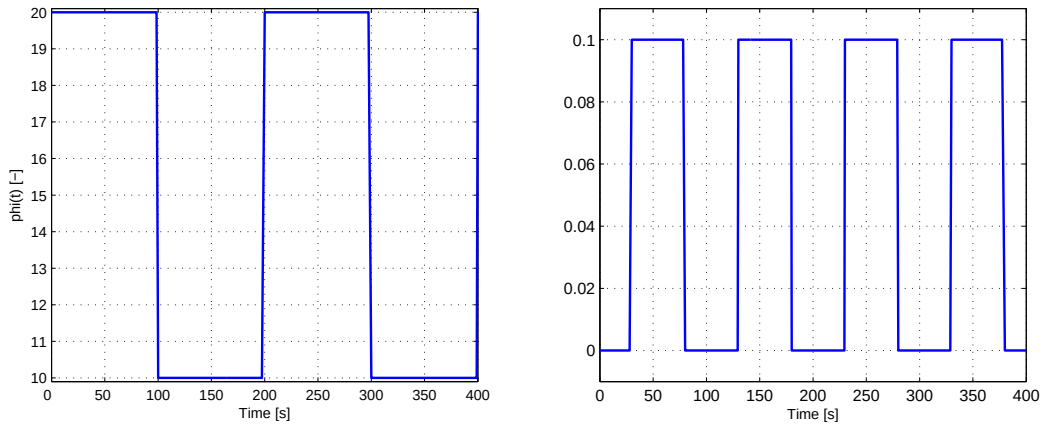

(a) $\phi(t)$ (b) $\psi(t)$

Figure B.1: Time evolution of $\phi(t)$ and $\psi(t)$

flow, here is modeled as square signal depicted in figure B.1(a) which change every 100 seconds. This choice is principally due to the necessity of change the operating point of the system.

The $\psi(t)$ signal, which is multiplied with the parameter θ (see eq. (B.1), is associated with the observers estimation convergence and so with the observability condition. For reasons that would be cleared during the analysis, it has been choosen to guarantee intervals in which there were no observability thus $\psi(t) = 0$ at all and others in which is different from zero, so the signal is a square signal included between zero and 0.1, moreover to avoid simultaneous switch of the signal, $\psi(t)$ has been shifted of 30 seconds as shown in Figure B.1(b).

The nominal value of the parameter θ^* has been set arbitrarily to a value of 5 and it has been kept constant all along the simulation. In term of noise ν two types of signal

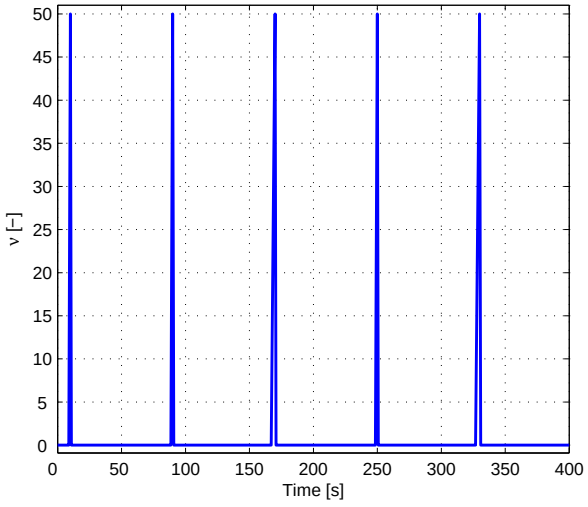

Figure B.2: Time evolution of $\nu(t)$ when is a pulses generator

have been employed:

- a white noise, simulated as random number generator with a zero mean and a variance set to a value of 2;
- a pulses train (see Fig. B.2), which has been generated with a PWM signal generator with a maximum value set to 50;

.

A final consideration regarding the initial condition used in the simulation. They have been set to 1 for $x(0)$ and, as told previously, $\theta(0)$ equal to 5.

The presented system it will be referred as reference system in the rest of this analysis.

B.2 Performance Analysis

The aim of this section is to compare the observer performances in order to better characterise the behaviour of the two dynamical estimators.

From a simulation point of view, to avoid that the observers start from initial condition close to the real one used in the reference model and in order to allow to evaluate the dynamical responses the initial condition of both the observers have been set to the same values: $\hat{x}(0) = 10$ and $\hat{\theta}(0) = 50$.

B.2.1 Same Gains

The first test was design to look at the observers behaviour when exactly the same gains where applied to both of them. The intent here was to understand the effect that the $\psi(t)$ introduces in the observer responses both in the state than in the parameter θ and to assess the impact of the additional term that appear in the modified observer: the integral term (3.17).

For this test, with respect with notation used in the section 3.3, we set the gain to a common arbitrary value:

- Lyapounov observer with $gains = [K_0\ \gamma] = [1\ 1]$
- Modified observer with $gains = [K_1\ K_\theta] = [1\ 1]$

With this choice of gains the results obtained are reported in Figure B.3.

Looking to the results and in particular to the parameter estimation B.3(b) is possible to observer two interesting dynamical behaviours:

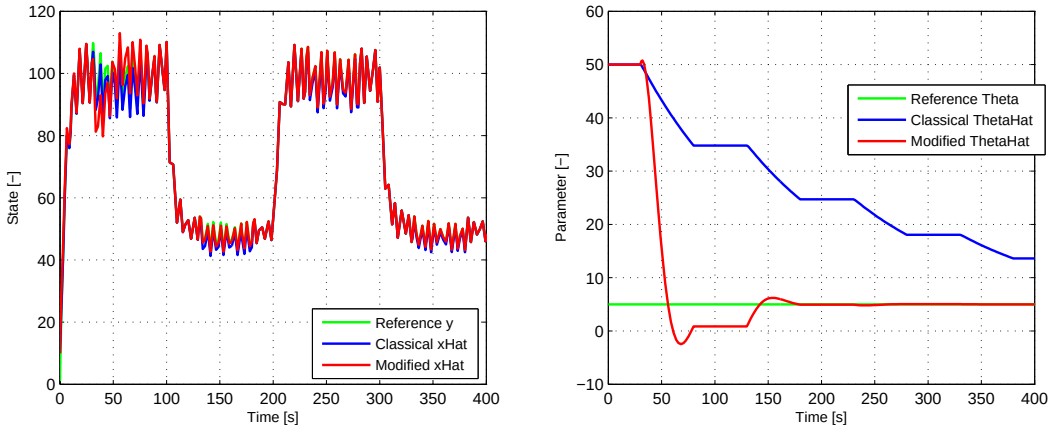

(a) $\hat{x}(t)$

(b) $\hat{\theta}(t)$

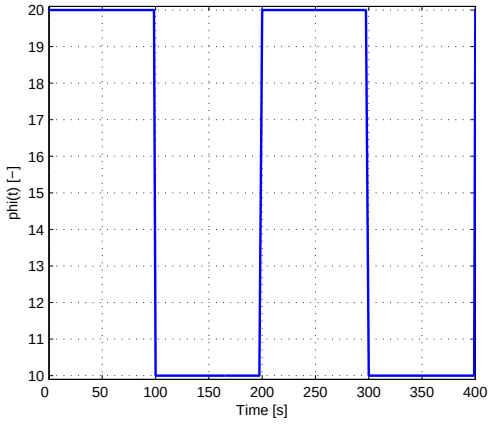

(c) $\phi(t)$

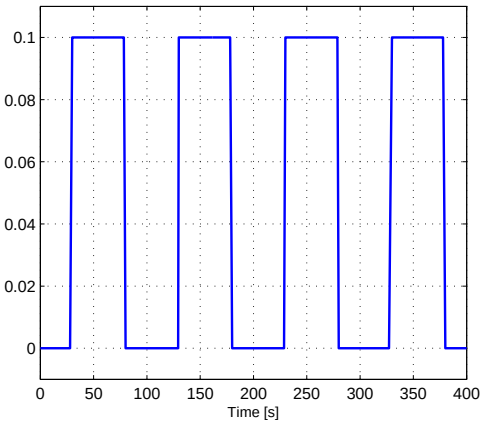

(d) $\psi(t)$

Figure B.3: Performance Analysis - The two observers have the same gains

- both the observers freeze the $\hat{\theta}(t)$ estimation when the observability condition (Fig. B.3(c)) is loss

- the modified obsever, due to the integral term and when the observability condition is satisfied, has a faster convergence.

In term of state convergence, the faster convergence of the parameter estimation in the modified observer, allow the observer with the integral term to have better behaviour.

B.2.2 Same behaviour: different gains

The following test was designed to understand if it was possible to find a set of gains in order to have comparable behaviour of the two observers. In other words, in the first test it seemed that the modified observer was faster, now we look if it would be possible to speed up the Lyapounov observer in order to have the same behaviour of the modified one.

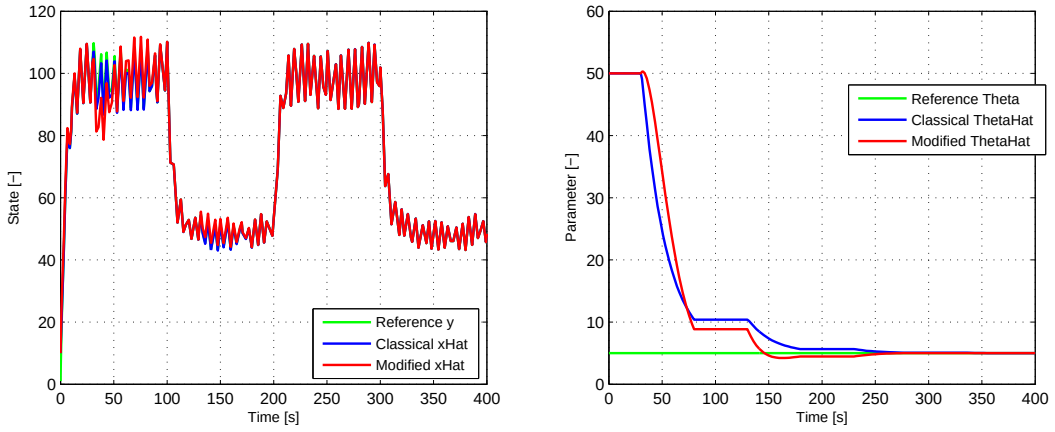

(a) $\hat{x}(t)$

(b) $\hat{\theta}(t)$

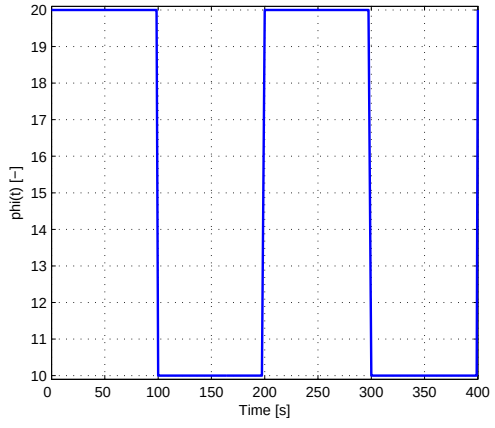

(c) $\phi(t)$

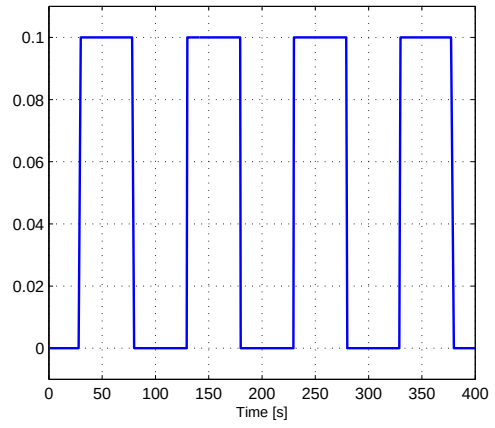

(d) $\psi(t)$

Figure B.4: Performance Analysis - The two observers have the same gains

By choosing the gains as follow

- Lyapounov observer with $gains = [K_0\ \gamma] = [1\ 5]$

- Modified observer with $gains = [K_1\ K_\theta] = [1\ 0.4]$

as shown in Figure B.4, the two observers behave very closely and the performances of the dynamical response of the parameter and the state convergence confirm the hypothesis (see Fig. B.4(a) and B.4(b)).

It is important here to remark that in order to have a close behaviour of the Lyapounov observer to the modified, it has been necessary to increase the gain γ of a factor 4 and reduce therefore reduce K_θ.

B.2.3 Conclusions

The performance analysis shows that, if the observability condition is satisfied, it is always possible to find a set of gains that allow the two proposed observer to behave in a similar way: convergence time. In general it is possible to see that the modified observer is faster, if the same gains are applied to both the estimators. The reason is that the integral term contributes to the convergence because of the state error $\tilde{x}(t)$ that is integrated over the time.

B.3 Robustness Analysis

The second aspect worth to be investigated is the robustness of the proposed observers to exogenous signals as noise and spikes.
Both these disturbances reflect possible communication problems and that is the reason why $\nu(t)$ has been applied directly to the measurement $y(t)$.

In order to make comparison simpler the same tests sequence will be proposed in the next part of this section: same gains and different gains.

B.3.1 Same gains: Impulses and noise

The first test is with the same gains for both the observers as described in B.2.1 applying a white noise to the measurement $y(t)$.

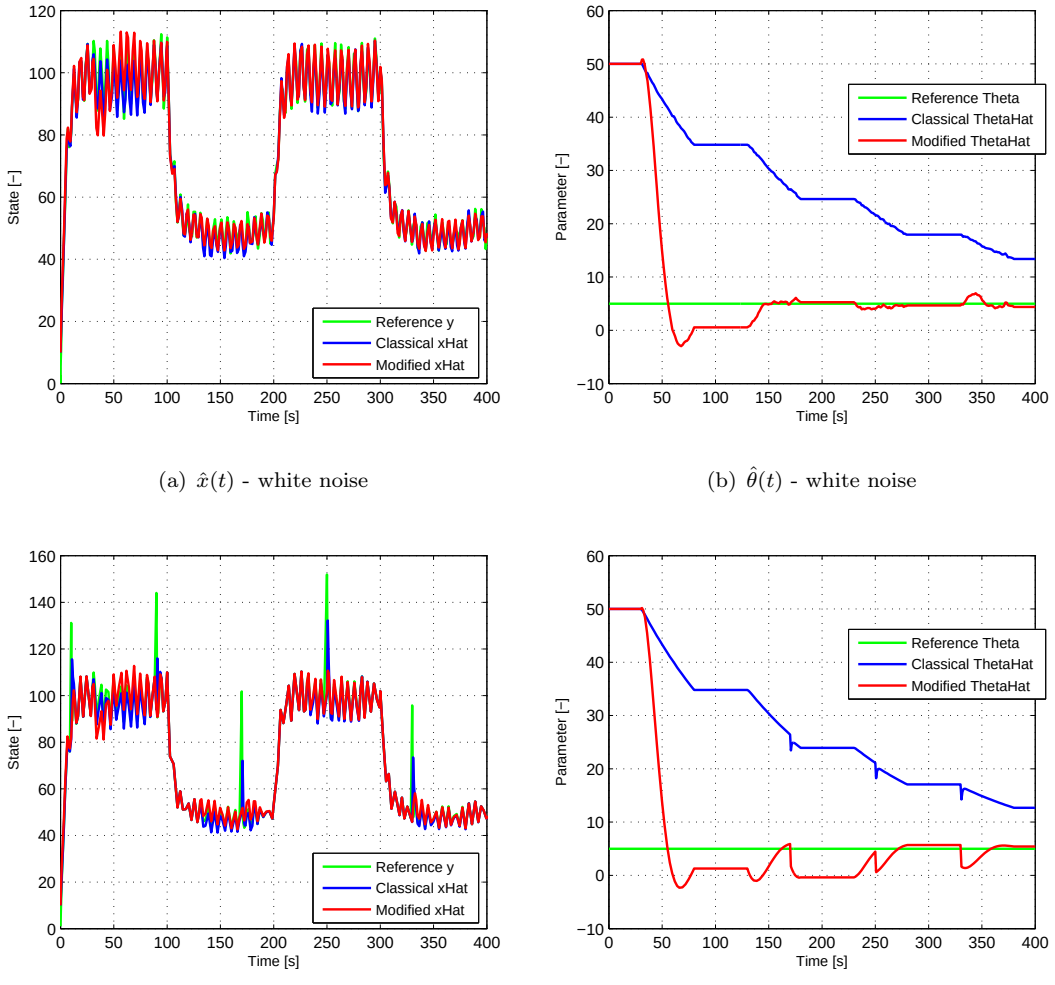

(a) $\hat{x}(t)$ - white noise

(b) $\hat{\theta}(t)$ - white noise

(c) $\hat{x}(t)$ - impulses

(d) $\hat{\theta}(t)$ - impulses

Figure B.5: Robustness Analysis - The two observers have the same gains

The results shown in Figure B.5 show in the upper row the observer responses both for the state (Fig. B.5(a)) than for the parameter (Fig. B.5(b)) and in the lower row the same when only impulses as shown in figure B.2 are applied.
In term of noise, the two observers parameter estimation are partially affected by the

noise in a very limited manner.
The spikes effect instead, even if limited seems, seems to be more evident in the modified observer than in the Lyapounov one with respect to the parameter estimation (Fig. B.5(d)). In the state estimation instead the modified observer acts as it was not sensitive to the spikes, the Lyapounov observer instead filter much less the spikes as it possible to see in Fig. B.5(c).

B.3.2 Different gains: Impulses and noise

The previous test shows how good the modified observer was to reject impulsive disturbances on the system output from the state estimation and a reduce effect of those on the parameter estimation having anyway a faster convergence response.

With respect to this consideration, the aim of this test is to assess the impact of these disturbances in the estimation dynamic when the convergence speed is similar between the two observers: they have different gains.

As already stated, to simplify the comparison between the test results, the gains chosen are the same presented in the section B.2.1.

The results of this test are shown in Figure B.6 where the effect of increase the gain of the Lyapounov observer for having a convergence rate similar to the modified observer lead to a unwanted effect on both the estimations.
In more details, the effect of the noise is now more evident on the parameter estimation (Fig. B.6(b)) even if limited, for the modified observer due also to a decrease of its adaptive gain K_0 the noise is completely filtered.

The key result, in terms of robustness, is the evaluation of the spikes effect on both the state and the parameter estimation: in both the case the modified observer reacts better to these perturbations (see Figure B.6(c) and B.6(d)).

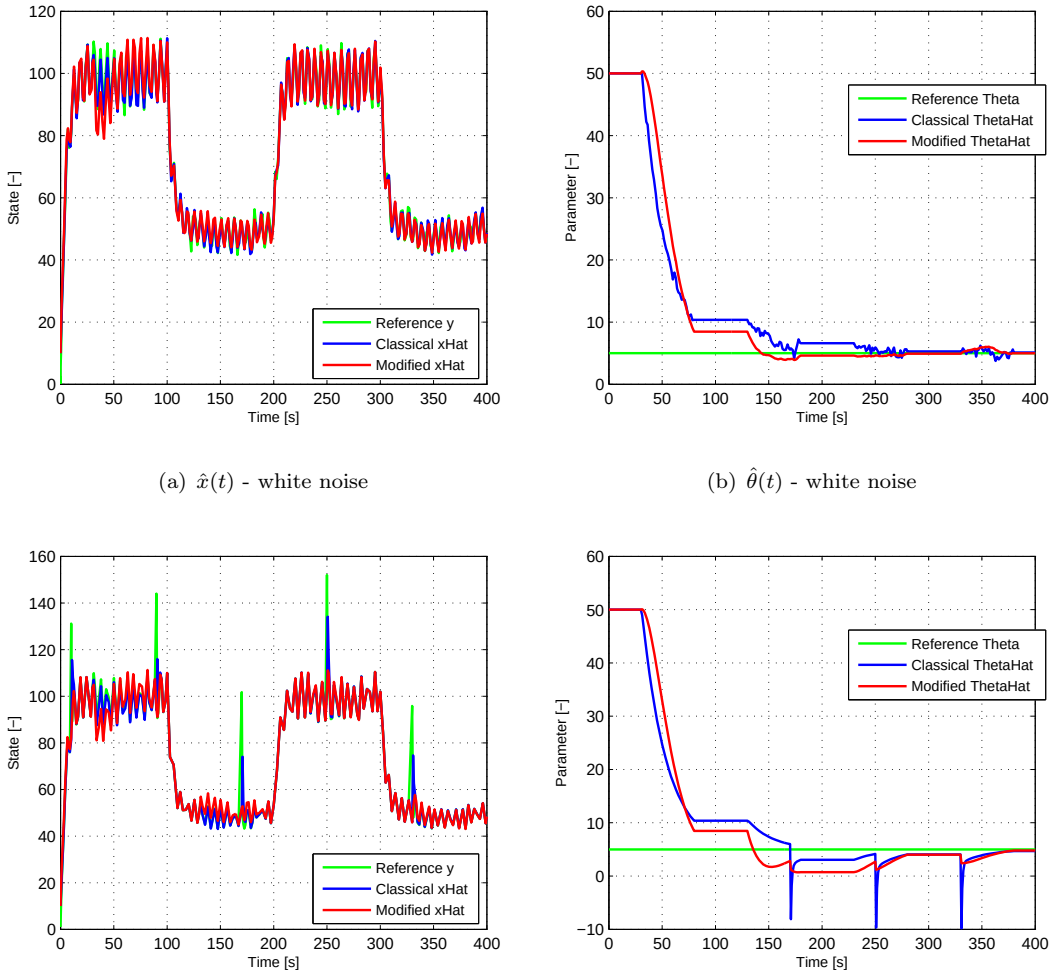

(a) $\hat{x}(t)$ - white noise

(b) $\hat{\theta}(t)$ - white noise

(c) $\hat{x}(t)$ - impulses

(d) $\hat{\theta}(t)$ - impulses

Figure B.6: Robustness Analysis - The two observers have the different gains

B.4 Conclusion

In the design of a dynamical system, such as an observer, there is always a trade-off between performances and robustness. The qualitative analysis provided was intended to assess both those aspects with respect to the fault detection and identification problem.

The presented results show that from a performance benchmark the two proposed observers show differences in term of convergence speeds: the modified observer due to its additional integral feedback term can be faster. However, it has been possible to show

that it is possible to find a set of gains for the Lyapounov observer to behave in a very similar way like the modified one.

This possibility of having a closer dynamical behaviour it is obtained in practice by increasing the adaptation gain of the Lyapounov observer to higher values.

The effect of increasing the gain has a counter productive effect on the observers robustness, in particular to reject noise and spikes from the system output measurement.

These considerations make the modified observer more suitable for FDI problems that are casted in the way of model based approach with the use of adaptive observers and parameter estimation.

Appendix C

Sensitivity Analysis: a tool

In Chapter 4 we studied the fault detection for a variable geometry turbine by the design of an observer which relies on many measurements equally potentially affected by biases and drifts. For those reasons, the sensitivity analysis has been used to understand which measurement error would have the major effect on the turbine efficiency estimation and so drive the strategy to possible false alarms.
The results of this analysis provide the constituent element of the variable threshold which is cover in discuss in that chapter.

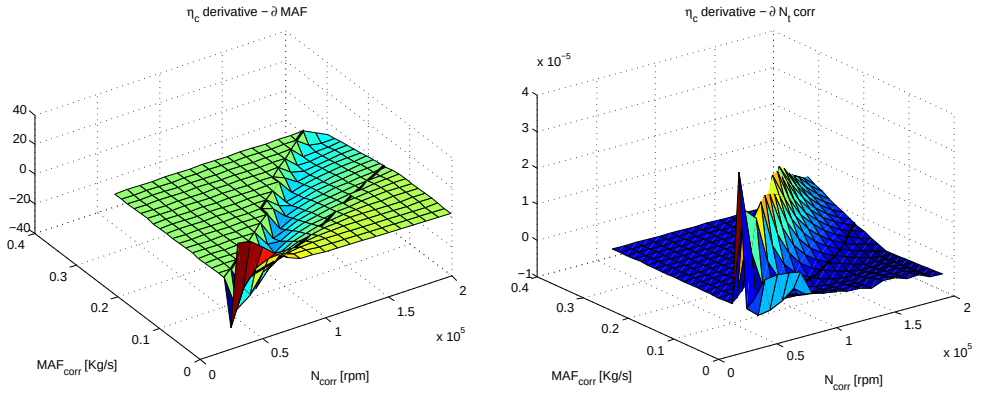

(a) Compressor Efficiency Map derive wrt MAF (b) Compressor Efficiency Map derive wrt turbocharger speed N_t

Figure C.1: Compressor Maps

The aim of this section is to present a different use of the sensitivity analysis not for understanding the impact of each sensors error on the estimation but as a tool to

identify the operating conditions in which the observer parameter estimation has a sensitivity equal to zero with respect to a specific measurement variation. In other words, if the sensitivity is equal to zero it means that a small variation of the measurement will not affect the estimation so those points are the most likely to be use in the FDI strategy in order to reduce possible sources of errors.

In section 4.3.1 this analysis has been done with respect to some measurement for a specific operating point: 2000 rpm. The result was that all the signals affect the estimation with different magnitudes and in particular the exhaust pressure was the most critical measurement, it introduces by its own a minimum error of 10%. In the same section we consider variation of the compressor efficiency map as global error and not as potential bias of the measurement used to evaluate it:

- N_t - Turbocharger shaft speed;
- MAF - Air mass flow sensor.

Figures C.1(a) and C.1(b) show the derivative of the compressor efficiency map (Fig. 2.10(a)) with respect to its arguments: N_t and MAF. In Figure C.2 it is shown the isolevel contour corresponding to where the compressor map derivative with respect to the turbocharger shaft speed N_t (red solid line) and the derivative with respect to the mass air flow measurement are equal to zero. In addition, for different engine speeds used in the calibration process, in figures C.2(a), C.2(b), C.2(c) and C.2(d) they are reported the steady state condition values of the two measurements for different loads (green squares) showing that there are operating points that are across the zero sensitivity lines: this points could be used then for running, in that case, the turbine efficiency FDI strategy knowing that it will be less sensible to small MAF of N_t biases. In reality we are only interested in the MAF bias because, for the specific problem, we supposed to have a very good estimation of the turbocharger, i.e p_{int} is fault free.

To conclude this analysis, the same approach have been taken for the turbine efficiency map used as a reference for generating the residual. The turbine η_t (eq. 2.21) depends on the turbocharger shaft speed, the variable geometry turbine wings position

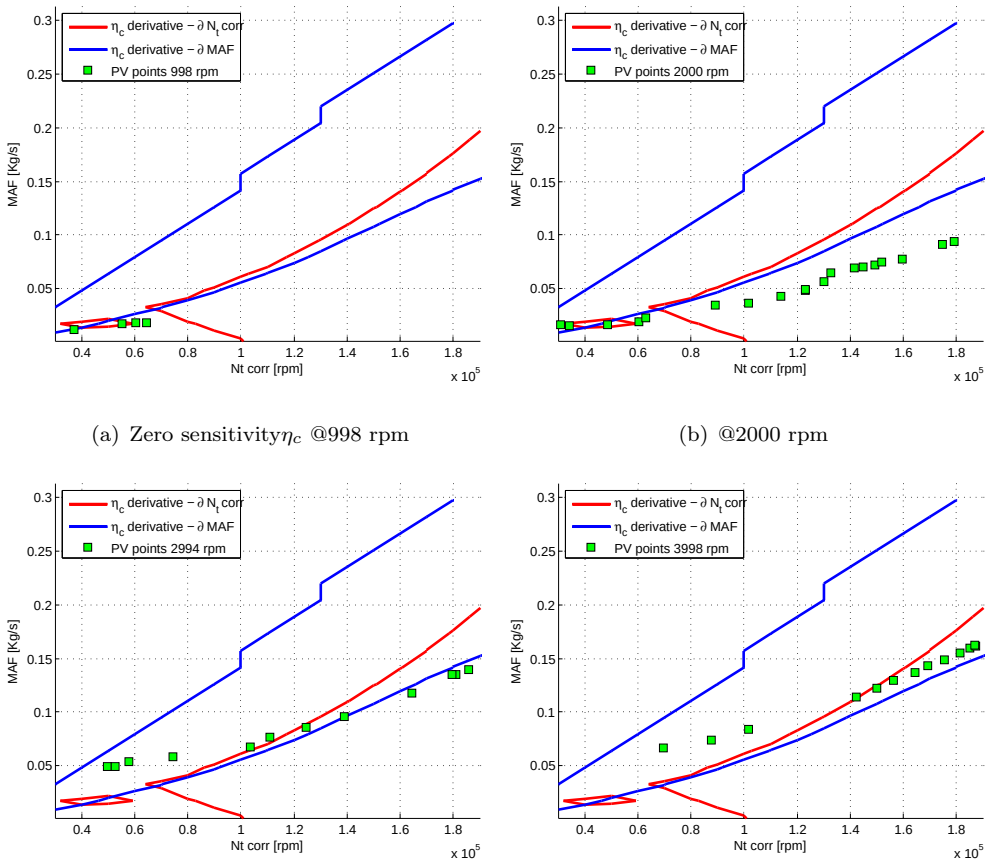

(a) Zero sensitivityη_c @998 rpm

(b) @2000 rpm

(c) @2994 rpm

(d) @3998 rpm

Figure C.2: Steady state calibration points for G9T evaluate on the compressor zero sensitivity function at different engine speeds

and the turbine gas flow (eq. (2.23)) which is function on the the delta pressure across the turbine and so it is subject to p_{exh} biases. The first two signals are fault free and so the same analysis did previously for the compressor map is now presented for the turbine efficiency map.

Figure C.2 shows the zero sensitivity curves (parametrised with respect to the u_{VGT} position) for a Π_t variation. In addition the same engine operative calibration points has been superposed (green squares) and the same if a 200 mbar bias would be added to the exhaust pressure measurement p_{exh} (black squares).

The results show that there are operating points at low engine speed and relative low loads (Fig. C.3(a) and C.3(b)) that are over the zero sensitivity curves (green square)

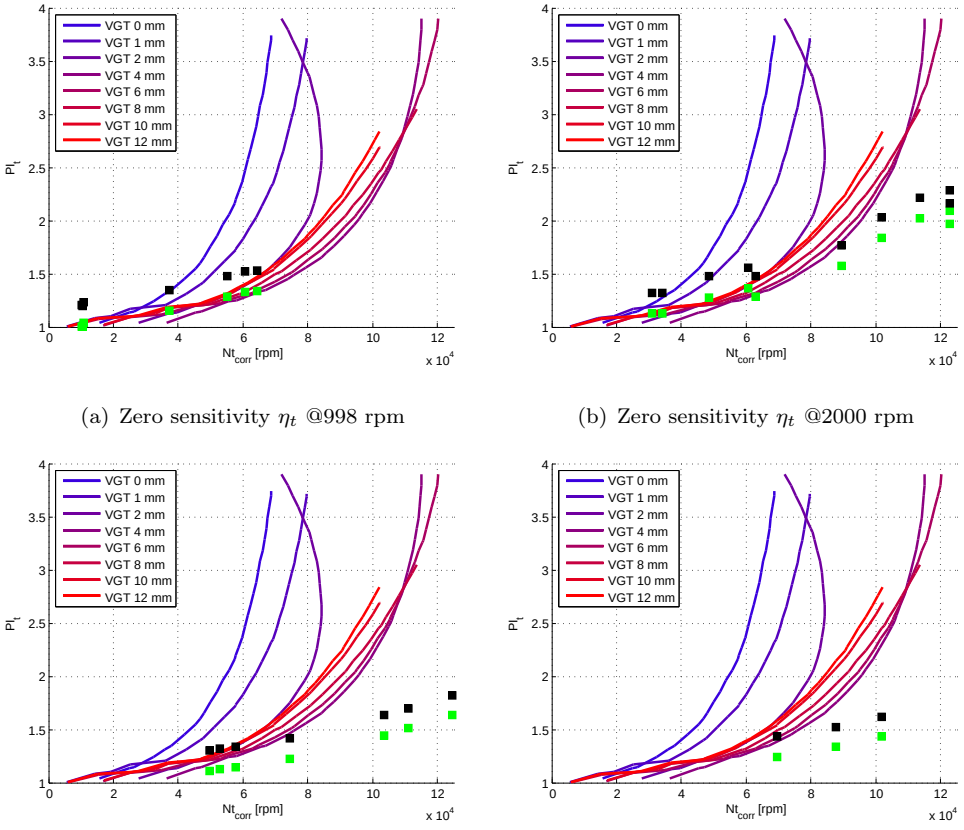

(a) Zero sensitivity η_t @998 rpm

(b) Zero sensitivity η_t @2000 rpm

(c) Zero sensitivity η_t @2994 rpm

(d) Zero sensitivity η_t @3998 rpm

Figure C.3: Steady state calibration points for G9T evaluate on the turbine zero sensitivity function at different engine speeds

even if a positive bias is applied to the p_{exh} measurement (black squares). In reality all the points that are not on the zero sensitivity curves for high engines speed are on a iso-surface in which the derivative of the turbine efficiency map with respect to Π_t is zero (Fig. C.4). This last fact confirm what already discovered in simulation in Chapter 4 and, moreover, it provides an important information about the reliability of the estimation we use as reference for built our residual term: the turbine efficiency map evaluation, at high engine speed, it is not affected by exhaust pressure measurement errors.

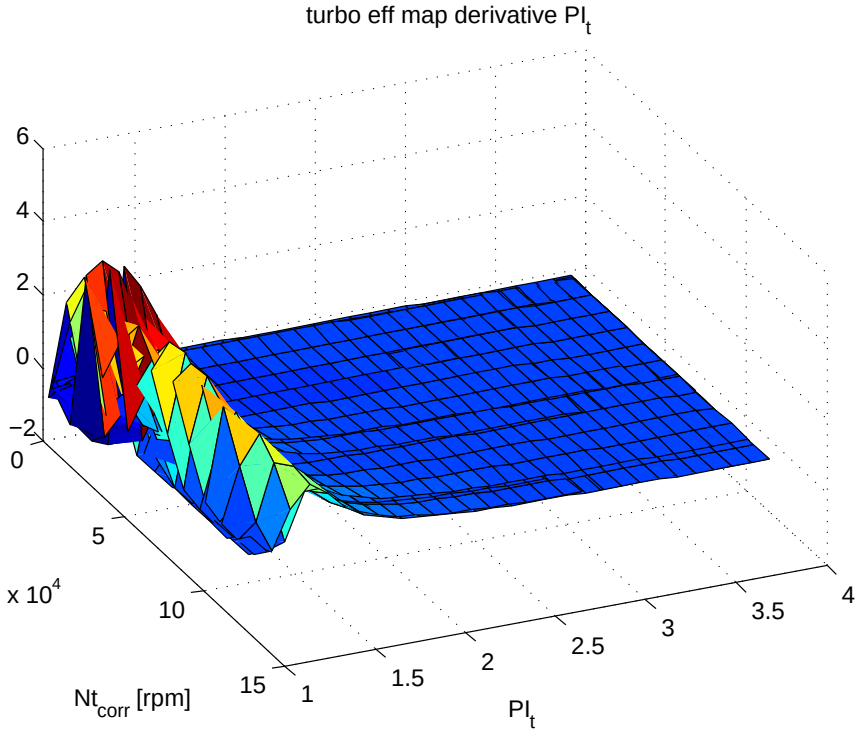

Figure C.4: Turbine efficiency map derived with respect to Π_t

Appendix D

Publications

Conferences

- Ceccarelli, R., Moulin, P., Canudas de Wit, C., *"Robust Strategy for Intake Leakage Detection in Diesel Engines"*, Multi-conference on Systems and Control 2009
- Ceccarelli, R., Canudas de Wit, C., Moulin, P., Sciarretta, A., *"Model-based Adaptive Observers for Intake Leakage Detection in Diesel Engine"*, in Proc. of American Control Conference 2009

Journal

- Ceccarelli, R., Moulin, P., Canudas de Wit, C., *"Turbine Efficiency Estimation for Fault Detection Application"*, Engine Control and Calibration, SAE Technical Paper Series, 2010

Bibliography

[1] A. P. O. Adilson de Jesus Teixeira, Marcelo Lopes de Oliveira e Souza. Multiple Fault Detection and Isolation in Sensors of Dynamic System. *SAE Technical Paper Series*, (2005-01-4136), 2005.

[2] A. Albrecht, J. Chauvin, F. Lafossas, and S. Potteau. Development of Highly Premixed Combustion Diesel Engine Model: From Simulation to Control Design. *SAE Paper*, 2006-01-1072, 2006.

[3] E. Alcorta Garcia and P. Frank. Deterministic nonlinear observer-based approaches to fault diagnosis: a survey. *Control Engineering Practice*, 5(5):663–670, 1997.

[4] A. Astolfi, D. Karagiannis, and R. Ortega. *Nonlinear and adaptive control with applications*. Springer Verlag, 2008.

[5] K. Astrom and B. Wittenmark. *Adaptive control*. Addison-Wesley Longman Publishing Co., Inc. Boston, MA, USA, 1994.

[6] G. Besancon. *Nonlinear Observers and Application*. Springer, 2007.

[7] C. Canudas De Wit and S. Ge. Adaptive friction compensation for systems with generalizedvelocity/position friction dependency. In *Decision and Control, 1997., Proceedings of the 36th IEEE Conference on*, volume 3, 1997.

[8] C. Canudas de Wit and R. Horowitz. Observers for Tire/road Contact Friction using only wheel angular velocity information. *Proceedings of the Conference on Decision & Control Phoenix, Arizona USA*, 1999.

[9] C. Canudas-de Wit, M. Petersen, and A. Shiriaev. A new nonlinear observer for tire/road distributed contact friction. *Proceedings of the Conference on Decision and Control - Hawai, USA*, pages 9–12, 2003.

[10] R. Ceccarelli, C. Canudas de Wit, P. Moulin, and A. Sciarretta. Model-based Adaptive Observers for Intake Leakage Detection in Diesel Engine. *American Control Conference - St. Louis*, 2009.

[11] R. Ceccarelli, P. Moulin, and C. Canudas de Wit. Robust Strategy for Intake Leakage Detection in Diesel Engine. *IEEE Multi-conference on Systems and Control*, 2009.

[12] M. Celik and R. Bayir. Fault detection in internal combustion engines using fuzzy logic. *Proceedings of the Institution of Mechanical Engineers, Part D: Journal of Automobile Engineering*, 221(5):579–587, 2007.

[13] J. Chauvin. *Estimation et controle d'un moteur HCCI. Estimation des systemes periodiques.* PhD thesis, Ecoles des Mines de Paris, September 2006.

[14] J. Chen and R. Patton. *Robust model-based fault diagnosis for dynamic systems.* Springer, 1999.

[15] A. Chevalier, M. M
"uller, and E. Hendricks. On the validity of mean value engine models during transient operation. *SAE Technical Paper Series*, 2000.

[16] S. X. Ding. *Model-Based Fault Diagnosis Techniques.* Springer, 2008.

[17] P. Dolcini, H. Bechart, and C. Canudas de Wit. Observer-based optimal control of dry clutch engagement. In *Decision and Control, 2005 and 2005 European Control Conference. CDC-ECC'05. 44th IEEE Conference on*, pages 440–445, 2005.

[18] S. Drakunov and V. Utkin. Sliding mode observers- Tutorial. pages 3376–3378, 1995.

[19] J. Gertler. *Fault Detection and Diagnosis in Engineering Systems.* CRC Press, 1998.

[20] L. Guzzella and C. Onder. *Introduction to modeling and control of internal combustion engine systems*. Springer, 2004.

[21] E. Hendricks. Isothermal vs. adiabatic mean value engine models. In *IFAC Workshop: Advance in Automotive Control*, Karlsruhe, Germany, March 2001.

[22] J. Heywood. *Internal combustion engine fundamentals*. McGraw-Hill New York, 1988.

[23] E. Höckerdal, E. Frisk, and L. Eriksson. Observer design and model augmentation for bias compensation with a truck engine application. *Control Engineering Practice*, 17(3):408–417, 2009.

[24] P. Ioannou and J. Sun. *Robust adaptive control*. Prentice Hall PTR, 1996.

[25] R. Isermann. Model Based Fault Detection and Diagnosis Methods. *Proceedings of the American Control Conference - Seattle*, 1995.

[26] R. Isermann. Supervision, fault-detection and fault-diagnosis methods. An introduction. *Control Engineering Practice*, 5(5):639–652, 1997.

[27] R. Isermann, A. Schwarte, and F. Kimmich. Model-based fault detection of a Diesel engine with turbo charger. A case study. In *1st IFAC Symposium on Advances in Automotive Control, University of Salerno, Italien*, 2004.

[28] H. Khalil. *Nonlinear systems*. Prentice Hall Upper Saddle River, NJ, 2002.

[29] Y. Kim, G. Rizzoni, and V. Utkin. Automotive engine diagnosis and control via nonlinear estimation. *Control Systems Magazine, IEEE*, 18(5):84–99, 1998.

[30] E. Larson, B. Parker Jr, and B. Clark. Model-based sensor and actuator fault detection and isolation. In *American Control Conference, 2002. Proceedings of the 2002*, volume 5, pages 4215–4219. IEEE, 2002.

[31] B. Lee, Y. Guezennec, and G. Rizzoni. Model-Based Diagnosis of Spark-Ignition Direct-Injection Engine Using Nonlinear Estimation. *SAE Paper*, 2005-01-0071, 2005.

[32] N. McDowell, G. McCullough, X.Wang, U. Kruger, and G. W. Irwin. Fault Diagnostics for Internal Combustion Engines - Current and Future Tecniques. *SAE Paper*, 2007-01-1603, 2007.

[33] J. Mohammadpour, K. M. Grigoriadis, M. A. Franchek, and B. Zwissler. Real-Time Diagnostics in the EGR System of Diesel Engines. *American Control Conference*, 2008.

[34] C. Montes-Solano and P. Pisu. Fault Detection in Idle Speed Control of IC Engines. 2009.

[35] P. Moraal and I. Kolmanovsky. Turbocharger modeling for automotive control applications. *SAE transactions*, 108(3):1324–1338, 1999.

[36] P. Moulin, J. Chauvin, and B. Youssef. Modelling and control of the air system of a turbocharged gasoline engine. In *Proc. of IFAC World Congress (submitted)*, 2008.

[37] M. Nyberg. Model-based diagnosis of an automotive engine using several types of fault models. *Control Systems Technology, IEEE Transactions on*, 10(5):679–689, 2002.

[38] M. Nyberg and A. Perkovic. Model based diagnosis of leaks in the air-intake system of an SI-engine. *SAE Paper*, 980514, 1998.

[39] M. Nyberg and T. Stutte. Model based diagnosis of the air path of an automotive diesel engine. *Control Engineering Practice*, 12(5):513–525, 2004.

[40] E. Parliament and of the Council. Regulation (ec) no 715/2007 of the european parliament and of the council of 20 june 2007 on type approval of motor vehicles with respect to emissions from light passenger and commercial vehicles (euro 5 and euro 6) and on access to vehicle repair and maintenance information., 2007.

[41] R. Patton and J. Chen. Observer-based fault detection and isolation: Robustness and applications. *Control Engineering Practice*, 5(5):671–682, 1997.

[42] A. Schwarte and R. Isermann. Model-Based Fault Detection of Diesel Intake With Common Production Sensors. *SAE technical paper*, 2002-01-1146, 2002.

[43] R. Sharma and M. Aldeen. Fault detection in nonlinear systems with unknown inputs using sliding mode observer. pages 432–437, 2007.

[44] S. Sorenson, E. Hendricks, S. Magnusson, and A. Bertelsen. Compact and accurate turbocharger modelling for engine control. *SAE transactions*, 114(3):1343–1353, 2005.

[45] S. K. Spurgeon. Sliding mode Observers: a survey. *International Journal of Systems Science*, 39:8:751–764, 2008.

[46] Q. Zhang. Adaptive Observer for MIMO Linear Time Varying System. Rapport de recherche n.4111, INRIA, 2001.